2014

Design And Analysis Of Reconfigurable Sensing Antennas For Wireless Sensing Applications

Qian Qiao
University of Mississippi

DESIGN AND ANALYSIS OF RECONFIGURABLE SENSING ANTENNAS FOR WIRELESS SENSING APPLICATIONS

A Thesis

Presented for the

Doctor of Philosophy

The University of Mississippi

Qian Qiao

ABSTRACT

Reconfiguration sensing antenna (RSA) is a novel antenna concept, which not only can transmit or receive radio waves but also can sense the surrounding environment. The environment sensing is realized by reconfiguring the antenna's characteristics, such as resonant frequency, and radar cross section (RCS). The RSAs possess the advantages of passive and low cost, which make them suitable for the large-scale wireless sensing networks (WSNs) deployment. In this dissertation, the RSAs concept is demonstrated, and two sensing mechanisms performed in the RSAs are investigated. In order to verify these sensing mechanisms, four RSAs are designed, analyzed, and measured. All the RSA designs in this dissertation are temperature monitoring RSAs, and they realize the temperature sensing by reconfiguring the antenna resonant frequency.

About the two sensing mechanisms, one utilizes the electrical properties of materials, and the other utilizes thermal properties of the materials. For each sensing mechanism, there are two RSA designs using different sensing materials. As sensing antennas, sensitivity is a crucial factor in the RSA designs. Thus, a sensitivity evaluation method is also defined in this dissertation. There are three factors used to evaluate the RSA performance, which are $\Delta f/\Delta T$, realized gain, and realized gain bandwidth.

For the sensing mechanism using electrical properties of materials, water and high density polyethylene-Ba0.3Sr0.7TiO3 (HDPE-BST) are investigated and selected as the sensing materials.

Patch antennas are properly designed to easily implement these sensing materials as their substrate. Simulation and measurement results show that these two designs provide 4MHz/10°C and 8MHz/10°C frequency shift with temperature, respectively. Their realized gain is -3.2dB with 4.33% 3dB bandwidth, and -3.9dB with 0.6% 3dB bandwidth, respectively. And their corresponding read range is 5.8m and 4.2m.

For the sensing mechanism using thermal properties of materials, mercury and Polytetrafluoroethylene (PTFE) are used as sensing materials. To magnify the materials' thermal expansion impact on antenna performance, cavity backed slot antennas are designed to integrate the sensing materials. The simulation and measurement results show that these two designs provide 13MHz/10°C and 40MHz/10°C frequency shift with temperature, respectively. Their realized gains are 5.47dB with 1.33% 3dB bandwidth and 4.2dB with 0.66% 3dB bandwidth, respectively. And their corresponding read range can achieve 17m and 14m, respectively. In addition, the size reduction method of the PTFE cavity RSA is also investigated. A new compact cavity RSA is presented at last, which provide comparable sensitivity but 30% size reduced, when compared with the conventional PTFE used cavity RSA.

DEDICATION

This work is dedicated to my mother, my father, my uncles, my brothers, and my sisters

without whose love and support

I could not finish it.

ACKNOWLEDGMENTS

This work is supported in part by Tsinghua National Laboratory for Information Science and Technology（TNList）Cross-discipline Foundation, and the Natural Science Foundation of China (Grant No.51221291).

I would like to sincerely thank my advisors Dr. Atef Z. Elsherbeni and Dr. Fan Yang for their guidance, patience, attention, valuable discussion. I learned a lot from them, not only the knowledge of EM and antenna, but also the attitude for research. They are idols for me for their personality and solid knowledge. I feel lucky that I met them in olemiss and being students of them. They helped me a lot to improve my presentation skills, and have been always open for my ideas, motivate me to execute it, follow up and give suggestions to my results and findings. They also gave me the chance to conclude and decide the next steps in light of their mentorship. I'm in addition, very grateful for their advices and undeniable help in my career development first steps.

I want to thank my parents, without their love and support; I would not come to the US to finish my Ph.D study. The study life in oxford will be a beautiful memory in all my life.

I would also like to thank my best friends Yilin Mao, Suping Xia, Xiaoliang Liang for their always accompany with me during the tough time in my graduate study. Especially Yilin, she is with me all the five years. I would also like to thank my colleges in olemiss and Tsinghua.

TABLE OF CONTENTS

LIST OF FIGURES

FIGURE PAGE

LIST OF TABLES

TABLE PAGE

CHAPTER I

INTRODUCTION

1.1 Introduction of Antenna Development

Antennas are the electrical devices which are used to transmit or receive radio waves. In transmitting mode, they convert electrical power to radio waves, and vice versa in receiving mode. They are essential elements in the telecommunication systems. From the first antenna build by Hertz in 1888, antennas have been developed for more than one century. Generally, the development of antennas can be classified into three steps: conventional antennas, reconfigurable antennas (RAs), and the novel reconfigurable sensing antennas (RSAs). The conventional antennas have fixed characteristics like resonant frequency, pattern, etc., when they are designed. They are the normal used antenna types, which can be found anywhere in our daily life, for example the Yagi-Uda antennas for TV broadcasting, and the reflector antenna for satellite communications. Nowadays, in many applications, such as cell phone, satellite communications, etc., compact, high gain, and wideband antennas are desired. In this situation, most of the conventional antenna designs focus on how to reduce antenna size, broaden its bandwidth, and improve antenna gain to meet the emerging application requirements [1]-[3].

With the evolution of technologies, the antennas are required to possess more functionality. In some cases, such as Multiple-input and Multiple-output (MIMO) [4], and Antenna

SYstem Reconfiguration in Orbit (ASYRIO) [5], the antennas are required to have reconfigurable characteristics such as frequency, pattern, to meet their adaptive systems requirements. In this condition, RAs are introduced and developed. Different technologies like Microelectromechanical systems (MEMS) [6], Pin diodes [7], optical switches [8], and varactors [9] are utilized in the RA designs to control the frequencies and radiation patterns of the antennas. Although the RAs have reconfigurable patterns or frequencies, they cannot transmit more information other than electromagnetic waves. In order to make the antenna transmit more information, reconfigurable sensing antennas are introduced.

The RSAs are the antennas which not only can transmit or receiver electromagnetic waves, but also can sense the surrounding environment variation. The reason they called reconfigurable sensing antennas are because they sense the environment by reconfiguring the antennas characteristics such as resonant frequency, RCS. In this dissertation, all the RSAs are frequency reconfigurable RSAs. The idea is that by directly integrating sensing materials in the antennas, the antennas' characteristics are reconfigured by the environmental parameters. By checking the antennas' characteristics, the environment information is detected. The important features of RSA are passive and simple structure which implies low cost and low power consumption. These features make it a good candidate in many applications, such as wireless sensor networks (WSN). Meanwhile, by integrating the radio frequency identification (RFID) used IC chip, the RSA can also be used for both wireless sensing and wireless identification, which broaden its application areas.

1.2 Research Background

Wireless sensing network (WSN) plays an important role in many areas such as environment monitoring, air pollution monitoring, forest fire detection, etc. The current sensor networks are built of various sensor nodes. A sensor node usually consists of a radio transceiver, a microcontroller, a sensor interfacing circuit, and a battery. The cost of the sensor nodes could be as high as hundreds of dollars depending on its complexity. Meanwhile, the usage of batteries restricts the sensor nodes' operation time and increases their maintenance fee. Thus, the big challenge of a WSN is to develop low-cost and passive sensor node. In this situation, reconfigurable sensing antenna becomes a promising candidate because of its important features stated before.

Reconfigurable sensing antennas are the antennas that possess the sensing capabilities. As mentioned before, their characteristics, such as resonant frequency, RCS are reconfigured by the environment. This parameter reconfigurable property enables the RSAs to transmit more information than traditional antennas.

On the other hand, the RFID technology has attracted lots of attentions because of its wireless identification and tracking features. If IC chip used in RFID is integrated in the RSA design, it can realize both wireless identification and wireless sensing. Thus, the RSAs can also be deployed in the RFID applications with more functions like environment sensing.

Generally, a RSA consists of three parts: an antenna, a sensor unit, and an IC chip. In most cases, the sensor units in the RSAs are low cost physical sensors, which can be directly integrated in the antennas. On the other hand, as mentioned before, the integration of IC chip in RSA design

can make it also possess wireless identification. No batteries are needed in the RSAs, which make them lifetime operation and suitable for harsh environment. The RSAs provide a possible solution for today's economic deployment of WSNs and other wireless sensing applications, because of their simple structures, low cost, and passive characteristics.

According to their sensing targets, the RSA can be classified into temperature, humidity, gas, etc. Taking temperature sensing as an example, in many areas, instantaneous temperature sensing is important. For example, in cold chain, temperature is critical for the product quality. In this case, the RSAs can be deployed through the cold chain to wireless monitor the temperature variation. In addition, the sensor node maybe placed in harsh environment, which means it is not easy to replace. In such a situation, the passive feature of RSA is favorable, which can operate in lifetime. Fig. 1-1 shows the environmental applications for the temperature RSAs, one is cold chain, and the other is energy efficient house. Both of them are suitable environment for RSAs deployment.

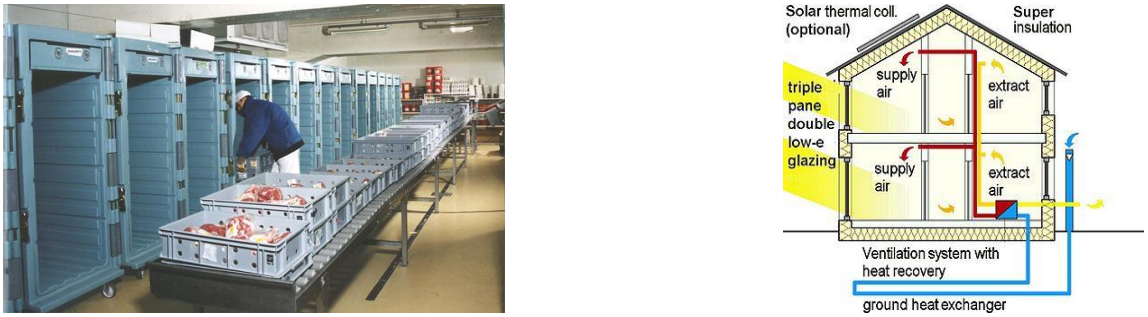

(a) (b)

Fig. 1-1 Application areas of temperature RSA: (a) cold chain [10], (b) energy efficient house [11].

1.3 Review of the State-of-the-Art RSA Technologies

RSAs have received great interests recently, and a number of designs have been published. As mentioned before, the RSAs can be classified into temperature RSA [12]-[15], humidity RSA [16-17], gas RSA [18], motion RSA [19], etc. The designs in [12] and [17] use water and Kapton as sensing materials to realize temperature and humidity level monitoring. Water has a temperature-dependent dielectric constant, and is integrated in the substrate of a patch antenna [12]. When the temperature changes, the dielectric constant of water also changes accordingly, which in turn affect the resonant frequency of the patch antenna. This is because the resonant frequency of a patch antenna is proportional to its substrate permittivity. So we can get the temperature information by checking the resonant frequency of the RSA. Similar to water, Kapton has a humidity level dependent dielectric constant. It is used as substrate of a capacitive-load dipole. The dielectric constant variation will affect the loaded capacitance of the dipole, and in turn change the resonant frequency of the dipole. Thus, we can also obtain the humidity information by checking the resonant frequency of the RSA.

Ice is used in the design in [15] to realize a critical temperature sensing. When temperature is above 0°C, the ice melts, which will change the backscattered signal strength of the RSA. Thus, the 0°C temperature can be detected by checking the backscattered signal strength of the RSA. The thermal switches in [14] have the same functionality as the ice has in [15]. The thermal switches have two states "on" and "off" which are determined by the temperature. Different switches can sense different temperatures. When the temperature is below the sensing value, the switch keeps the "on" state, which is usually short circuit. However, when the temperature is above the sensing

value, the switches will switch to the "off" state, which is the open circuit. In [14], the switches are integrated in a dipole antenna. The resonant frequency of the dipole antenna is determined by its length. The switches in the dipole antenna can reconfigure the length of the dipole by converting between its two states "on" and "off". Therefore, the resonant frequency of the dipole RSA in [15] is controlled by the states of the switches. Accordingly, the specific temperature is sensed by checking the resonant frequency of the RSA.

For the gas RSA in [18], the resistance of the sensing material, single walled carbon nanotube (SWCNT) is ammonia dependent. The SWCNT is designed as part of the antenna. As the ammonia concentration varies, the resistance of the SWCNT is changed, which will affect the match between the antenna and the IC chip. For a high ammonia concentration level, the radar cross section (RCS) of the antenna becomes smaller due to the poor match. As a result, the ammonia level can be detected by the RCS of the RSA. All the advantages and limitations of the aforementioned designs are summarized in Table 1-1.

Table 1-1 Summary of current RSA designs

Publication time	Sensing parameter	Reconfigurable parameter	Advantages	Limitation
2010	temperature [15]	RCS	Cost effective, ease of fabrication, safe	Critical temperature detection, short read range (1m)
2011	temperature [12]	Resonant frequency	Cost effective, safe	Low Q factor, Limited sensitivity (4MHz/10°C)

2012	temperature [14]	Resonant frequency	Low cost, short response time, long read range	Critical temperature detection
2010	humidity level [16]	Resonant frequency	low cost, continuous humidity detection	Low Q factor, Limited sensitivity (4MHz/10°C)
2009	Ammonia [18]	RCS	Simple, low cost	Limited sensitivity

According to this summary, most of the current RSA designs possess the merits of low cost, and passive operation. However, few of them can realize a high sensitivity when they are designed to monitor the continuous target variation at a long distance. Thus, in this dissertation, the goal is to design high sensitivity RSAs for continuous target monitoring at a long distance.

The design of RSAs requires the knowledge of antenna theory, RFID technique, and sensor information. There are two key steps in the RSA designs. One is the sensing mechanism selection. Another is the sensor and antenna integration, which is to design proper antenna configurations that can integrate the sensor unit and make it effectively reconfigure the antennas' characteristics. In addition, the RFID chips are also considered to incorporate into the RSAs. Therefore, the knowledge of the RFID technology is necessary. The following section is about the RFID technique.

1.4 Organization and Contribution of This Dissertation

The scope of this dissertation pertains to the usage of different sensing mechanisms in the RSA designs, and how to improve the RSAs' sensitivity. Two different sensing mechanisms are investigated and implemented in this dissertation. One utilizes electrical properties of sensing materials, and the other utilizes thermal properties of sensing materials. Each of them has two specific designs to demonstrate its working principle. Meanwhile, as a sensing antenna, sensitivity is important to determine its performance. In this dissertation, three parameters are used to evaluate the RSA sensitivity which are $\Delta f/\Delta T$, realized gain, and realized gain bandwidth. As stated above, the goal of this dissertation is to realize a high sensitivity RSAs for continuous target monitoring at a long distance. To achieve this goal, the first step is to select appropriate sensing materials which possess the features such as good sensitivity, low cost, and easy to integrate in the RSAs. Secondly, antenna configurations should be properly designed which can magnify the sensing materials effects on the RSA performance.

In this dissertation, all of the RSAs are designed for monitoring temperature. Temperature is selected as the sensing parameter, because it is closely related to our daily life, such as food production, healthcare, cold chain, energy efficiency house, etc. In chapter 2, the RSA concept will be introduced including its components and operation principle. Also because the usage of IC chip in the RSAs, the RSA is related to the RFID technology, thus, RFID is also introduced. And a comparison is made between the RSA and RFID sensor tag. In chapter 3 and 4, two specific designs of using electrical properties of the sensing materials are introduced and analyzed. They are water embedded RSA design and HDPE-BST based RSA design. After that, in chapter 5 and 6,

two specific designs using the thermal properties of sensing materials are introduced and analyzed. They are mercury used capacitively-loaded cavity backed slot RSA and PTFE used capacitively-loaded cavity backed slot RSA. It is observed that from chapter 3 to chapter 6 the sensitivity of the RSAs is increased. Fig. 1-2 shows the flow chart of the organization of this dissertation.

The research of the existing RSAs focus on using electrical properties of sensing materials in the antenna designs. And they have limited sensitivity of 4MHz/10°C [12] and 4MHz/20%RH [17]. In this dissertation, the RSA design which uses HDPE-BST as sensing material can provide an improved sensitivity of 8MHz/10°C. Besides that, HDPE-BST is firstly discovered and used as the temperature sensing materials in RSA designs. In addition, the thermal properties of materials are used in the RSA designs for continuous temperature monitoring. By integrating the sensing material mercury and PTFE in cavity backed slot antennas, a competitive sensitivity is achieved under the passive condition. The PTFE used cavity RSA has 40MHz/10°C frequency shift with temperature and more than 14m read range. This result is the best one in the published designs. Additionally, the thorough systematic research and analysis of the RSAs have not been investigated before, and this dissertation is the first one to do it.

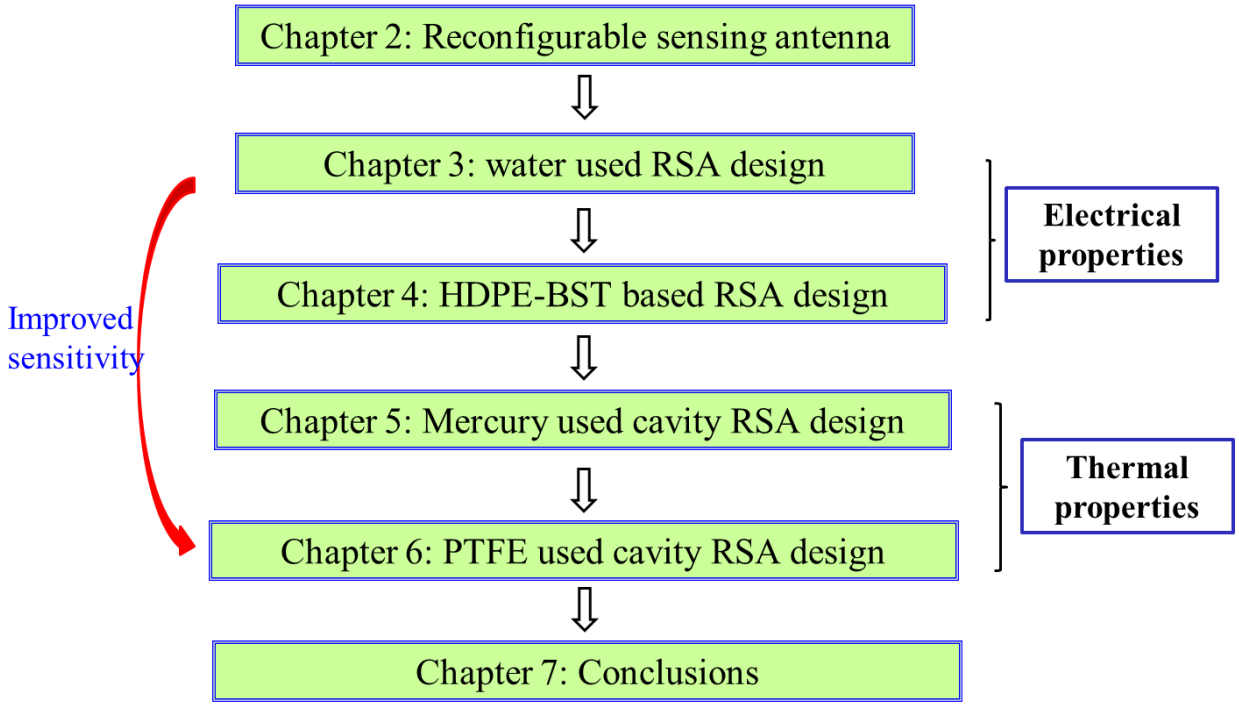

Fig. 1-2 Flow chart of the organization of the dissertation.

CHAPTER II

RECONFIGURABLE SNESING ANTENNA

Reconfigurable sensing antenna is introduced in this chapter, including its concept and operation principle. Generally, the RSA mainly consists of three parts: an antenna, a sensor unit, an IC chip. The IC chip with a unique identification number is the same as the one used in radio frequency identification (RFID) systems. Hence, the RFID technology is also introduced in this chapter. The relation between RFID and RSA is illustrated and organized. Finally, the parameters used to determine the RSA sensitivity are illustrated, which are $\Delta f/\Delta T$, realized gain, and bandwidth.

2.1 Reconfigurable Sensing Antennas Concept

As mentioned before, reconfigurable sensing antennas are the antennas which not only can transmit electromagnetic waves, but also can sense the surrounding environment. For sensing antennas, sensor units are the essential elements in the RSAs. In most cases, the sensor units are simple and low cost physical sensors, which can be directly integrated in the antenna. According to their sensing parameters, the RSAs can be classified into temperature RSA [12]-[15], gas RSA [18], humidity RSA [16]-[17], movement RSA [19], etc. In this dissertation, all of the research works focus on temperature sensing RSA designs. The reason for selecting temperature as a

sensing target is that temperature is closely related to our daily life. For example, temperature is important in food production, medical management, etc.

To obtain more functionality, the RSAs are usually integrated with the RFID chips, which are low cost and low power consumption. For example, the Alien Higgs 3 chip has a sensitivity of -18dBm [20]. With the integration of RFID chip, the RSAs can work as passive RFID tag without battery and any other power source. The energy used in the RSAs operation is based on the incoming EM wave from the interrogator. In this case, the RSAs can realize both the wireless sensing and the wireless identification. The RSAs represent a new wireless sensing and identification approach, which is much simpler comparing with the traditional approach. For the comparison purpose, a traditional wireless sensing and identification approach is shown in Fig. 2- (a). Its architecture includes a CPU, a sensor, a RF interface, and an antenna. The ID information is usually stored in the read only memory (ROM). It is known that this complicated structure will consume more energy. Thus, in most cases, batteries are used to supply power in this traditional approach. Accordingly, the maintenance fee is increased. On the other hand, the new wireless sensing and identification approach shown in Fig. 2- (b), has no CPU and RF interface. The main components are antenna, sensor, and chip. This structure is much simpler, easier to maintain, and cost efficient. The RSAs belong to the new sensing approach. In the RSAs, the sensors are directly integrated in the antennas. The advantages of RSAs are simple, low cost, and passive.

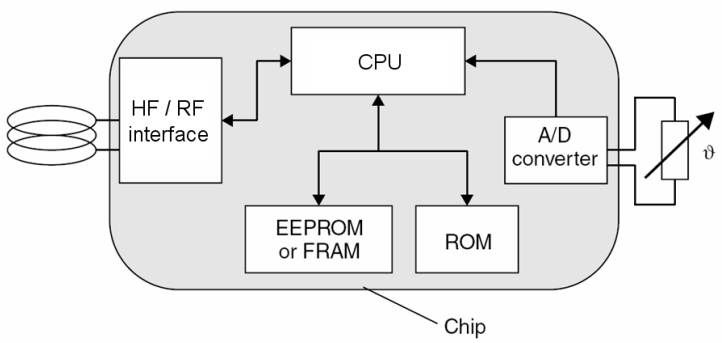

(a)

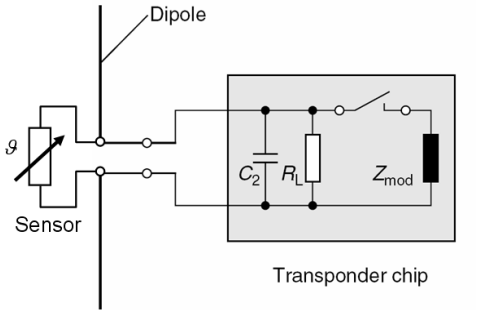

(b)

Fig. 2-1 Wireless sensing and identification architectures: (a) traditional architecture [26], (b) new architecture.

2.2 RSA Components and Operation Principle

A RSA consists of three components: an antenna, a sensor unit, and a load, which is usually an IC chip. Fig. 2-2 shows an illustrative configuration of RSA.

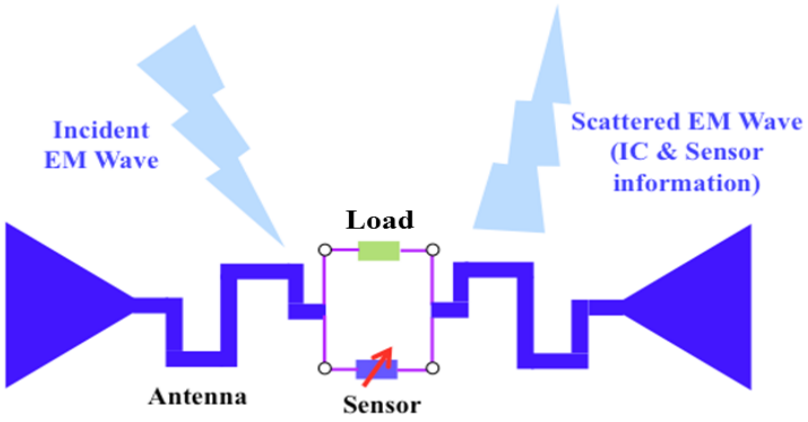

Fig. 2-2 An illustrative configuration of the normal RSA.

The antennas of the RSAs are used to harvest the EM power. Besides that, it can also scatter the EM wave under the control IC and sensor. Dipole antennas and microstrip patch antennas are the two commonly used antenna configurations in the RSA designs. These antennas have the advantages of being simple, cost-effective, and ease of integration. Dipole antennas have omni-directional radiation patterns, which can equally receive energy from many directions. On the other hand, the microstrip patch antennas have the advantages, such as low profile, conformable for planar and non-planar surfaces, inexpensive to manufacture using modern printed-circuit technology, etc. These features make patch antenna very popular in many applications. And patch antenna consists of patch, substrate, and ground, where the ground plane enables the patch to work on the metal surface without degrading its match.

The IC chips in RSAs are used to store the ID information of the RSAs. The ID information in each chip is ubiquitous, and can be modulated on the scattered EM wave by the IC. Thus, the

RSAs can realize wireless identification. The IC chips have the advantages of being low cost and low power consumption. The IC integrated RSA designs can realize the wireless sensing and wireless identification, which makes them more attractive in wireless sensing applications.

The sensor units in RSAs are usually physical sensors. The sensors reflect the surrounding environment variation by changing their resistance, capacitance, dielectric constant, and thermal expansion, etc. According to their sensing target, sensors can be divided into temperature, humidity, gas, motion, etc. According to their forms, the sensors can be categorized into lumped and distributed. For example, thermistor is a lumped sensor whose resistance depends on the surrounding temperature, and then water is a distributed sensor whose dielectric constant depends on the temperature. In most cases, the sensors are integrated in the antennas. Then the sensors will directly affect the antenna performances.

The operation principle of the RSAs is described as follows: when the ambient environments such as temperature, humidity, and gas concentration changes, the sensors will be affected in terms of inductance, capacitance, resistance, dielectric constant, thermal expansion, etc. These sensor properties variations will result in the change of antenna performance parameters such as resonant frequency, and radar cross section (RCS). Thus, the environment parameters can be sensed by detecting the radiation properties of the antennas. A flow chart in Fig. 2-3 is used to demonstrate the operation principle of the RSA.

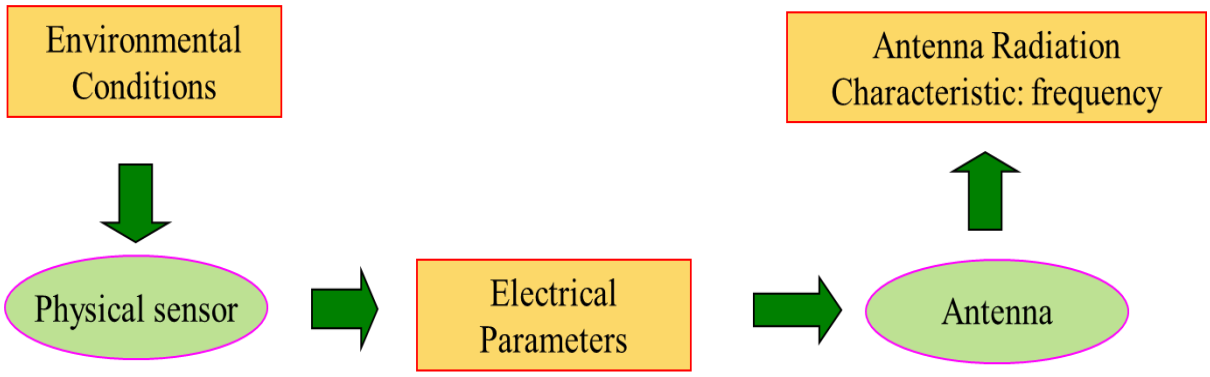

Fig. 2-3 Flow chart of the RSA operation principle.

2.3 Radio Frequency Identification Technology

During the RSA designing procedure, the knowledge of RFID technique is necessary and helpful. The following are the descriptions of RFID including its components, RFID tag, and RFID sensor tag. The relation between RFID sensor tags and RSAs are also demonstrated.

2.3.1 Introduction of RFID Technology and RFID Components

Radio frequency identification (RFID) is the use of radio communications to identify a physical object. The RFID system is composed of a reader which is also called an interrogator, and a tag (transponder). The reader usually radiates the interrogating EM wave to detect whether the tags are in the areas where its signal can cover. The tags, in most cases, a simple dipole antenna with an IC chip are attached to the object which needs to be identified. The unique ID information is stored in the IC. When the tag receives the incoming EM wave from reader, it will backscatter the EM wave under the modulation of IC. Thus, the backscattered EM wave including the ID

information of the tag can be recognized by the reader. Fig. 2-4 shows the basic scheme of a RFID system.

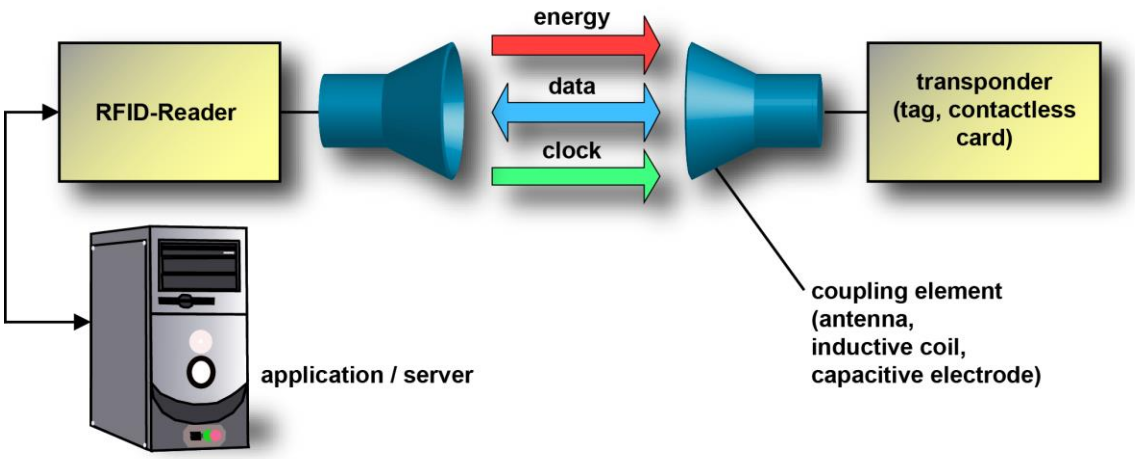

Fig. 2-4 Basic scheme of a RFID system [22].

The RFID can be classified into different types according to the power supply method it select, or the different frequency band it use. The RFID tag can be passive, semi-passive, and active. A passive tag has no battery to drive the circuitry in the tag and has no radio transmitter of its own [21]. Passive tag depends on rectification the received power from the reader to support operation of their circuitry, and modulate their ID information on the backscattered wave to the reader. So it is simple and cheap. A semi-passive tag has a small battery to power the tag circuitry. However, it still uses the backscattered communication for the tag-to-reader communications. An active tag has its own battery and periodically transmits its ID signal. It is reconfigured as a traditional bidirectional radio communication device. According to its operation frequencies, the

RFID can be classified into high frequency (HF), ultra high frequency (UHF) and microwave (MW) which are shown in Fig. 2-.

The most commonly used frequency bands are the 125/134 KHz, 860-960 MHz, and 2.4-2.5GHz, which are corresponding to LF, UHF and MW band. Readers and tags in the 900MHz region are referred to UHF band readers and tags. In different frequency bands, the methods used to transfer energy from reader to tag are different. In the LF and HF band, readers and tags use the inductive coupling. Both the UHF and MW band systems use the radiative coupling. The inductive coupling denotes the operating wavelength is much larger than the antenna. This means the inductive coupling takes place in the near field region of the reader antenna. The radio frequency field created may be treated as a simple alternating magnetic field. The radiative coupling is the systems where the antenna size is comparable to the wavelength. In different operating band, the RFID tags also have different configurations. Fig. 2- shows examples of tag antennas designed for different operating frequencies.

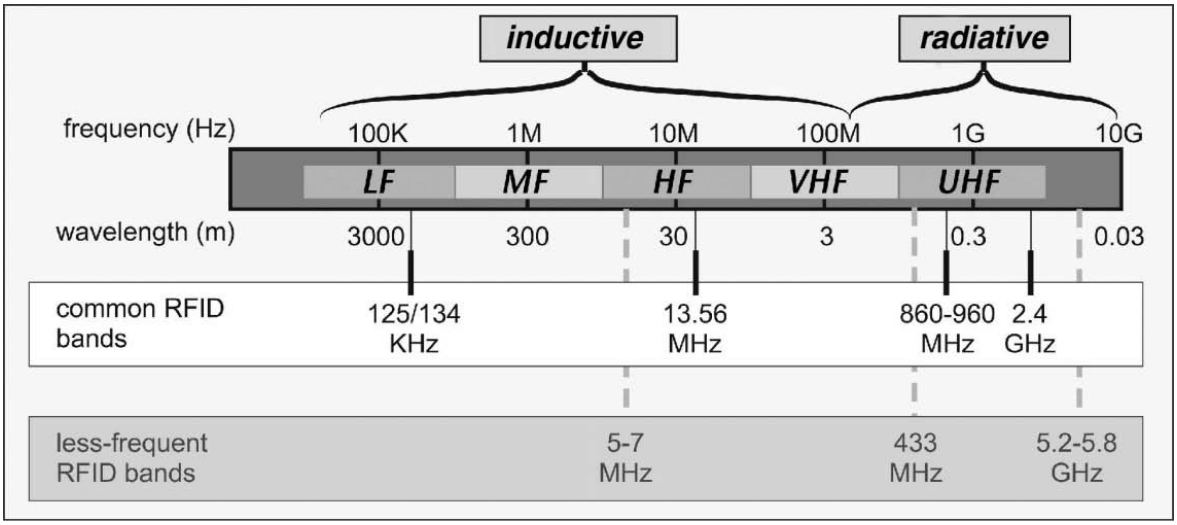

Fig. 2-5 RFID frequency bands [21].

The amount of information you can send over a link is constrained by the amount of bandwidth you have available. Based on this principle, the speed of data transfer in LF band is the slowest. In most cases, it just sends binary "0" and "1" symbols. The UHF tags can operate at a much higher speeds. In the United States, a UHF tag can send data to a reader at hundreds of kilobit per second (kbps). The different characteristics associated with each frequency band mean that the optimal applications are different for each band. Table 2-1 is a summary of the RFID characteristics in each band. The read range mentioned in the Table 2-1 for the UHF band is determined by the Friss formula. For the reader side, the equivalent isotropic radiated power (EIRP) is already defined by the speculations. And for the tag side, since in most cases, dipole antenna is selected as the tag antenna, so its gain is also determined. So the read range of the UHF band RFID system is several meters. Comparing with the LF and HF, this longer read range really benefits the

UHF band system. According to Table 2-1, because of its low cost, long read range, and high data rates, the passive UHF band RFID are of great interests of researchers. Since tags have individual serial numbers, the RFID system design can discriminate several tags within the range of the RFID reader simultaneously.

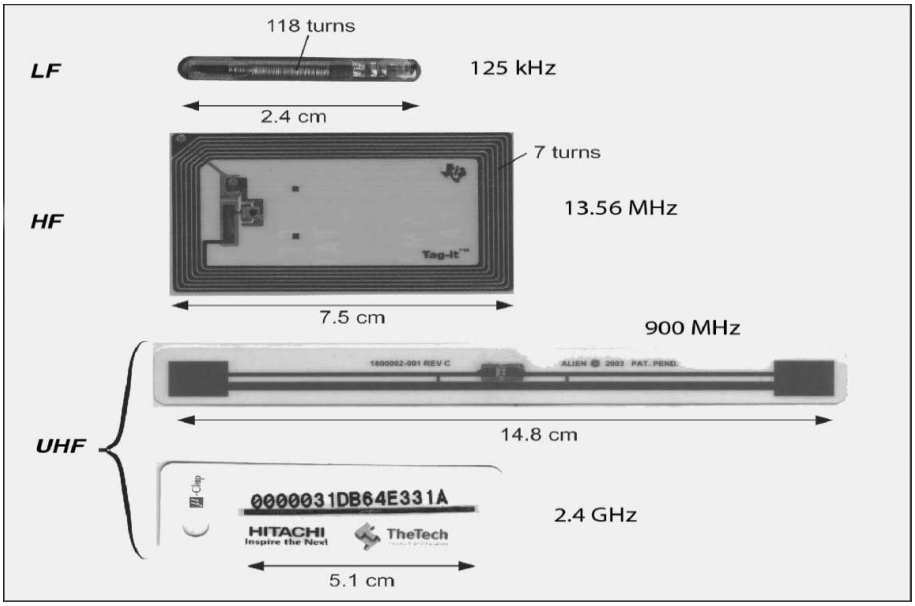

Fig. 2-6 RFID tag antenna configurations of different frequency bands [21].

2.3.2 Introduction of UHF RFID Sensor Tag

A RFID system uses tags attached to objects to be identified. According to their power source, the tags can be classified in to passive, semi-passive, and active tags. Among these, the passive tags are the most simple and low cost ones without batteries and transmitters. Thus, they are popular in the economic deployment of RFID systems. On the other hand, the RFID tags can also be classified by the working frequencies, such as LF, HF, UHF, and MW. As mentioned

before, the UHF tags have a longer reader range, faster data rates, so they have attracted a lot of interests. An electronic product code (EPC) global standard is established for them. Their application areas include items tracking, supply chain, etc. The RFID tags contain at least two parts: an integrated circuit (IC), which is used to store its information and modulate it on the backscatter wave; an antenna, which is used to receive the incoming wave from reader. The information stored in the IC chip maybe a unique tag serial number, or may be product-related information such as a stock number, lot, or batch number, production date, or other specific information.

Table 2-1 Summary of RFID characteristics

Frequency	Communication method	Read range	Applications	benefits	drawbacks
12.5/13.4 KHz (LF)	inductive coupling	<0.5m	animal ID access control product authentication	Works well around metal and water products.	Short read range and slower read rates
13.56MHz (HF)	inductive coupling	<1m	smart card library book	Low cost	Higher read rates than LF
860-960 MHz (UHF)	raidiative coupling	3m	supply chain baggage tracking electronic toll access	EPC standard build	not work well around items with

					water and metal
2.4GHz (MW)	Radiative coupling	1m	airline baggage electronic toll collection	most expensive	fastest read rates

Now we are thinking, can we transfer more information through the tag response besides the above mentioned? For example, the surrounding environments like temperature, humidity, fire, gas, motion. In the state of art, it is impossible to integrate the sensor element in the RFID IC chip. However, we can use another way to transfer the surrounding information by the RFID tag. That is using sensing element in the tag design. The tags with the capability of sensing environment are called sensor tags. According to their sensing targets, the sensor tags can be classified into temperature sensing tag [23], humidity sensing tag [16], gas sensing tag [18], motion sensing tag [19], etc. The sensor element can be either lumped such as thermistor, or distributed such as Kapton, SWCNT. Fig. 2- shows an example of UHF temperature sensor tag using thermistor. We can see a complex circuit is designed to implement the thermistor. This sensor tag can provide a high sensitivity of 0.1°C from 35°C to 45°C; however the read range is only around 1m due to the high power consumption of the circuitry. Fig. 2- shows a humidity sensor tag of using Kapton as sensing material. The Kapton is used as substrate of a capacitively-loaded dipole. The dielectric constant of the Kapton material depends on the humidity level. As the humidity changes, the substrate dielectric constant also changes, which alters the resonant frequency of the sensor tag accordingly. All of the designs in Fig. 2- and Fig. 2- are passive. Besides passive sensor tags, there

are also active ones. The active sensor tags have longer working distance and high sensitivity, and of course, are high cost.

2.3.3 Relation between RSAs and RFID Sensor Tags

Reconfigurable sensing antennas (RSAs) and RFID sensor tags both can sense the surrounding environment through the EM wave transmission. Integrated with IC chips, the RSAs can also realize wireless identification. Although RSAs and sensor tags have common points, they are different from each other in some aspects. As shown in Fig. 2-, a classic RSA is composed of a physical sensor, a load, and an antenna. There is no battery in the RSA. However, for the sensor tags, there are passive sensor tags and active sensor tags. In this case, RSAs are similar to the passive sensor tags. Another difference is IC chip. The IC chip is necessary in the sensor tags, because identification is the basic function of tags. However, ICs are not the essential element in RSAs. Although in this dissertation, we use IC integrated in the RSA to make it possess more functionality, the RSA basically can be in other types. For example, we can use RCS of RSA to transfer environmental information. In this case, no battery and no IC are needed. Meanwhile, for the sensor tag designs, as shown in Fig. 2-, they can use a complex circuit integrating sensor element to realize environment sensing. However, in the RSAs, only simple physical sensors are employed. Additionally, in most sensor tags, antenna is not a big concern, they always use dipole antenna because it is simple and easy to fabricate. However, in the RSAs, we pay more attention to the antenna designs, and select suitable antenna configurations to increase the RSAs working

distance and to improve their sensitivity. The RSA research needs the knowledge of antenna, RFID, and sensor materials, and their relation is illustrated in Fig. 2-.

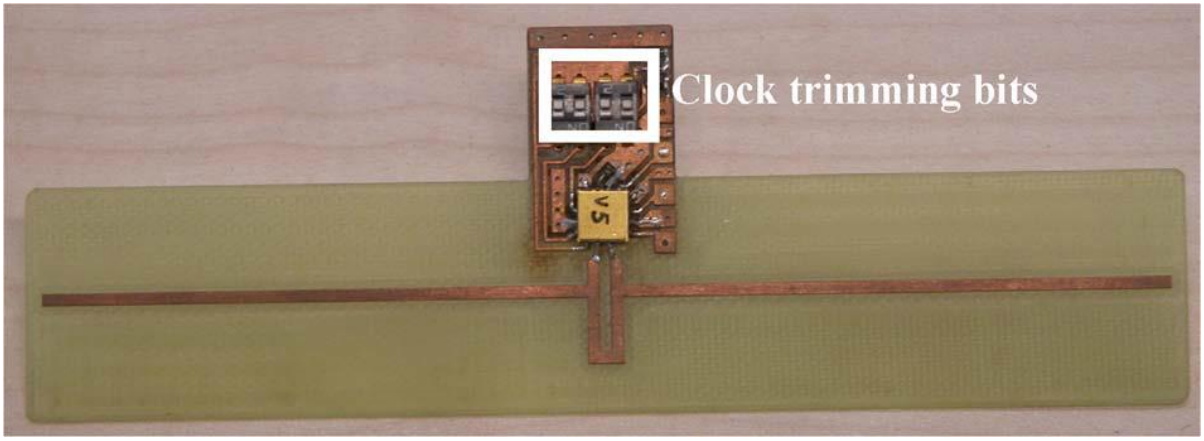

Fig. 2-7 The prototype of a sensor tag using complicate circuit [23].

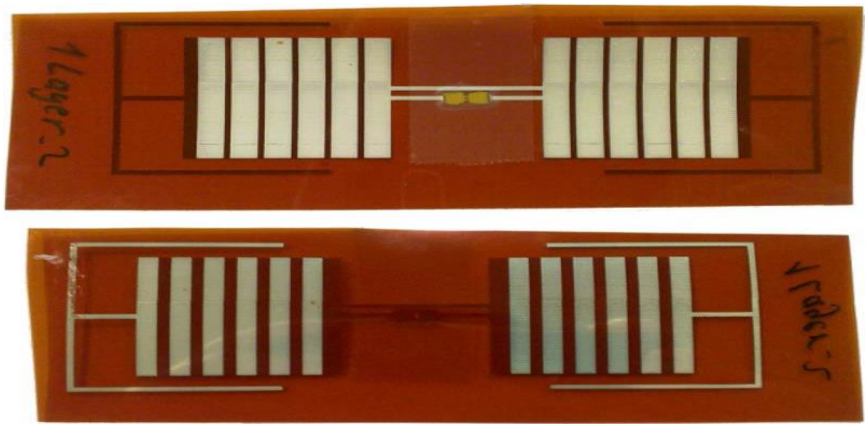

Fig. 2-8 The prototype of a sensor tag using Kapton as substrate [17].

In one word, RSA is a simple passive device using a physical sensor to realize the wireless environmental sensing. The purpose of RSA designs is to use the simplest method to obtain the maximum sensitivity. The main concerns of RSA designs are described as follows:

- How to select the sensing mechanism
- How to integrate the sensing mechanism in the RSA design
- How to improve sensitivity without sacrificing working distance and increasing cost.

For the RSA sensitivity, more details will be found in the following section.

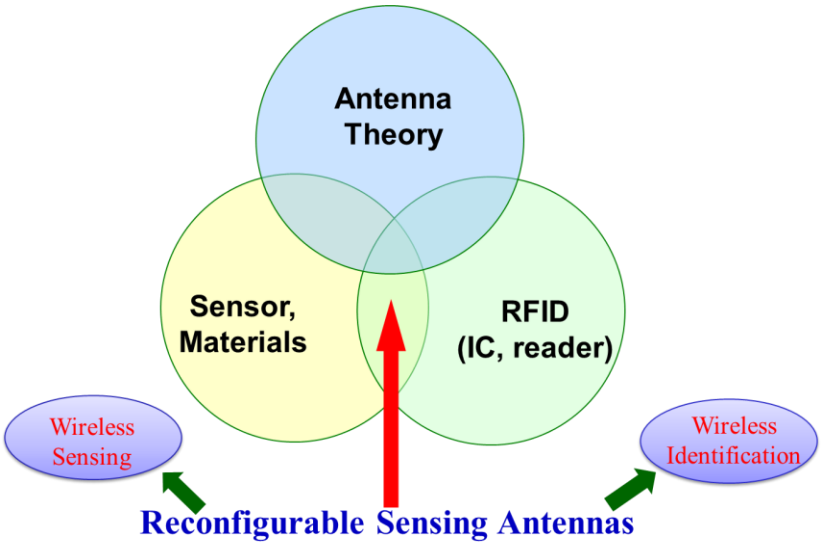

Fig. 2-9 RSA, a multidisciplinary topic.

2.4 Key Parameters to Evaluate RSA Sensitivity

For a sensing antenna, sensitivity is a crucial factor to evaluate the performance of RSAs. In this dissertation, all the temperature sensing RSA designs are frequency reconfigurable RSAs, which means the resonant frequency of the RSA is controlled by temperature. Thus, by distinguishing the resonant frequency, the temperature information is obtained. In this case, the resonant frequency shift with temperature ($\Delta f/\Delta T$) becomes an import parameter to determine the RSA sensitivity. For a good sensitivity, the much frequency shift with temperature is preferred.

For example, the RSA with 10MHz/°C is obviously more sensitive than the one with 1MHz/°C, because the temperature has a much effectively impact on its characteristics.

As mentioned above, $\Delta f/\Delta T$ is a parameter used to evaluate the RSA sensitivity. In order to get the resonant frequency at different temperatures, one needs to easily figure out the resonant frequency. Thus, the second parameter related to the RSA sensitivity is emerging, which is the antenna bandwidth. Usually, it is easy to find out the resonant frequency of the antenna with narrow bandwidth, which can be observed from Fig. 2-. In this figure, the broadside realized gains of two RSAs with different bandwidth under various temperatures are depicted. It is clear that the resonant frequency of the RSA with narrow bandwidth is easy to find out. Therefore, bandwidth becomes another factor which can determine the RSA sensitivity. On the other hand, bandwidth is directly related to the Q value of antenna. Approximately, it is inversely proportional to the antenna Q value. In order to get a narrow bandwidth, the antenna should have high-Q. Designing high-Q antenna is one objective in this dissertation, which meets the special requirements of sensing antenna.

The RSAs work in far field to monitor environmental parameters. According to the Friis formula, the working distances of the RSAs are mainly determined by the antenna gains. And a long working range is a merit of the RSAs. Hence, antenna gain is also used to determine RSA sensitivity. The antenna gain is directly determined by the antenna directivity and loss, where loss includes dielectric loss and conductor loss. In order to obtain high gain, there are two ways. One is to increase the antenna directivity, and the other is to reduce the antenna loss. The antenna directivity is determined by the antenna aperture size and other parameters. For example, the

directivity of patch antenna is also related to its ground size. Apparently, there would be compromise between antenna gain and antenna size. An optimum design should consider both gain and size.

As a summary of above information, there are totally three parameters used to determine the sensitivity of frequency reconfigurable RSAs, which are Δf/ΔT, bandwidth, and antenna gain. To obtain a high sensitivity, the RSA should have high gain, large Δf/ ΔT, and narrow bandwidth. Improving sensitivity is the guideline of the RSA designs through this dissertation.

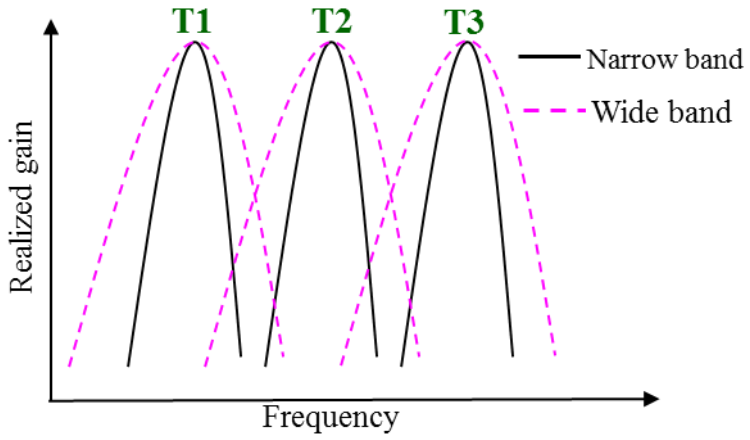

Fig. 2-10 An illustrative figure showing the relation between bandwidth and sensitivity.

CHAPTER III

RSA USING ELECTRICAL PROPERTIES OF MATERIALS: WATER EMBEDDED RSA

In conventional antenna designs, radiation characteristics, such as input impedance, and radiation patterns, are fixed. In recent years, reconfigurable antennas have attracted increasing attentions, because their radiation characteristics can be reconfigured by integrating the control electronics such as pin diodes, varactors, and MEMS switches in the antenna [6], [7], [9]. This chapter proposes a reconfigurable sensing antenna design, where water is used as the control unit instead of conventional active electronics. In this design, the function of the antenna is not only to transmit and receive electromagnetic waves, but also to sense the variation of surrounding temperature. Selecting water as sensing material is due to the variation of its dielectric constant with temperature. In the design, water is integrated in the substrate of a patch antenna. The resonance frequency of patch antenna is inversely proportional to its substrate dielectric constant. Thus, as temperature varies, the changes of water's dielectric constant will alter the resonant frequency of antenna accordingly. The temperature information can then be determined by checking the resonant frequency of the antenna. Integrating the sensing material in the antenna is an easy way to monitor the temperature instead of using complicate sensing circuit. Beginning with the water characteristics analysis, a slotted patch RSA with water embedded is then designed, analyzed and fabricated. It has a 4MH/10°C frequency shift with approximately 4.5m read range. To increase

the water embedded RSA sensitivity, the substrate material, substrate thickness, water thickness, and water location are analyzed. Finally, a compromise design is obtained with an improved sensitivity in terms of antenna gain and bandwidth.

3.1 Water Embedded Slotted RSA Design

3.1.1 Water Characteristics

Water covers 71% of the earth's surface, and it is vital for all known forms of life. Water is a safe and cheap liquid material. It is found that water's dielectric constant is related to temperature, and measurements are conducted to confirm this relationship. Fig. 3-1 shows the measured complex permittivity of water versus temperature at 900MHz [24]. It is observed that as temperature increases, real part of water decreases. Also the imaginary part of permittivity decreases with the increase of temperature. The dielectric constant is about 88 at 0°C and becomes 67 at 60°C. The temperature has an effective impact on the dielectric constant of water. Hence, water can be selected as temperature sensing material. It also has other advantages such as low cost, and environmental safe. Properly placement of water in the RSA design can effectively reconfigure the resonant frequency of the antenna.

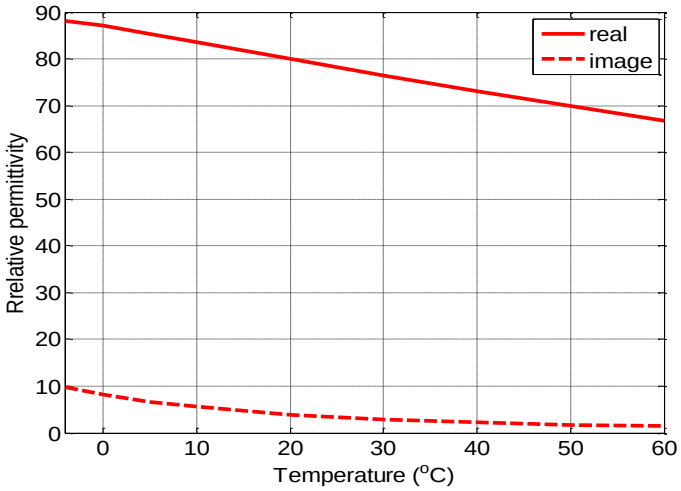

Fig. 3-1 The complex permittivity of distilled water at 900MHz.

3.1.2 Water Embedded Patch RSA Geometry

In this section, a slotted patch antenna is designed. Distilled water is used as a distributed temperature sensor, and a commercial Alien Higgs-2 chip is used as the IC attached to the RSA. The antenna geometry is shown in Fig. 3-2, which consists of three layers: two FR4 layers to support the metal ground and patch, and a middle Duroid/5880 layer with a center square cavity to contain water. A patch antenna is selected in this design because of its low cost and ease of fabrication. Furthermore, the narrow antenna bandwidth, which is usually disadvantageous in many communication systems, is actually an advantage in the RSA design because it increases the frequency sensitivity to the environment. In addition, the ground plane helps to minimize the effect of the platform where the antenna is installed. Thus, this design can also work on metallic objects. In addition to a conventional probe feed that needs to drill a hole in the substrate or a microstrip

line feed that needs an extra feed line, a slot feed is adopted in the proposed design and a *Higgs-2* IC chip is easily mounted in the middle of the slot.

The antenna dimensions are initially designed using Ansoft HFSS [25] and then optimized using the in-house FDTD program to make it resonate at 900MHz at 20^{o} C [26]. The thicknesses of the FR4 and Duriod/5880 substrates are 1.6mm and 3.2mm, respectively. The overall ground plane size is 100×100 mm^2, and the patch size is 38×38 mm^2. The size of the water pocket is 40×40 mm^2. The slot length is 12mm and slot width is 11.5mm. From Fig. 3.1 we can obtain that the dielectric constant and loss tangent of water as 80 and 0.05, respectively.

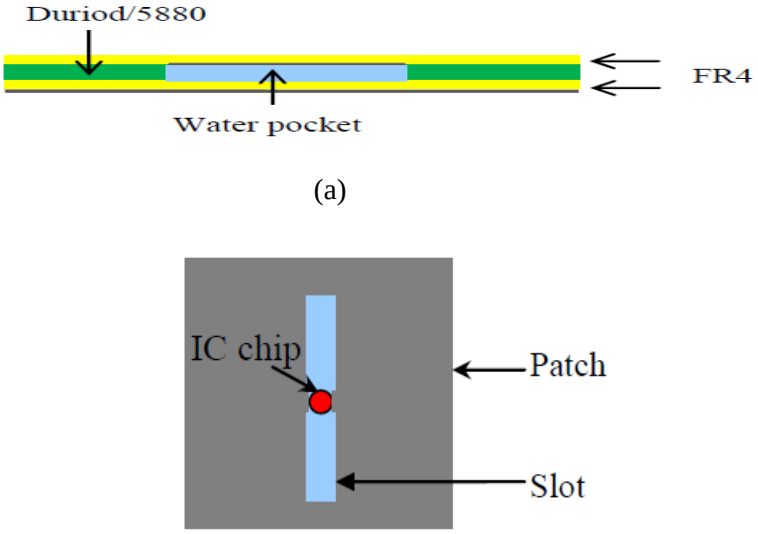

Fig. 3-2 Configuration of a slotted patch RSA design: (a) side view, (b) top view.

3.1.3 Temperature Sensitivity Analysis

Sensitivity is a crucial factor in RSA designs. In this dissertation, three parameters are used to evaluate the sensitivity of temperature-monitoring RSA, including the frequency shift per temperature change ($\Delta f/\Delta T$), the antenna bandwidth, and the antenna gain. A high sensitive RSA should have a larger $\Delta f/\Delta T$, a narrower bandwidth, and a higher gain. For the water RSA design, its sensitivity is mainly determined by the water performance and the method used to integrate it in the antenna.

Table 3-1 shows the detailed information about the water's dielectric constant and loss tangent at different values of temperature. Based on this information, one can establish a relation between the RSA characteristics and temperature. The simulated reflection coefficient (S_{11}) of the RSA is shown in Fig. 3-3. As the temperature increases, the dielectric constant of water decreases and the antenna resonant frequency increases. The realized gain (RG) of the RSA is shown in Fig. 3-4. It is illustrated that as temperature increases, the maximum realized gain of the RSA also increases. This is because the loss tangent of water decreases and also the reflection coefficient improves as temperature increases. The detailed information of the water embedded RSA are also included in Table 3-1. It is observed that the frequency shift with temperature is about 4MHz/10^{o} C with a -3.2dB realized gain at 20^{o} C.

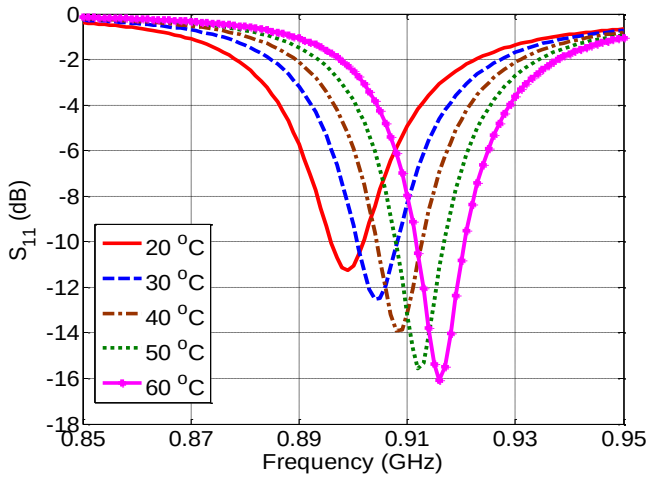

Fig. 3-3 Simulated S_{11} of the water RSA under various temperatures.

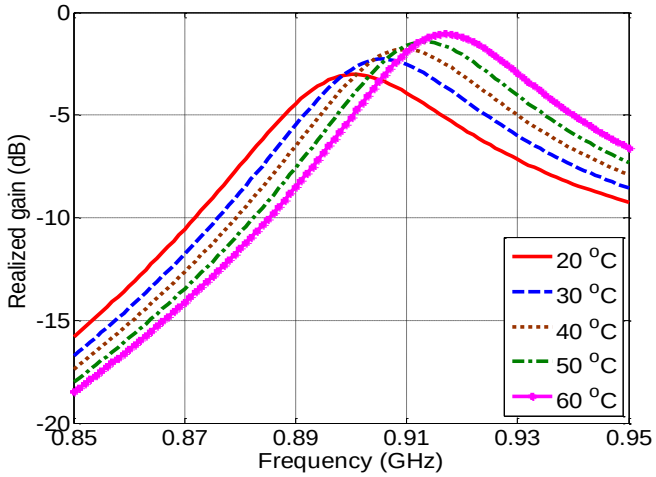

Fig. 3-4 Simulated realized gain (RG) of the water RSA under various temperatures.

Table 3-1 Detailed information of water and the water embedded RSA

Temperature (ºC)	20	30	40	50	60
Dielectric constant	80	76.44	73.1	69.84	66.67
Loss tangent (tanδ)	0.05	0.038	0.031	0.025	0.021
Resonant freq. (MHz)	899	904	908	912	916

Realized gain (dB)	-3.2	-2.31	-1.84	-1.46	-1.05

3.2 Fabrication and Measurements

3.2.1 Measurement Facility and Methods

The tagformance system, a product of Voyantic Company in Finland, is a complete RFID measurement solution for evaluating the functionality and performance of EPC Class1 Gen2 RFID system [27]. The Tagformance system consists of Tagformance lite measurement device, one software package, and accessories that complete the system. A Tagformance system is shown in Fig. 3-5. It is clearly that the system is composed of hardware part, software part, and accessory part. The measurement device is the hardware part which has a standard frequency sweep from 800MHz to 1000MHz. Its output power is from 0 to 27dBm with the receiver sensitivity as low as -70dBm. On the other hand, the software installed in a computer has the functionalities of measuring different parameters including: threshold transmitted power to active tag, backscatter power from tag, orientation sensitivity of tag, etc. The threshold power measurement is to measure the minimum transmitted power used to active the tag and gets correct tag response at selected frequency point. It can measure the threshold power during a specified frequency range. The backscatter measurement is a measure of tag's response signal strength at specified frequency points. The measurements that we mostly use are the threshold transmitted power measurement and backscatter measurement. Based on the threshold transmitted power measurement, one can obtain the theoretical read range, power on tag, etc. A reader antenna is also found in the Fig. 3-5,

which is connected to the measurement suit and used to transmit and receive electromagnetic waves.

The whole measurement procedure is that the reader antenna connecting to the measurement device firstly sends out the interrogating wave. The tag antenna with the IC chip receives the incoming wave, and backscatters it with the modulation of chip information. These backscattered signals are received by the reader side and processed through the software. Fig. 3-6 shows the figure of the theoretical read ranges of different tags. The read ranges are post-processed results based on the measured threshold transmitted power by the software. The equation used to calculate the read range is shown in the (3-2), which is obtained from Friis formula [1]. The read range is about the reader-to-tag distance. Because the reader has a very high sensitivity of -70dBm, thus the read range is mainly limited by the tag side including its chip sensitivity and antenna gain.

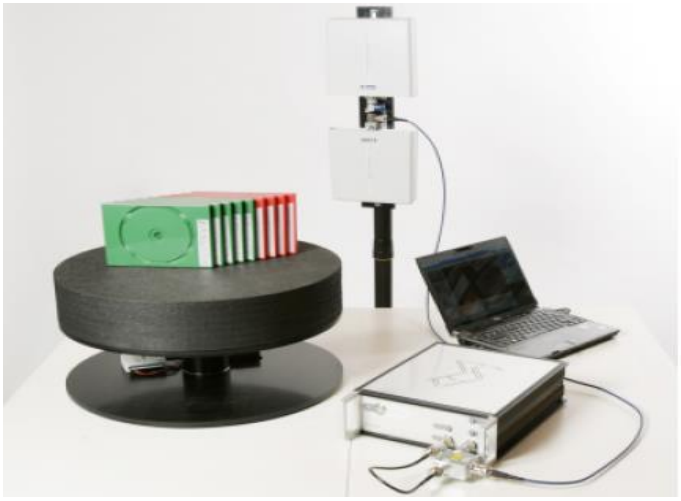

Fig. 3-5 The Tagformance system.

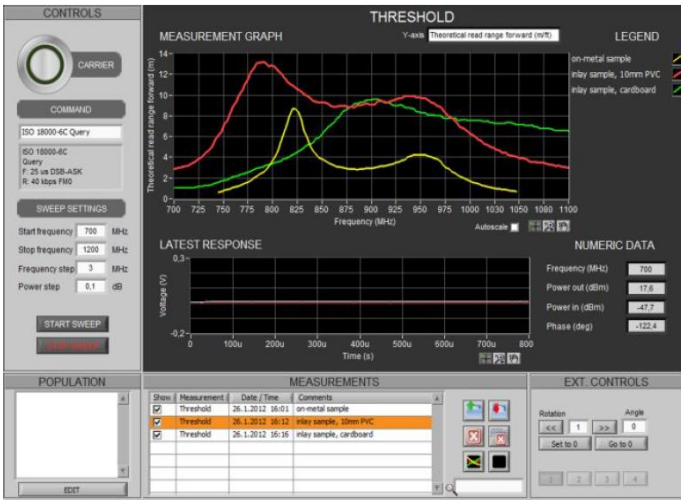

Fig. 3-6 The interface of measuring theoretical read range using the software.

3.2.2 Fabrication and Measurement

An antenna prototype is fabricated and tested. Fig. 3-7 shows the three layers of the proposed RSA. In the figure, from left to right are the Duriod/5880 with cavity for water, top FR4 substrate with an IC attached to the slotted patch, and bottom FR4 with ground. Fig. 3-8 is the photo of the final RSA prototype.

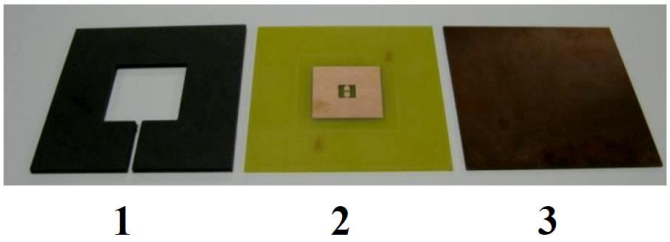

Fig. 3-7 Three layers of the proposed water RSA.

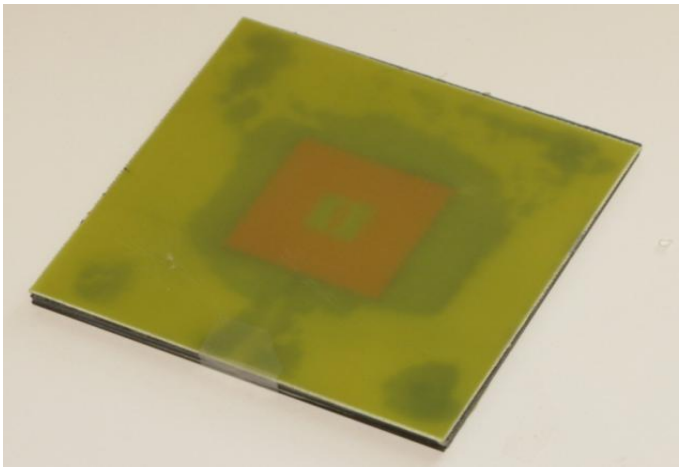

Fig. 3-8 Final prototype of the proposed water RSA.

The measurement of the RSA is conducted in an anechoic chamber, as shown in Fig. 3-9. The RSA is placed inside an empty plastic container and is attached to its back wall. The reason for doing this is to limit the airflow and control the temperature around RSA. The ambient temperature is held stable by using a heater and an air cooler simultaneously. The measurements were performed with the Tagformance device that can read both the IC information and the transmit/receive power levels.

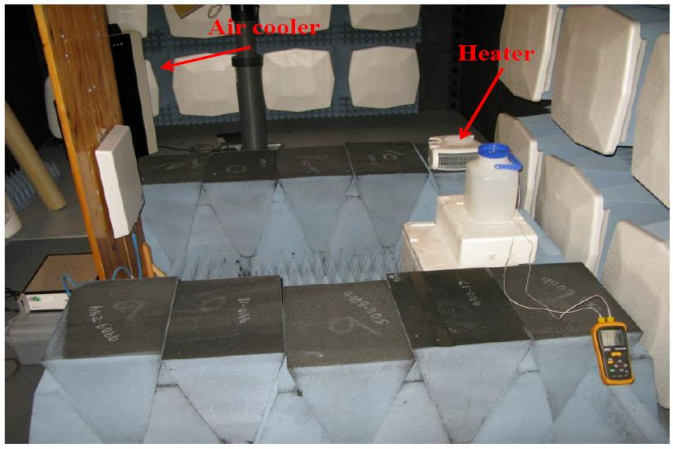

Fig. 3-9 Measurement setup for the proposed water RSA prototype.

The minimum transmitted power (P_{TS}) that can activate the RSA is measured. It is the threshold power used to active the RSA IC chip and makes it work correctly. The relation between the minimum transmitted power and the threshold IC received power (P_{IC}) is given in (3-1):

$$P_{IC} = L_{fwd} P_{TS} G_{RSA} \tag{3-1}$$

Here L_{fwd} is the measured path-loss between the TX-port and the tag, which includes the cable loss, reader antenna gain, and free space loss. The G_{RSA} is the temperature-dependent realized gain of the RSA antenna. The maximum read range (d_{RSA}) of the RSA can be determined based on Friss formula as given in (3-2):

$$d_{RSA} = \frac{l}{4\rho}\sqrt{\frac{EIRP}{P_{IC}/G_{RSA}}} = \frac{l}{4\rho}\sqrt{\frac{EIRP}{P_{TS} L_{fwd}}} \tag{3-2}$$

The equivalent isotropic radiated power is 3.28W [28]. The (3-2) shows the methods of calculating the read range based on simulation results and measurement results. The P_{IC} of a Higgs 2 chip is -14dBm, which is known from the company datasheet [29]. And from the HFSS simulation, we

can obtain the realized gain of the RSA. So according the above equation (3-2), we can calculate the maximum simulated read range based on the known P_{IC} and G_{RSA}. About the measured read range, EIRP is known from the hardware speculation, and the Tagformance system can measure the threshold transmitted power to active the RSA and path loss, thus the software can easily provide the measured read range by post-processing.

3.2.3 Results Analysis

Fig. 3-10 compares the simulation and measurement read ranges. Simulated results are obtained by substituting P_{IC} (-14 dBm) and simulated realized gain (G_{RSA}) into (3-2), while the measured results are obtained by measuring P_{TS} and L_{fwd} and substituting in the equation as shown (3-2). It is shown in Fig. 3-10 that the measured and simulated read ranges are generated during a frequency range from 900MHz to 970MHz. The RSA sensitivity is determined by the $\Delta f/\Delta T$. In order to figure out the resonant frequency shift with temperature variation, we need first determine the resonant frequency of the RSA under different temperatures. At the resonant frequency, the RSA possess almost the maximum realized gain, hence, the minimum power is required to active the RSA IC from the reader side. And according to (3-2), the maximum read range is obtained. So the resonant frequency is the frequency point where the longest read range is achieved.

It is observed from Fig. 3-10 that as the temperature increases, both the antenna resonant frequency and read range increase. It is worthwhile to point out that the resonant frequency in

measurement is higher than those in Fig. 3-3 at comparable temperatures, because the water layer in the RSA prototype is slightly thinner than the designed value.

Fig. 3-11 is the sensitivity curve of the temperature sensor. A 2nd order polynomial function is used to describe the dependency between the temperature and resonant frequency:

$$f(\mathrm{MHz}) = C_2 T^2 + C_1 T + C_0 \tag{3-3}$$

Here, T is the ambient temperature in Celsius degrees, and the coefficients (C_2, C_1, C_0) = (0.0049, -0.0259, 924.8424). The average error between the measurement and empirical (3-3) is 0.025MHz.

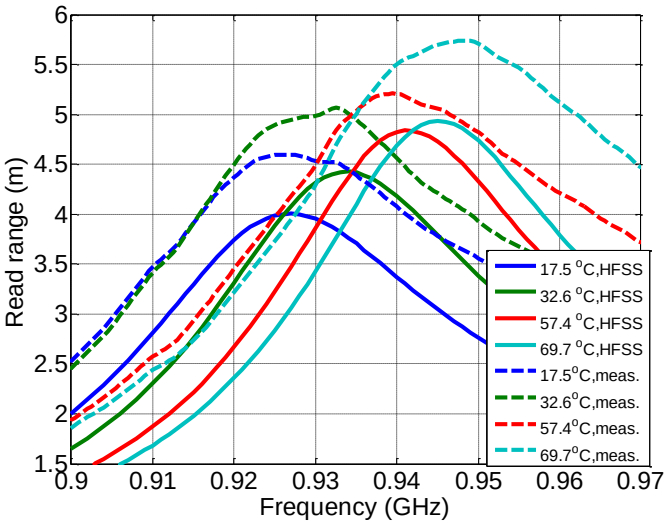

Fig. 3-10 Read range comparison of the water RSA under different temperatures, where the water layer thickness is set to 3.165mm in the simulation.

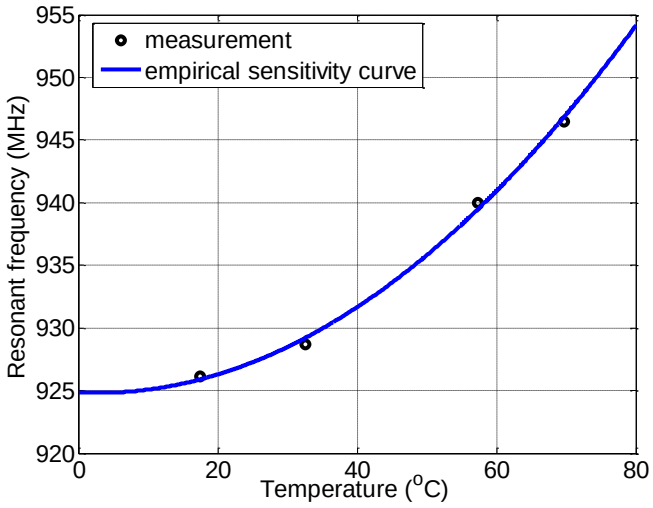

Fig. 3-11 An empirical temperature sensitivity curve based on the measured data.

3.3 Sensitivity Improvement Study

As mentioned before, for the frequency reconfigurable RSA designs, the narrower the bandwidth, the easier to distinguish the frequency, and the better the sensitivity. It is noticed from Fig. 3-4 that the water RSA's 3dB realized gain bandwidth is as wide as 4.33%. This wide bandwidth does degrade the RSA sensitivity. Meanwhile, the maximum realized gain value is around -3dB, which also limits the RSA sensitivity. So the following studies are towards the purpose of reducing the water RSA bandwidth and improving the antenna gain. The tunable parameters include the substrate thickness, substrate material, water thickness, and water pocket configuration.

3.3.1 Substrate Thickness and Material Study

In this part, the impacts of substrate thickness and substrate material on RSA performance are investigated. Fig. 3-12 shows the configuration of the new RSA structure with a thinner FR4 layer. The thickness of FR4 is decreased from the original 1.6mm to 0.8mm, and other parts of the design are the same as shown in Fig. 3-2 except the patch side length. In the original one, the patch length is 40mm. Now in order to keep the 900MHz resonant frequency, the patch size is decreased to 33.7mm. The simulated S_{11} and realized gain comparison are shown in Fig. 3-13 and Fig. 3-14, respectively.

As we can see from the Fig. 3-13, decreasing the FR4 thickness has a slight impact on the S_{11} performance. The two curves almost cover each other. However, from Fig. 3-14, it is observed that the gain, realized gain, and realized gain bandwidth between the original one and the new one with thinner FR4 layer have bigger differences. The detailed comparison information is shown in Table 3-2.

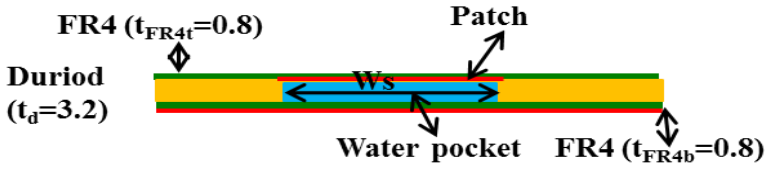

Fig. 3-12 The water RSA design with thinner substrate.

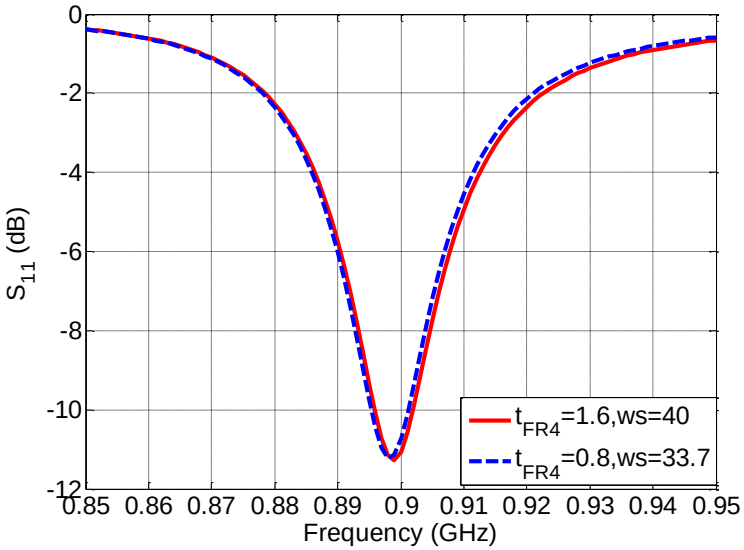

Fig. 3-13 S_{11} comparison of the water RSAs using different substrate thickness.

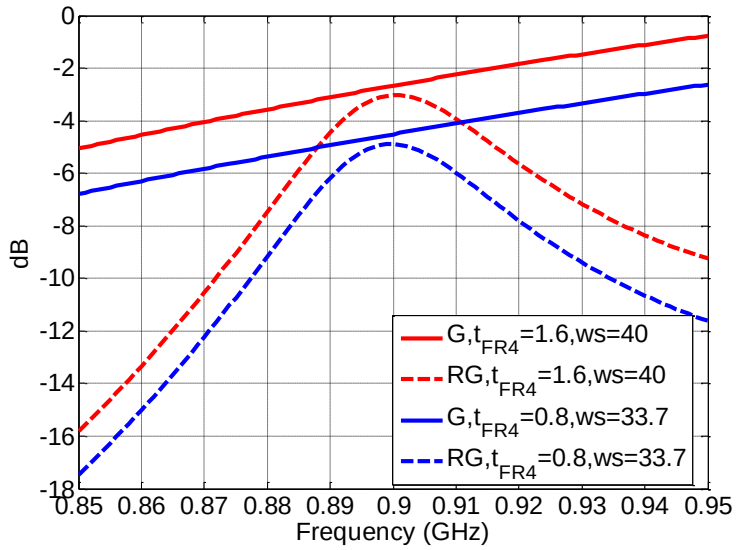

Fig. 3-14 Gain and realized gain comparison of the water RSAs using different substrate thicknesses.

Table 3-2 Gain and bandwidth comparison for the RSAs with different FR4 thickness

t_{FR4}	patch length	gain	realized gain bandwidth

1.6mm	40mm	-3dB	4.33%
0.8mm	33.7mm	-5dB	4.12%

According to the information in Table 3-2, decreasing the substrate thickness will make the bandwidth a little narrower; however, the antenna gain drops a lot. The low gain of the thin substrate RSA is caused by two reasons: one is the radiation characteristics of the patch itself. The radiation of patch is mainly due to two parallel magnetic slots formed by the patch edges and the ground. The substrate thickness is actually the slot width. Thus, the thinner the substrate, the less the energy is radiated which results in a lower gain. The other reason is that as we reduce the patch size to maintain the resonant frequency, the aperture size becomes smaller which will results in a lower gain. So the method of decreasing substrate thickness to enhance the RSA sensitivity should be used carefully.

After the investigation of substrate thickness, the impacts of substrate material on RSA performance are studied. Fig. 3-15 shows the antenna with different substrate materials. The original Duriod/5880 is replaced with FR4, RO3006, and RO2310, respectively. The characteristics of these materials are shown in Table 3-3. The patch size is the same for all designs.

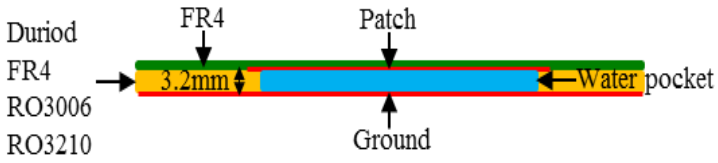

Fig. 3-15 The water RSA design with various supporting substrate material.

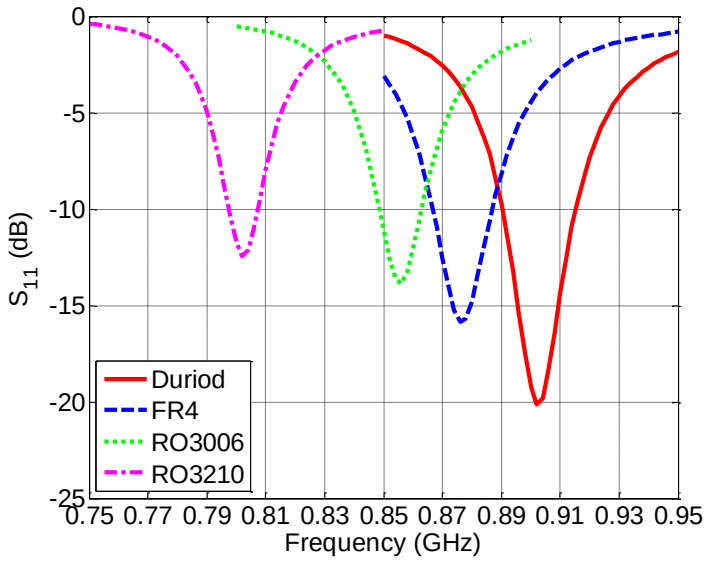

Fig. 3-16 S_{11} comparison of the water RSAs using different substrate materials.

The simulated S_{11} of the RSA with different substrate materials are shown in Fig. 3-16. It is noticed that the resonant frequency of the RSA decreases effectively as its substrate dielectric constant increases. This conforms to the characteristics of patch antenna. Fig. 3-17 shows their realized gain comparison. We can see that the RSA's realized gain increases as the dielectric constant of the substrate increases. This is because, the higher the dielectric constant of substrate, the less the E field constrained in the water which has a much higher loss. As a result, when the substrate is high dielectric constant material, the smaller the loss in total, and thus the higher the realized gain. Meanwhile, the realized gain bandwidth becomes narrower as the substrate permittivity increases. The realized gain bandwidth is also shown in Table 3-3. It is observed that the influence of the dielectric constant on the antenna bandwidth is much effective than that of the substrate thickness.

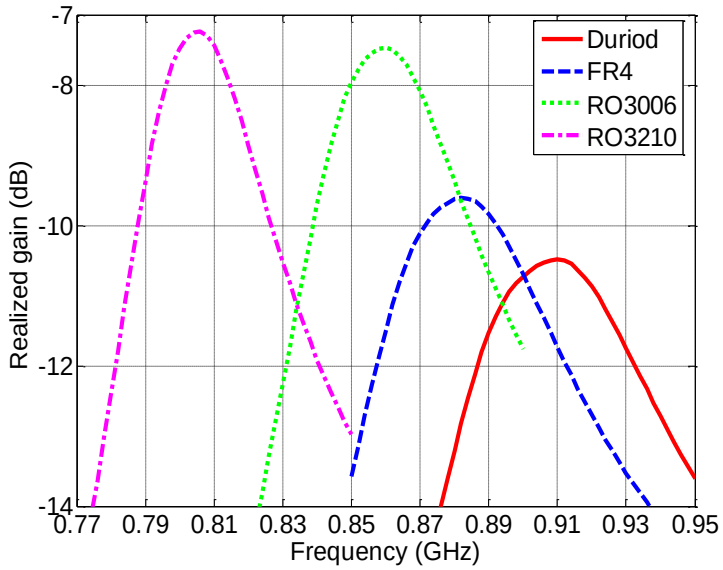

Fig. 3-17 Realized gain comparison using different substrate materials.

Table 3-3 Material information and realized gain bandwidth comparison

Material	Duriod/5880	FR4	RO3006	RO3210
Dielectric constant	2.2	4.4	6.5	10.2
Loss tangent	0.0009	0.02	0.0025	0.003
Realized gain bandwidth	7.69%	7.5%	6.05%	5.21%

3.3.2 Water Thickness and Location Study

As mentioned before, selecting the substrate material with thin thickness and high dielectric constant in the water RSA design can reduce the RSA's bandwidth; however the antenna gain is sacrificed. In this section, the impact of water thickness and location on the RSA sensitivity is investigated. Fig. 3-18 shows the RSA configuration with a 1.6mm water thickness, which is

thinner as compared with the 3.2mm of the original design. The total substrate thickness is the same as the original one, which is also 4.8mm. In order to effectively reduce the RSA bandwidth, RO3210 is selected as the substrate material. And to maintain the 900MHz resonant frequency, the patch's length is set to 36.5mm rather than the original 40mm.

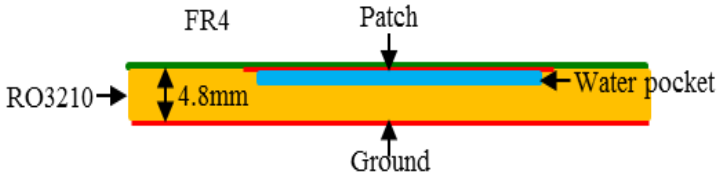

Fig. 3-18 The RSA design with thinner water thickness.

Fig. 3-19 shows the simulated S_{11} and realized gain under various temperatures. It is found that the $\Delta f/\Delta T$ is only 2MHz/10°C in this case. This is due to less water used in the substrate. More specifically, the frequency shift of the design is mainly determined by the water, since its dielectric constant is temperature dependent. The less the water used, the poor the RSA sensitivity. On the other hand, water is a high loss material with pretty high permittivity. All of these features of water constrain the gain of the water used RSA. Thus, as we use less water, the realized gain of the antenna is effectively improved. As shown in Fig. 3-19 (b), the realized gain at 20^{o} C now becomes more than 1dB which is effectively improved. This is the merit of using less water. It is noticed that there is a tradeoff between the antenna sensitivity and the antenna gain. How to improve the sensitivity without sacrificing much gain is a challenge.

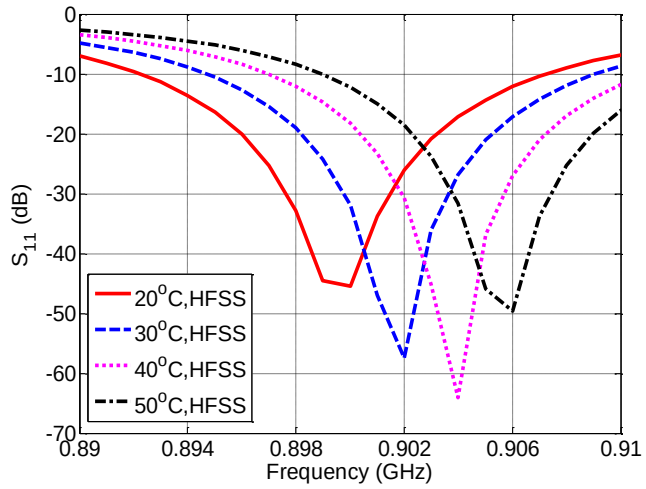

(a)

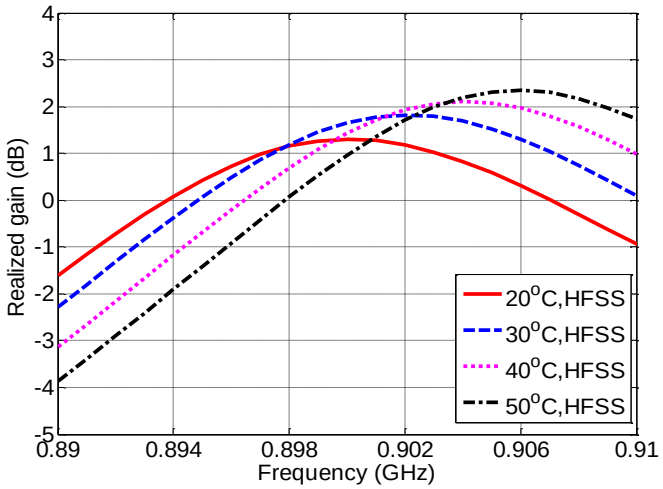

(b)

Fig. 3-19 The characteristics of the water RSA with 1.6mm water thickness: (a) S_{11} comparison under various temperatures, (b) realized gain comparison under various temperatures.

The knowledge of patch antenna tells us that a patch antenna radiates energy from its edges. Based on this, in order to improve the impact of water on the antenna's radiation property, the water pocket is located under the two radiating edges instead of placing under the center of the

patch. Fig. 3-20 shows the configuration of the RSA with water under its edge. Considering the fabrication issues and the available laminates thickness, three layers of the RO3210 laminates are used. Each layer has a thickness of 1.24mm. So the total thickness of substrate is 3.72mm. The water pocket is cut out from the top layer RO3210 which is close to the patch. The patch is etched on a FR4 layer with a thickness of 1.6mm. And it is flipped in order to make the patch and water close to each other. Fig. 3-21 shows the simulated S_{11} and realized gain at different temperatures. We can see that the frequency shift becomes 3MHz/10°C when the water is located under the radiating edges. However, the realized gain is 0.5dB at 20°C, which is around 0.7dB smaller compared to the previous structure shown in Fig. 3-18. The smaller gain is caused by the thinner substrate thickness. As the temperature increases, the water loss decreases, so a higher realized gain is observed from Fig. 3-21. Based on the results in Fig. 3-19, it is noticed that placing water under the radiating edges of patch can enhance the RSA sensitivity in terms of $\Delta f / \Delta T$.

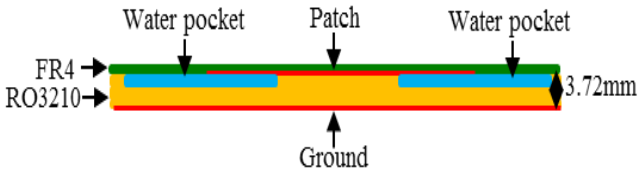

Fig. 3-20 The water RSA with water located under its radiating edges.

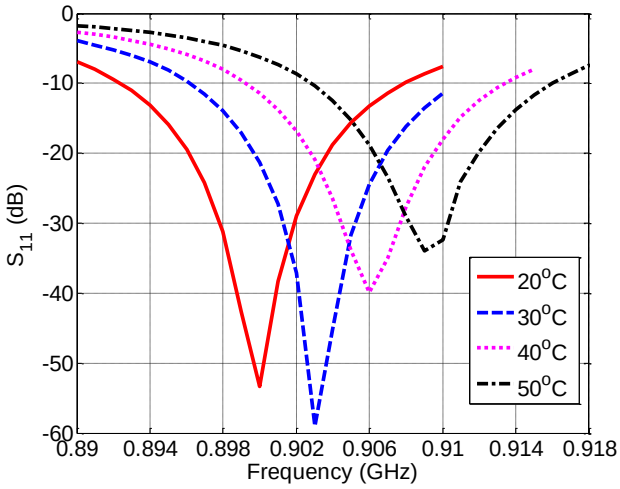

(a)

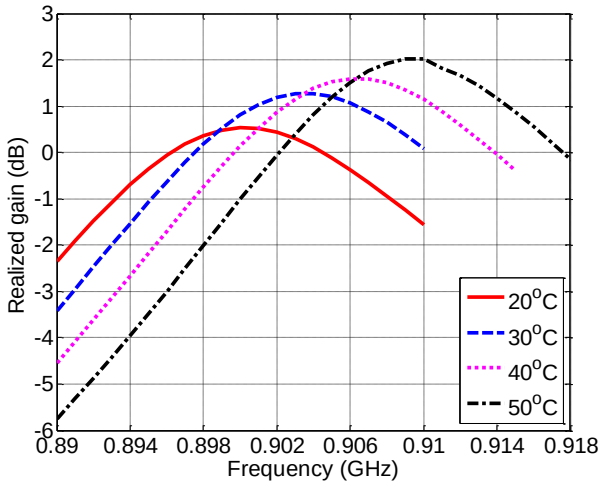

(b)

Fig. 3-21 The characteristics of the water RSA with water locating under patch edges: (a) S_{11} comparison for different temperatures, (b) realized gain comparison for different temperatures.

Through the above parameters studies, we can summarize the following guidelines of improving the water embedded RSA sensitivity:

- The thinner the substrate thickness, the narrower the antenna bandwidth, but a smaller gain is obtained. Decreasing the substrate thickness will heavily decrease the antenna gain, but its impact on bandwidth reduction is small.
- The higher the substrate's dielectric constant, the narrower the antenna bandwidth, a higher gain is obtained. For the specific water embedded RSA design, a high dielectric constant material will effectively improve the antenna gain and reduce its bandwidth. So it is beneficial for the RSA sensitivity.
- The thinner the water layer, the poorer the $\Delta f/\Delta T$, and a higher gain is obtained. From here, we learn that there is a tradeoff between the $\Delta f/\Delta T$ and antenna gain. A good RSA design should have large $\Delta f/\Delta T$ and high gain.
- Placing the water under the RSA's radiating edges has an effective impact on improving $\Delta f/\Delta T$. Properly selecting the water location does benefit the RSA sensitivity.

3.3.3 An Optimum Design

According to the aforementioned guidelines, an optimum design of the water embedded RSA is shown in Fig. 3-22. The two layers of Duriod/5880 with thickness of 0.787mm of each layer are used as the superstrate with patch and the bottom substrate with ground. And two layers of RO3210 are also selected as the substrate material. One of the RO3210 layer is used to store water. The dimension of the RSA is 100mm×100mm×4.074mm. The thickness of each layer is presented in Table 3-4. Water is located under the radiating edges of the antenna. The simulated

S_{11} and realized gain of the optimum design are shown in Fig. 3-23. We can see that the frequency shift is 4MHz/10°C, and the maximum realized gain at 20°C is -0.5dB. Additionally, the 3dB realized gain bandwidth is 2.89%.

Table 3-5 shows the sensitivity comparison between the optimum RSA design and the original design. These two designs have the same $\Delta f/\Delta T$ of 4MHz/10° C. However, the optimum one has a much higher gain which is -0.5dB as compared to the original -3.2dB. And the optimum one also has a narrower bandwidth, which is good to enhance the sensitivity. Thus, it is obvious that the water embedded RSA's sensitivity can be improved by selecting proper substrate material and water location.

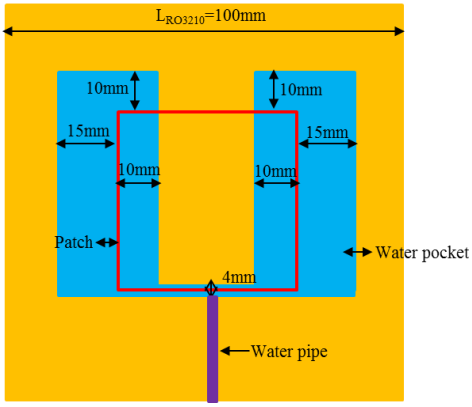

(a)

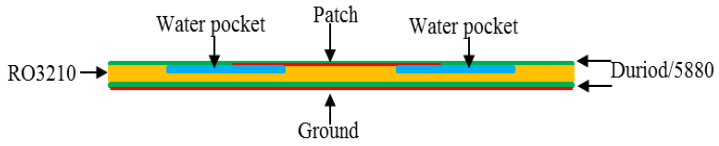

(b)

Fig. 3-22 The optimum design configuration: (a) Top view of the optimum design, (b) Side view of the optimum design.

Table 3-4 Thickness of each material layer

Duroid	RO3210	water pocket
0.797*2=1.594 mm	1.24*2=2.48 mm	1.24 mm

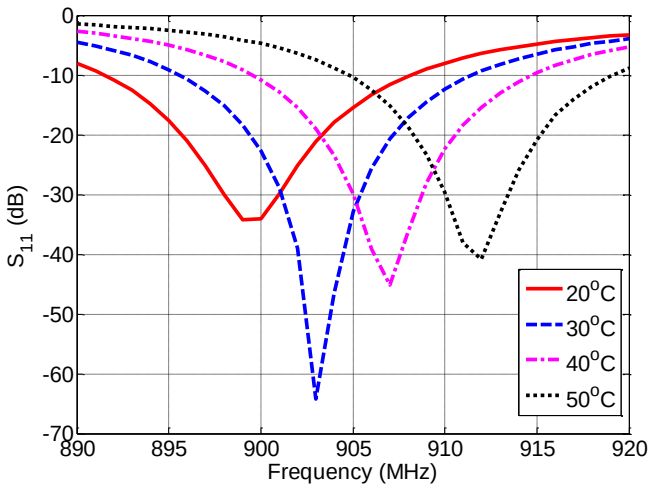

(a)

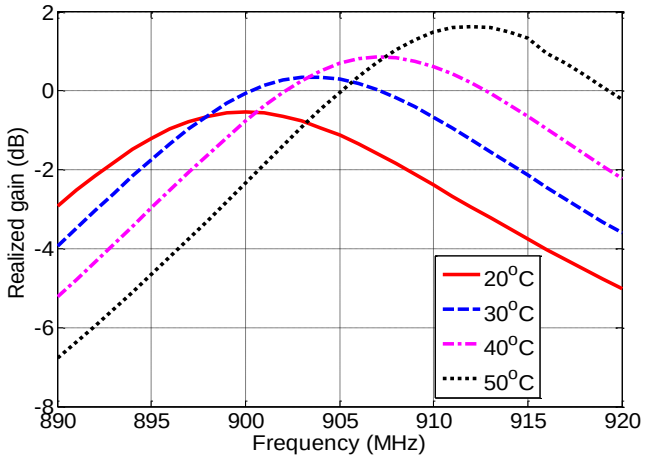

(b)

Fig. 3-23 The characteristics of the optimum design: (a) S_{11} comparison under various temperatures, (b) realized gain comparison under various temperatures.

Table 3-5 Sensitivity comparison between original RSA and optimum RSA

Parameter	Original RSA	Optimum RSA
Δf/ΔT	4MHz/10°C	4MHz/10°C
bandwidth	4.33%	2.89%
realized gain	-3.2dB	-0.5dB

3.4 Summary

This chapter presents the RSA designs that use water as their temperature sensing material. Water can be used as temperature sensing material because its dielectric constant is temperature dependent. Slotted patch antennas are selected because of their narrow bandwidth and easy to mount the IC chip on it. Water is embedded in the patch's substrate, thus the resonant frequency of the antenna can be reconfigured by the temperature. The operation principle of the RSA is

described in details. Operating at the UHF band (900 MHz), the RSA prototype demonstrates a temperature sensing range from 17°C to 70°C, which is the effective scope of the measurement facility. In practice, the water can work from 0°C to 100°C as the sensing material. The measurement results show that the water embedded RSA has a 4MHz/10^{o} C, and a -3.2dB realized gain with a 3dB bandwidth of 4.33%. For a sensing antenna, -3.2dB realized gain and 4.33% bandwidth is still need to be improved. In this situation, a thorough study of improving its temperature sensitivity is carried out. Substrate thickness, material, water thickness and location are investigated separately. It is noticed that using a high dielectric constant material as the water RSA substrate, while placing the water under the radiation edges of the patch will definitely increase the RSA's sensitivity. Finally, an optimum design is introduced, with a -0.5dB realized gain 2.89% bandwidth.

CHAPTER IV

RSA USING ELECTRICAL PROPERTIES OF MATERIAL: HDPE-BST COMPASITE MATERIAL BASED RSA

The water embedded RSA designs are presented in the previous chapter. The optimum water embedded RSA offers 4MHz/10°C frequency shift and -0.5dB antenna realized gain whose 3dB bandwidth is 2.89%. Water is safe and low cost, however, in reality, as a liquid material, it is not easy to integrate in the design. In addition, the water embedded RSAs have limited sensitivity, such as 4MHz/10°C frequency shift and 2.89% antenna bandwidth.

In order to design an easily fabricated RSA with higher sensitivity, a novel solid composite material, namely, high density polyethylene-Ba0.3Sr0.7TiO3 (HDPE-BST) is developed and utilized in this chapter. It is a solid material, and has a large temperature coefficient of dielectric constant, which varies from 7.10 at 20˚C to 6.66 at 80˚C. We can see the HDPE-BST has a similar temperature property as water. Its dielectric constant also depends on the temperature.

In this chapter, the HDPE-BST material is used as the temperature sensing material. In order to increase the temperature sensitivity, the bandwidth of the RSA should be as narrow as possible. To this end, a microstrip line feed slotted patch RSA resonating at 900MHz is designed, fabricated, and measured. The HDPE-BST material is directly used as the patch RSA substrate. Similarly, the resonant frequency of the HDPE-BST based patch RSA is also reconfigured by the

environmental temperature. The slot used in the patch can effectively reduce the patch size, because it can increase the current path length. The smaller patch size implies narrower antenna bandwidth. Finally, the HDPE-BST based RSA shows a 3-dB gain bandwidth of only 5.4 MHz (0.6%). Meanwhile, the experimental results show that an 8 MHz/10˚C frequency increment can be obtained in the temperature range from 20˚C to 80˚C.

Besides the microstrip line feed slotted patch RSA, other RSA configurations using HDPE-BST are also designed and analyzed. They are patch RSAs with shorting pins and slot feed patch RSA. Both of them have the merits of compact size, and narrow bandwidths. A comparison is done among these aforementioned RSA designs to evaluate their sensitivity. The comparison results show that all of the HDPE-BST used RSAs can achieve a high sensitivity in terms of $\Delta f/\Delta T$ and antenna bandwidth. The HDPE-BST has the advantages of large temperature coefficient of dielectric constant, good thermal conductivity, ease of integration, and light weight. All of these features make the HDPE-BST a good candidate in the temperature sensing RSA designs.

4.1 Introduction of HDPE-BST

An ideal temperature-dependent material to be used in sensing antennas should have a large temperature coefficient, high relative permittivity, and low dielectric loss. Polymer–ceramic composites, especially type 0–3, exhibit excellent comprehensive performance suitable for patch antennas, which combine the electrical properties of ceramics and the mechanical flexibility and processing possibilities of polymers. In order to develop high-permittivity composites, $Ba_{0.3}Sr_{0.7}TiO_3$ (BST) with dielectric constant 600, loss tangent 0.2%, and large temperature

coefficient of dielectric constant is used. The HDPE is selected as polymer matrix because of its high flexibility, excellent microwave dielectric properties, and low processing temperature (< 200℃). Based on these properties, 0-3 polymer-ceramic compositions with 30% volume fraction BST in the HDPE matrix through extrusion process is fabricated. A scanning electron microscopy (SEM) image is shown in Fig. 4-1. The composites show good surface texture, and it can be observed that the irregularly shaped ceramic particles with size 0.5-3μm are uniformed distributed through the HDPE matrix. So the HDPE-BST composite has a homogeneous performance. The relative permittivity and loss tangent of the HDPE–BST composite at different temperatures are measured at 900MHz by Agilent E4991A RF Impedance/ Material Analyzer, as shown in Fig. 4-2.

The data in Fig. 4-2 show that the relative permittivity of HDPE-BST decreases as the temperature increases. From 20℃ to 80℃, the relative permittivity of the HDPE-BST composite varies from 7.10 to 6.66. Meanwhile, the loss tangent increases from 0.0022 to 0.0034, respectively. The loss tangent of HDPE is mainly affected by relaxation of segment. Under low temperature, segment motion is hindered, so the loss tangent curve has a positive slope. The segment is fully relaxed in higher temperature, which is the reason for the saturation shape of the curve. The temperature coefficient of relative permittivity is -1033ppm/℃, which is much larger than conventional materials, such as -125ppm/℃ of RT/duroid 5880 [30]. Besides the merit of large temperature coefficient of permittivity, light weight and good thermal conductivity are also important advantages of the HDPE-BST material. Experimental results show that heating a HDPE-BST sample which has a 35mm radius with 1.524mm thickness from room temperature to

80℃ only takes half a minute. All of these features make the novel HDPE-BST suitable for RSA designs.

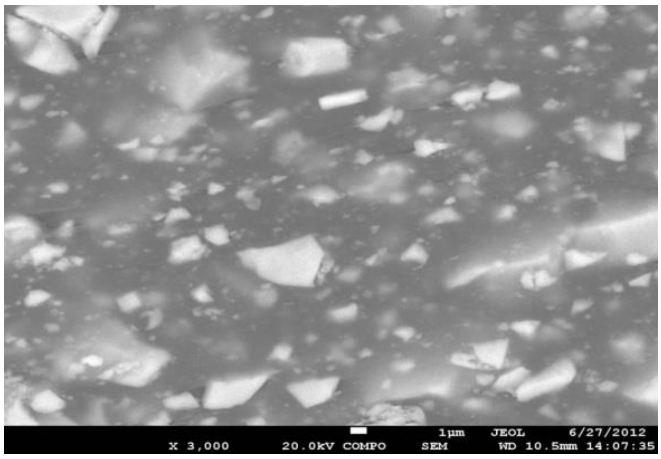

Fig. 4-1 SEM images of 30vol% BST ceramic powder loaded HDPE.

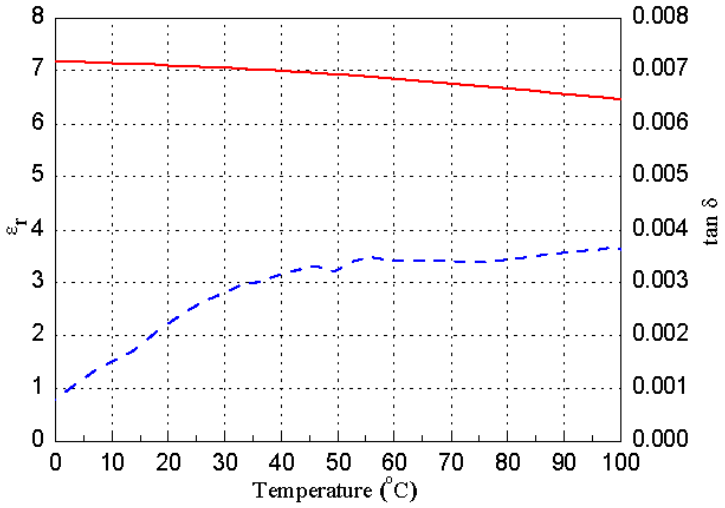

Fig. 4-2 Relative permittivity and loss tangent of the HDPE-BST material at 900MHz.

4.2 Microstrip line Feed Slotted RSA

4.2.1 RSA Configuration

In this section, we want to design a narrow bandwidth RSA for temperature sensing, which resonates at 900MHz. To this end, a patch antenna is selected in the RSA design, because it has narrow bandwidth and is easy to fabricate. HDPE-BST material is used as substrate, which has a 35mm radius and 1.524mm thickness. To reduce the antenna size, a slot is incorporated in the patch design. The slot can effectively increase the path length of the electric current on the patch, and make the antenna resonating at a lower frequency than the conventional one. The slot loaded patch RSA configuration is shown in Fig. 4-3. An Allien Higgs 3 chip is mounted on the microstrip line to realize wireless communication and identification. This microstrip line is shorted to the ground at the edge of the substrate.

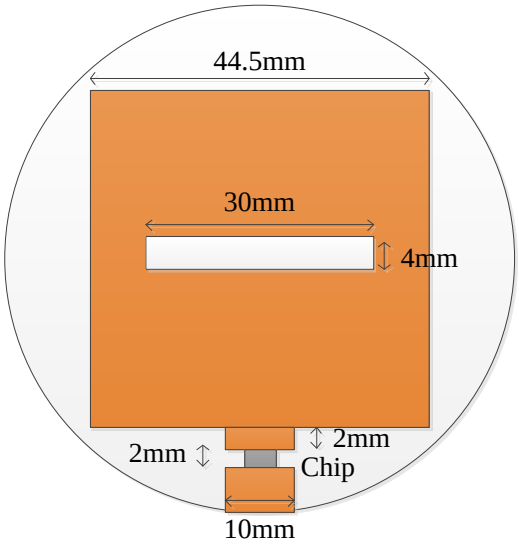

Fig. 4-3 The microstrip line feed HDPE-BST based slotted patch RSA configuration.

4.2.2 Slot Length and Width Study

Slot plays the role of increasing the current length of the patch antenna, and the current length is critical to determine the resonant frequency of antenna. In this section, the impacts of the slot length and width on the patch antenna performance are investigated. Fig. 4-4 shows the S_{11} and realized gain comparison of the RSAs with different slot lengths. In this case, the slot length is variable with a fixed slot width of 4mm. According to Fig. 4-4 (a), as the slot length increases, the resonant frequency of the antenna decreases. More specifically, the resonant frequency of the antenna decreases from 980MHz to 900MHz, when the slot length increases from 25mm to 30mm. On the other hand, the maximum realized gain decreases from -2dB to -3.9dB as the slot length increases from 25mm to 30mm. This is easy to understand. The longer slot length results in a lower resonant frequency, hence the directivity of the same antenna becomes smaller, which

consequently gives out a lower gain. In addition, the impedance match of the RSA using longer slot length also degrades, which definitely reduce the realized gain at resonant frequency.

Fig. 4-5 is the S_{11} and realized gain comparison among the RSAs using different slot widths. The slot length is fixed at 28mm. It is illustrated in Fig. 4-5 (a) that when the slot width increases, the resonant frequency of the antenna decreases. More specifically, the resonant frequency decreases from 935MHz to 900MHz, when the slot width increases from 4mm to 7mm. This is also due to the increased current path length by increasing the slot width. Meanwhile, the realized gain also decreases from -3.2dB to -4dB with the slot width increasing. This is due to the smaller directivity and degrading impedance match.

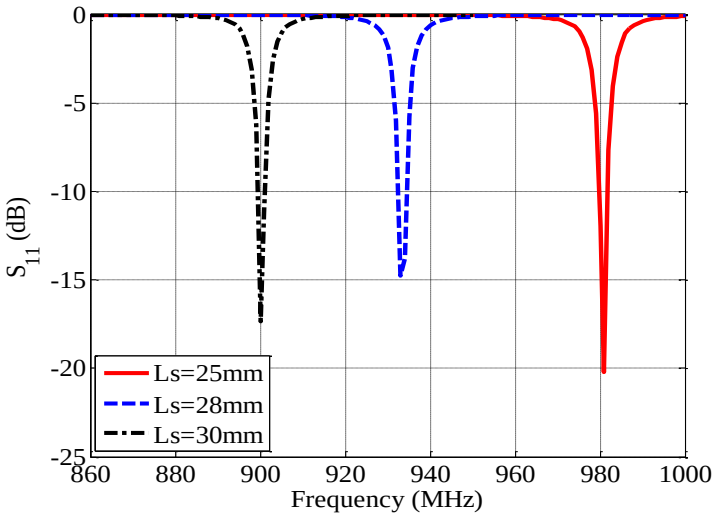

(a)

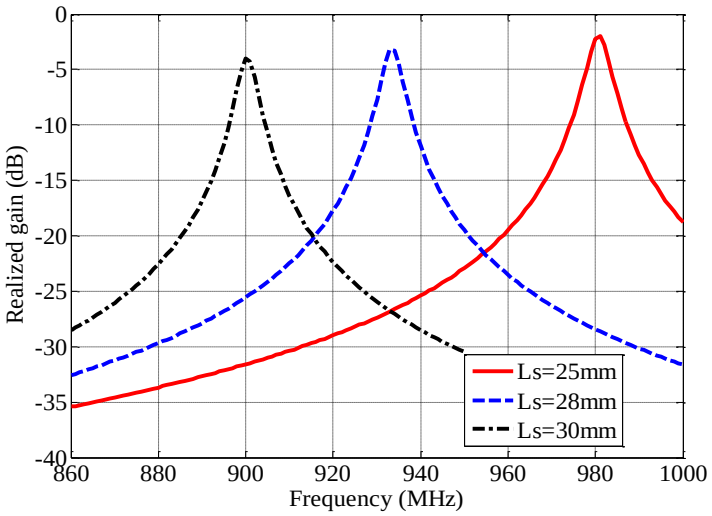

(b)

Fig. 4-4 The characteristics of HDPE-BST based slotted RSAs with different slot lengths: (a) S_{11} comparison, (b) Realized gain comparison.

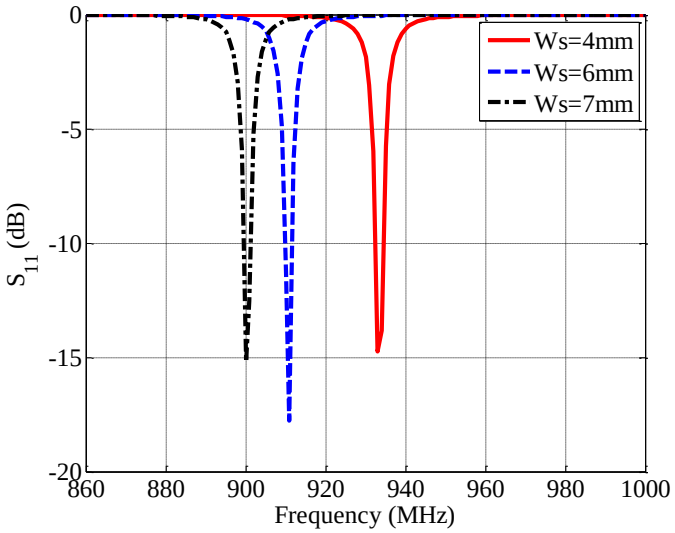

(a)

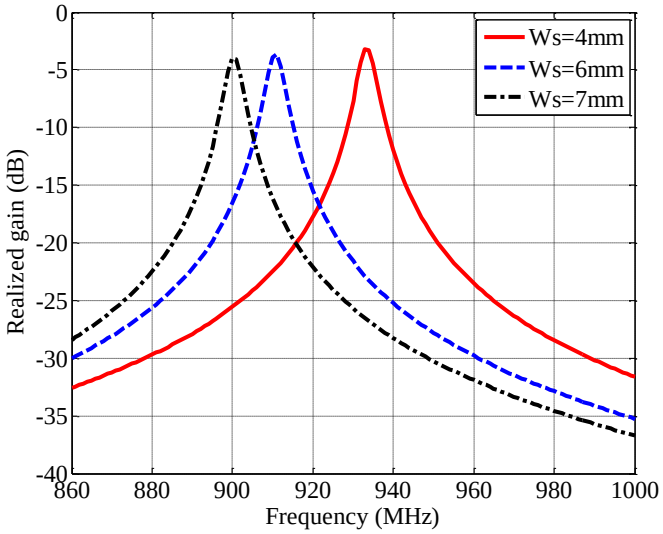

(b)

Fig. 4-5 The characteristics of HDPE-BST based slotted RSAs with different slot widths: (a) S_{11} comparison, (b) Realized gain comparison.

Based on the slot length and width studies, one can conclude that increasing the slot length and width will decrease the resonant frequency of the RSA. Thus, we can obtain a compact RSA size by incorporating the slot in the patch. This is the merit of using slot. However, the antenna gain is decreased by increasing the slot size. It is observed from the simulated cases above, the RSAs using 28mm slot length and 7mm slot width, and the one using 30mm slot length and 4mm slot width, both resonate at 900MHz. However, the realized gain of the later one is a little better. So, the slot length is set to be 40mm and the slot width is set to be 3mm.

4.2.3 Microstrip Line Width Study

The slot effects are studied in the previous section. In this section, the effects of microstrip line width are investigated. The purpose of using microstirp line feed is to add more freedoms to tune the impedance match. The IC chip can be simply treated as a parallel resistor and capacitor. It is impedance is around 13-j140 at 900MHz. For the maximum power transformation, the antenna should be conjugate matched to the chip, which means the antenna should possess high inductive reactance. The usage of micrstrip line is to add a parallel inductor to the antenna and make the antenna has a high inductive reactance. The impacts of microstrip line widths are investigated. Fig. 4-6 shows the impedance comparison of the RSA with three different microstrip line widths. It is observed that the imaginary part of the antenna impedance changes with microstrip line width. Before the resonance frequency of the antenna, where the reaction equals to 0, the wider the microstrip line, the higher the imaginary part of the antenna. Meanwhile, the resonant frequencies of the RSAs also change with the microstrip line width. Fig. 4-7 shows the S_{11} comparison between the three cases, which is matched to the chip impedance. It is illustrated from Fig. 4-7 that the value of S_{11} has slightly difference among the three different cases due to the impedance variation. However, different from the one shown in Fig. 4-5 (a), the mistrostip line width does not have effectively impact on the RSAs' resonant frequency. It is observed from Fig. 4-6 and Fig. 4-7 that by tuning the microstrip line width, good impedance matching between the antenna and the chip can be achieved. Finally, the microstrip line width is determined to be 10mm.

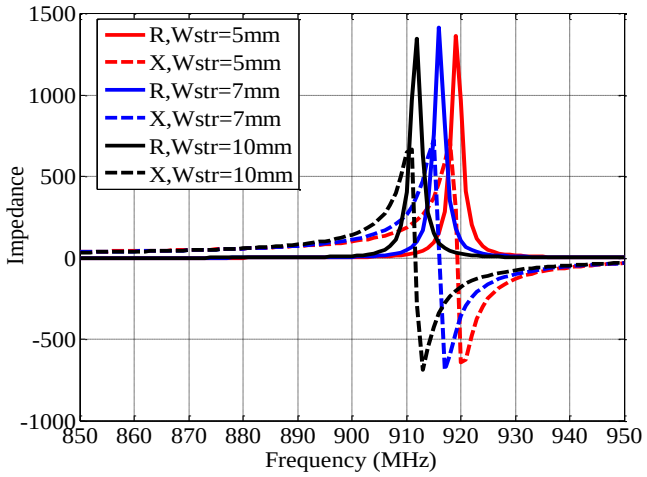

Fig. 4-6 Impedance comparison of the RSAs under different microstrip line widths.

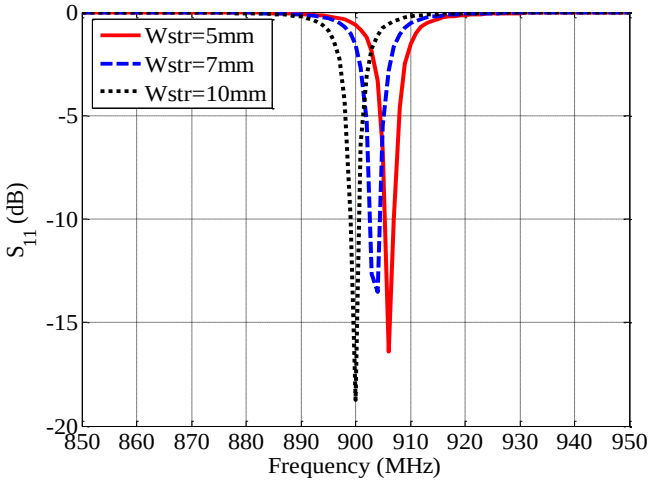

Fig. 4-7 S_{11} comparison of the RSAs under different microstrip line widths.

Based on the previous parameter study, we can learn that the slot length and width are important to increase the current path on the patch, thus control the resonant frequency of the RSA. The longer the slot, and the wider the slot, the lower resonant frequency is obtained. The microstrip line is mainly used to tune the impedance match of the RSA. The reason we choose a

wide microstrip line width is because it can provide a better match and easy to realize in fabrication.

4.2.4 Temperature Sensitivity of The HDPE-BST Based RSA Design

The RSA dimensions are designed with Ansoft HFSS. The simulated S_{11} at 20℃ is shown in Fig. 4-8, where the operating frequency of the RSA is 900MHz as expected. Meanwhile, the -10 dB S_{11} bandwidth is only 0.22%, which is preferable for RSA. This narrow bandwidth is beneficial to the RSA sensitivity. The E-plane RSA radiation pattern at 900MHz is shown in Fig. 4-9 (a), and realized gain at broadside is shown in Fig. 4-9 (b). According to Fig. 4-9 (a), the backward radiation of the RSA is larger than conventional patches due to its small ground size (0.21 λ_0). As a result, the broadside radiation is decreased, which has 3-dB directivity. At the same time, although the material loss is 0.003, it thin thickness (0.0046 λ_0) and high relative permittivity result in a -3.8 dB antenna gain. Although high permittivity and thin layer of the substrate degrade the gain of antenna, they will make the antenna bandwidth narrow, which are beneficial to RSA sensitivity. There is a tradeoff between RSA sensitivity and gain.

The proposed RSA is used for monitoring temperature, so its sensing capability should be considered. Fig. 4-10 shows the S_{11} performance of the RSA at different temperatures. It is clearly that the resonant frequency of the RSA increases as the temperature increases. This is because the HDPE-BST's dielectric constant decreases as temperature increases. Additionally, the relation between the resonant frequency and temperature is nonlinear. The higher the temperature, the

larger the frequencies shift. Fig. 4-11 shows the realized gain comparison at different temperatures. It is noticed that as temperature increases, the realized gain decreases. This is due to the increased loss of the HDPE-BST. The detailed information of the RSA performance including its resonant frequency, realized gain, and bandwidth at different temperature are listed in Table 4-1.

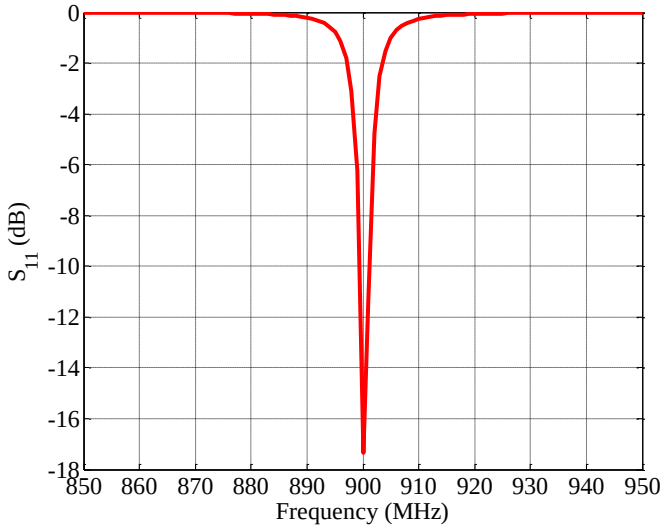

Fig. 4-8 Simulated S_{11} of the HDPE-BST based RSA at 20°C.

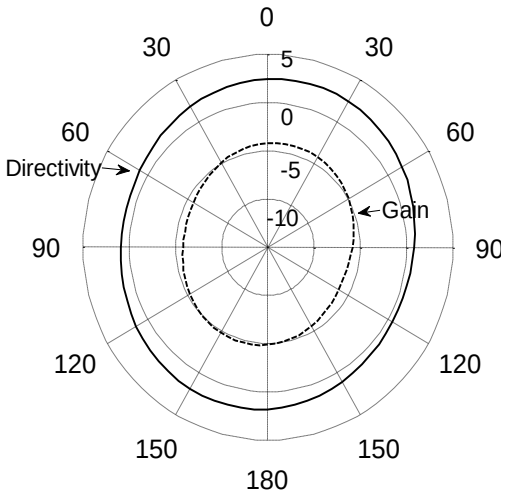

(a)

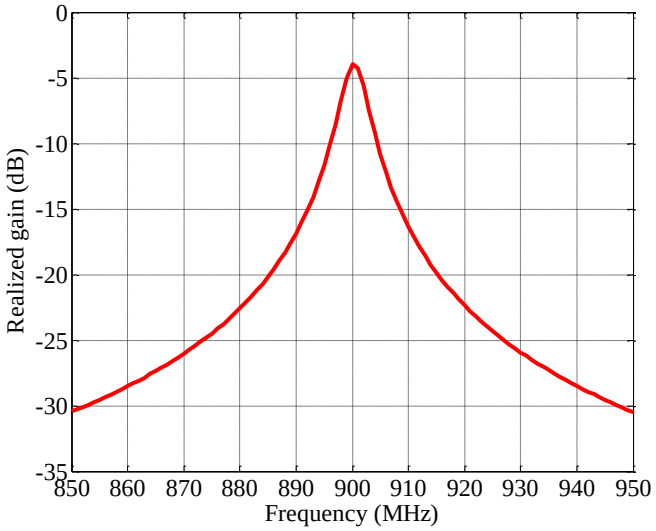

(b)

Fig. 4-9 The characteristics of the HDPE-BST based RSA: (a) radiation pattern at 900MHz, (b) broadside realized gain.

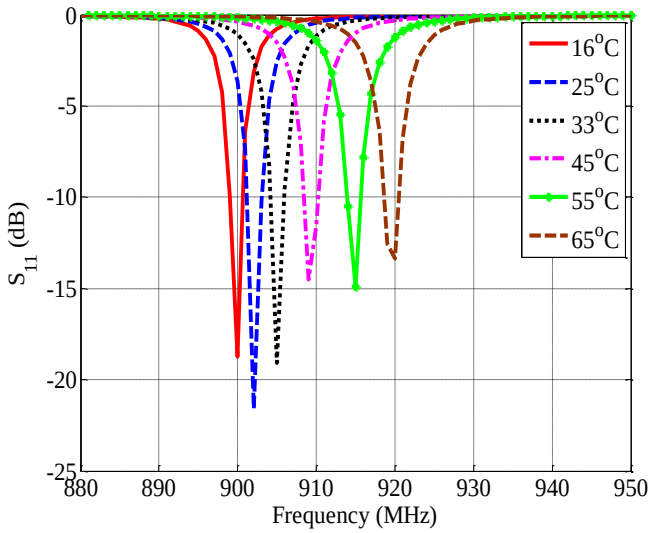

Fig. 4-10 Simulated S_{11} of the HDPE-BST based RSA under various temperatures.

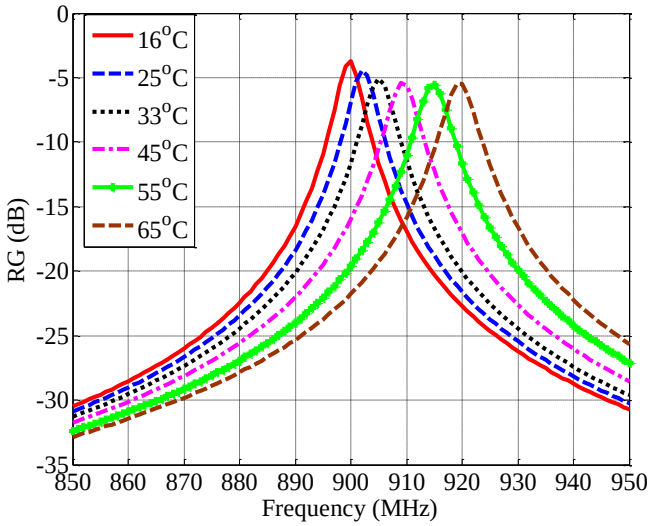

Fig. 4-11 Simulated broadside realized gain of the HDPE-BST based RSA under various temperatures.

Table 4-1 RSA performance at different temperatures

Temperature (°C)	16	25	35	45	55	65
HDPE-BST (ε_r)	7.12	7.08	7.04	6.96	6.88	6.8
HDPE-BST (tanδ)	0.002	0.0025	0.003	0.0033	0.0034	0.0034
Resonant freq. (MHz)	900	902	905	909	915	920
S11 (dB)	-17	-21.7	-19	-14.5	-14.9	-13.3
Realized gain (dB)	-3.7	-4.5	-5.1	-5.4	-5.6	-5.5

4.2.5 Measurement Setup and Results

The slot loaded patch RSA is fabricated and tested. Fig. 4-12 shows the RSA prototype, where an Alien Higgs 3 chip is mounted on the microstrip line to realize the wireless sensing.

The measurement of the RSA is conducted in an anechoic chamber, as shown in Fig. 4-13. The chamber is designed for the UHF band RFID antenna measurement. A reader antenna is used to send out the electromagnetic waves to the RSA as well as receive its backscattered information. The distance between the reader and the RSA is 0.5m. Temperature sensitivity is measure by the Tagformance device, which can read both the IC information and the transmit/receive power levels. The RSA is preheated outside the chamber with a heating device, and foam is used to cover the RSA to reduce the heat flow. The RSA temperature is measured by a digital thermometer, and it is ensured that the RSA temperature remains constant during the measurement.

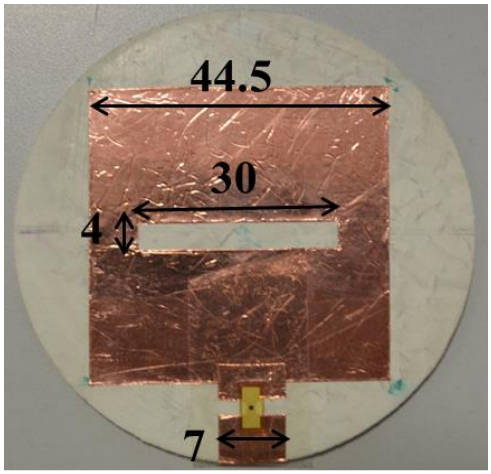

Fig. 4-12 Fabrication prototype of the HDPE-BST based RSA.

Fig. 4-13 Measurement Setup of meausring the HDPE-BST based RSA performance.

Fig. 4-14 shows the measured read range of the RSA at different temperatures. The read range d_{RSA} can be calculated as following:

$$d_{RSA} = \frac{\lambda}{4\pi}\sqrt{\frac{EIRP}{P_{TS}L_{fwd}}} = \frac{\lambda}{4\pi}\sqrt{\frac{EIRP}{P_{IC}/G_{RSA}}} \qquad (4\text{-}1)$$

where equivalent isotropic radiated power (EIRP) is 3.28W. The transmitted power (P_{TS}) is the measured threshold power to activate the RSA. L_{fwd} represents the measured path-loss between the TX-port and the RSA including the cable loss, reader antenna gain, and free space loss. Thus, P_{TS} L_{fwd} is the measured minimum power needed to active the chip on the RSA. The Higgs 3 chip has a sensitivity (P_{IC}) of -18dBm, and G_{RSA} is the simulated realized gain of the slotted RSA. So, P_{IC}/G_{RSA} is simulated minimum power to active the RSA. According to the measured results in Fig. , a 4.2 m read range is obtained at 16ºC. The frequency where the maximum read range is obtained increases as the temperature increases, as expected from simulations in Fig. 4-11. The resonant

frequencies discrepancy between Fig. 4-11 and Fig. 4-14 may be caused by the fabrication and measurement errors, including the chip impedance inaccuracy, fabrication tolerance, and temperature environment variation. Meanwhile, the read range decreases as the temperature increases. This is due to the characteristic of the HDPE-BST material, whose loss tangent increases as temperature increases. Since the bandwidth of the RSA is narrow, the resonant frequency where the maximum read range is obtained is easy to be distinguished, which can be used to derive the antenna temperature.

Fig. 4-15 shows the comparison of the RSA resonant frequency versus temperature between two rounds of measurements. The first round was measured at 20ºC, 29ºC to 37ºC; the second round was measured from 16ºC to 65ºC. The results agree with each other. According to the second measurement results, from 16ºC to 65ºC, the frequency varies from 903 to 934MHz, and a maximum 8MHz/10ºC frequency shift is obtained. Table 4-2 shows the sensitivity comparison between the current slotted RSA design and the measured water embedded RSA design. From the comparison, it is clear that the proposed HDPE-BST RSA has a higher sensitivity (in terms of $\Delta f/\Delta T$) and bandwidth than the previous water embedded one. In addition, the dimension of the HDPE-BST used RSA is much smaller comparing with the water embedded one.

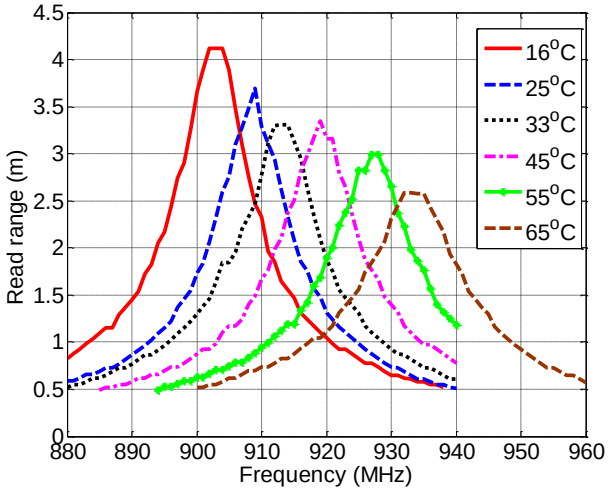

Fig. 4-14 Measured read range of the HDPE-BST based slotted patch RSA under various temperatures.

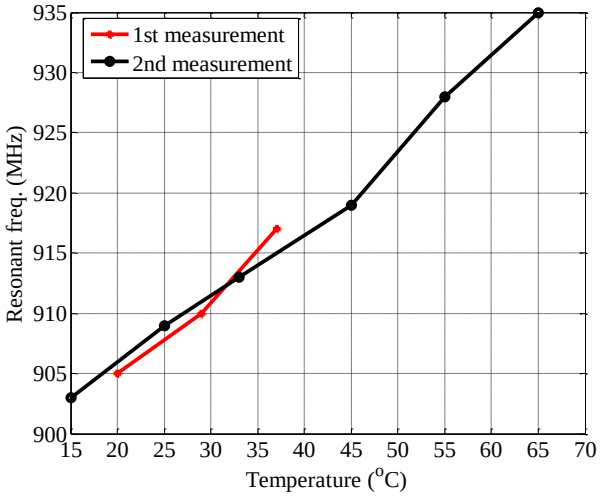

Fig. 4-15 Resonant frequency of HDPE-BST based slotted patch RSA under various temperatures.

Table 4-2 Sensitivity Comparison of the HDPE-BST RSA and water embedded RSA

Design	HDPE-BST RSA	Water embedded RSA
Δf/ΔT	8MHz/10°C	4MHz/10°C
3dB realized gain bandwidth	0.6%	4.33%

Realized gain	-3.8dB	-3.2dB
Dimension	D=70mm, t=1.524mm	100*100*6.4 mm^3

4.3 Various RSA Designs Using Different Size Reduction Methods

4.3.1 Microstrip Line Feed Patch RSA with Shorting Pins

Incorporating slot in patch antenna can reduce the patch size, because the existing of slot increases the current path length. This is one method to reduce the patch size. Besides using slot, there are other methods that can reduce the patch size such as integrating shorting pins in patch. The usage of shorting pins can effectively reduce the patch size to quarter wavelength and narrower the bandwidth. These features of shorting pins are beneficial to RSA designs.

In this section, the shorting pins are used in the patch to investigate its impacts on the RSA performance. Fig. 4-16 shows the configuration of the HDPE-BST based patch RSA using shorting pins. The antenna also works at 900MHz. It is a square patch with side length of 30.9mm. Five shorting pins are symmetrically located at the edge of the patch, and each of them has 1mm radius. There is a microstrip line on which an IC chip is mounted. The microstrip line width is 1mm. The HDPE-BST substrate has a diameter of 70mm and thickness of 1.524mm.

The simulated S_{11}, and realized gain at broadside comparison between the shorting pins RSA and the microstrip line feed RSA are shown in Fig. 4-17. It is noticed from the results, the two designs both resonate at 900MHz. The broadside realized gain of the one with shorting pins is around -4.4dB with a narrower 3dB bandwidth of 0.5%, when compared with the microstrip line

feed one. The narrower realized gain bandwidth is caused by the smaller patch size, which is only 30.9mm. As mentioned before, there is a tradeoff between antenna gain and bandwidth, as the Q factor is inversely proportional to the antenna size, and proportional to the antenna bandwidth. Hence, when the antenna becomes smaller, its bandwidth becomes narrower.

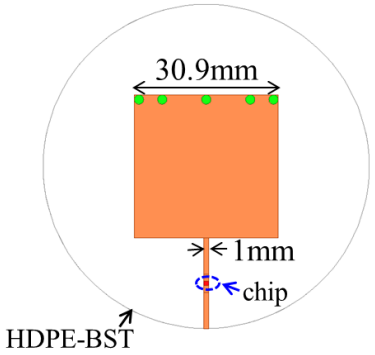

Fig. 4-16 Patch RSA with multiple shorting pins.

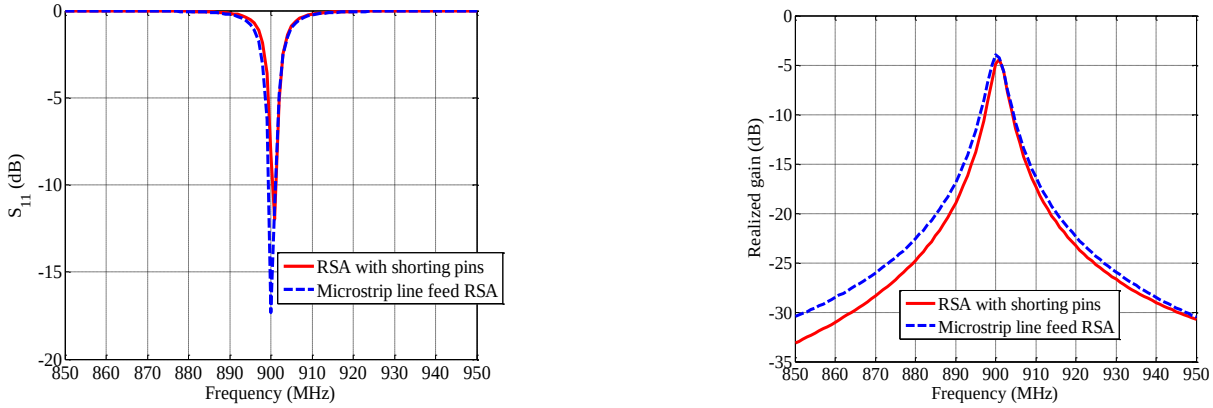

(a) (b)

Fig. 4-17 The characteristics comparison between RSA with shorting pins and microstrip line feed RSA: (a) S_{11} comparison, (b) realized gain comparison.

4.3.2 Slot Feed Patch RSA

The aforementioned microstrip line feed RSA has a compact size and narrow bandwidth. The IC chip is mounted on the microstrip line. In this section, a slot feed patch RSA using HDPE-BST is presented. Both of them adopt slot. The only difference is the feeding method. Instead of placing the IC chip on the strip line as shown in Fig. 4-12, the chip is mounted on the middle of the slot. In this case, the RSA is easiest to fabricate. The HDPE-BST is also used as the patch substrate with the same dimension. Fig. 4-18 shows the configuration of the slot feed RSA. The side length of the square patch is 47.5mm. The slot is cut out from the middle of the patch, which are 30mm in length and 3mm in width. The reason of choosing 3mm as the slot width is that this width is easy to mount the chip on it. Fig. 4-19 shows the S_{11} and broadside realized gain comparison between the strip-feed RSA and the slot feed RSA. We can see they have comparable S_{11} and realized gain. The only difference is that the realized gain bandwidth of the strip-feed RSA is narrower.

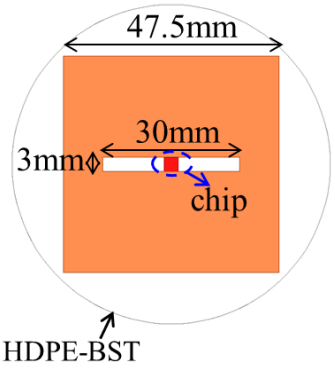

Fig. 4-18 Configuration of slot feed patch RSA using HDPE-BST.

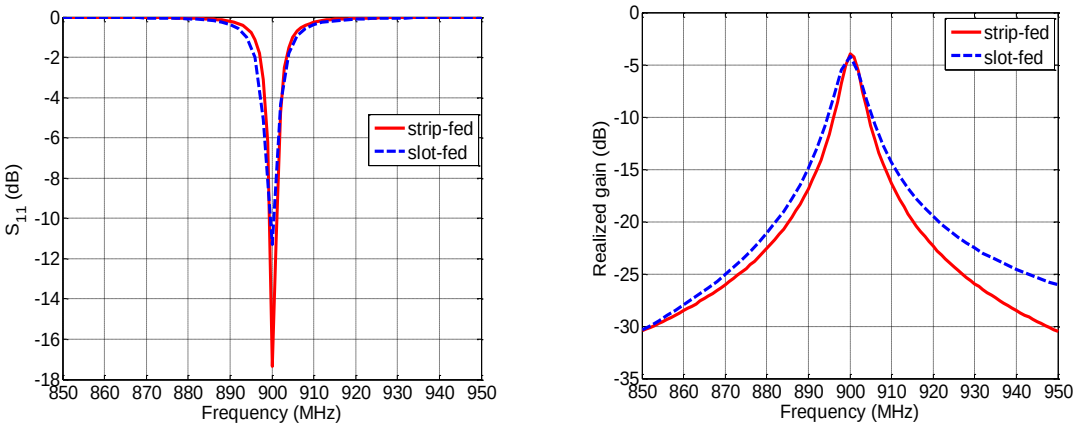

(a) (b)

Fig. 4-19 Simulation results comparison between strip feed patch RSA and slot feed patch RSA: (a) S_{11} comparison, (b) realized gain comparison.

4.3.3 Various RSA Designs Comparison

Till now, three different RSA designs are presented. All of them use HDPE-BST as substrate. As shown in Fig. 4-20, the three designs are strip-feed patch RSA, patch RSA with shorting pins, and slot feed patch RSA, respectively. Table 4-3 shows the detailed information of these designs, including patch size, maximum realized gain, and 3dB realized gain bandwidth.

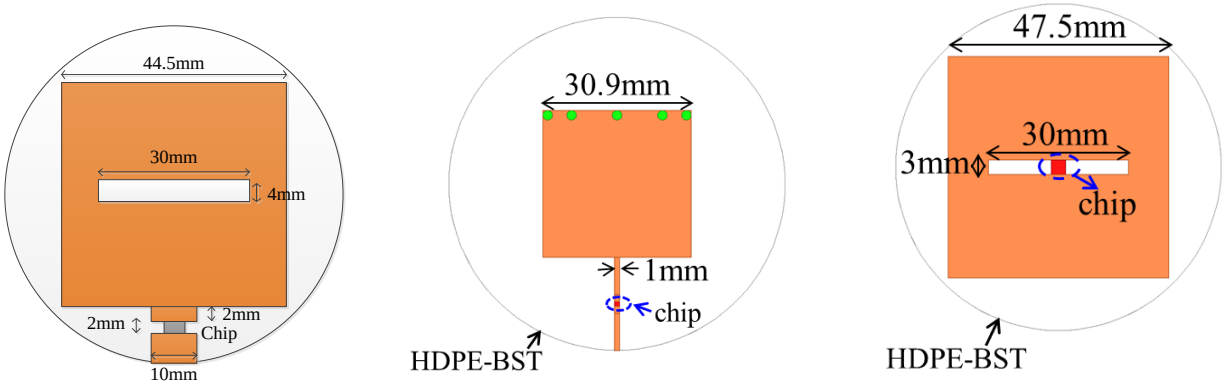

(a) (b) (c)

Fig. 4-20 Different RSA designs: (a) microstripline feed slotted RSA, (b) microstripline feed shorting pins RSA, (c) slot feed patch RSA.

Table 4-3 Comparison between three different RSAs

Configuration	Patch size	Maximum realized gain	3-dB realized gain bandwidth
Strip-feed RSA	44.5mm×44.5mm	-3.9dB	0.67%
RSA with shorting pins	30.9mm×30.9mm	-4.4dB	0.5%
Slot feed RSA	47.5mm×47.5mm	-4.17dB	0.78%

According to the Table 4-3, we can see the RSA with shorting pins has the smallest patch size and narrowest bandwidth. However, its realized gain is the smallest. The strip-feed RSA are the one with largest realized gain, with moderate patch size and bandwidth. And the slot-feed RSA is the one most easily to fabricate. However, its patch size and bandwidth are the largest. Which one is the best to use depends on the specific application requirements. Nevertheless, the HDPE-BST used patch RSAs has limited realized gain which will restrict their read range. This is

because of the high permittivity of the material, the thin layer of the structure, and relative small ground.

All of the three designs have similar frequency shift with temperature ($\Delta f/\Delta T$) of 8MHz/10ºC, which is much better comparing with the water RSA (4MHz/10ºC). However, it does not mean that 8MHz/10ºC is too good to further improve. The sensing mechanism of using materials' electrical properties provide limited sensitivity, which is due to the limited temperature coefficient of material and the constrained impacts of the material on the antenna performance. In this situation, to obtain a high sensitive RSA with larger $\Delta f/\Delta T$, higher gain, and narrow bandwidth, new sensing mechanism should be investigated.

4.4 Summary

In this chapter, a novel composite material, namely, HDPE-BST is introduced, and used as temperature sensing material in RSA designs. Similar to water, the HDPE-BST also has a temperature dependent dielectric constant. Thus, it is used as the substrate of patch antenna.

There are totally three different HDPE-BST used RSAs designed in this chapter. They are the microstrip line feed RSA, the RSA with shorting pins, and the slot feed RSA, respectively. Among the three designs, the microstrip line feed RSA is fabricated and measured. Experimental results show that the HDPE-BST based RSA has a higher sensitivity than the previous water embedded RSA in terms of $\Delta f/\Delta T$ and bandwidth. However, its gain is lower comparing with the water based RSA.

For comparison purpose, the microstrip line feed HDPE-BST used RSA has a $\Delta f/\Delta T$ of 8MHz/10 ºC, a bandwidth of 0.6% and a gain -3.8dB. And the water design has a $\Delta f/\Delta T$ of 4MHz/10ºC, a bandwidth of 4.3% and a gain of -3dB. The measurement results of the RSA prototype demonstrate a temperature sensing range from 16°C to 65°C. In practice, the HDPE-BST can work from -40°C to 120°C as the sensing material. Besides the microstrip line feed RSA, the other two RSA designs are also has similar $\Delta f/\Delta T$, can comparable realized gain and bandwidth. According to the specific application, either of them can be selected.

Although the HDPE-BST used RSA has an improved sensitivity comparing with the water embedded one, its sensing mechanism restricts the further improvement of sensitivity. Thus, a new sensing mechanism is investigated and introduced in the following chapters.

CHAPTER V

RSA USING THERMAL PROPERTIES OF MATERIAL: MERCURY USED CAPACITIVELY-LOADED CAVITY BACKED SLOT RSA

In the water and HDPE-BST based RSA designs, the materials' temperature-dependent electrical properties are used. The sensing materials water and HDPE-BST, whose dielectric constants depend on temperature, are designed as substrates of patch antennas. According to the characteristics of patch antennas, their resonant frequencies become temperature dependent. This kind of RSAs is simple and easy to fabricate. However, because the dielectric constant of material, its variation with temperature is always limited, which restrict the temperature sensitivity of the RSA. Meanwhile, the inherent characteristics of patch antenna constrain the impact of sensing materials on the RSA performance. Till now, the best sensitivity of the RSA using materials' temperature dependent dielectric properties is 8MHz/10^{o}C. Restricted by the sensing mechanism and optional antenna configuration, the sensitivity of the RSAs using the electric properties of materials is hardly to be further improved. Thus, in order to design high sensitive RSA, new sensing mechanism is adopted.

In this chapter, thermal properties of material is introduced and implemented in the RSA design. Thermal expansion properties of materials have been used to monitor temperature for a

long time, for example mercury thermometer, alcohol thermometer. Both mercury and alcohol are liquid materials with large thermal expansion coefficient. In this chapter, mercury is used as temperature sensing material because of its metallic property, and its 180ppm/°C large thermal expansion coefficient.

In order to implement mercury in the RSA design and magnify its effects on the RSA performance, a capacitively-loaded cavity backed slot RSA is designed. In this design, cavity backed slot antenna is selected as the antenna configuration to integrate mercury. And mercury is stored at the center of the cavity, which forms a loaded capacitor with the cavity ceiling. As temperature increases, the gap between mercury and cavity top is shrunk due to the thermal expansion of mercury. This gap variation will change the loaded capacitance of the RSA, and consequently change its resonant frequency. By checking the resonant frequency of the antenna, the temperature can be detected. Analysis results show that this new mercury used cavity backed slot RSA provides 13MHz/10°C frequency shift, 5.47dB realized gain and 1.33% 3dB realized gain bandwidth. Its sensitivity is much improved comparing with the water and HDPE-BST designs using electric properties of materials.

5.1 Tunable Cavity Resonator

The idea of capacitively-loaded cavity RSA stems from the tunable cavity resonator. In this section, the characteristics of tunable cavity resonator are introduced.

5.1.1 Characteristics of Cavity Resonator

Before the introduction of tunable cavity resonator, the conventional cavity resonator is demonstrated herein. Resonator is a device that exhibits resonance or resonant behavior that is naturally oscillating at some frequencies, called its resonant frequencies, with higher amplitude than at others [31]. Resonators are used to either generate wave of specific frequencies or to select a signal of the resonant frequencies. The electromagnetic wave resonator which also called microwave resonators has the forms of transmission line, cavity, dielectric, etc. And they have been used in a variety of applications, including filters, oscillators, tuned amplifiers, etc.

Cavity resonator is one type of microwave resonators. Most frequently used cavity resonator is empty waveguide with two ends short circuited. The most important feature of cavity resonator is high Q. If integrated with antenna, high Q means narrow bandwidth, which really benefits the RSA designs. Similar to waveguide, there also exist different modes in the cavity resonator, such as TE, TM mode, according to its field distribution. Different modes have different wavenumber *k*, and based on the *k*, the resonant frequency at different modes can be calculated through (5-1). In the equation, *m*, *n*, and *l* represents the periodical number of the field in *x*, *y*, and *z* direction, respectively, as shown in Fig. 5-1. It is noticed that, for the same cavity, the resonant frequencies of different modes are different. If b<a<d, the dominant resonant mode will be the TE101 mode, corresponding to the TE10 fundamental waveguide mode in a shorted guide of length λ/2. And similarly, the dominant TM mode is the TM110 mode. The resonant frequency of

the cavity resonator is fixed once its dimension is determined. In most cases, a frequency tunable cavity resonator is needed. For example, a tunable microwave filter needs a tunable resonator.

$$f_0 = \frac{c}{2}\sqrt{(\frac{m}{a})^2 + (\frac{n}{b})^2 + (\frac{p}{l})^2} \tag{5-1}$$

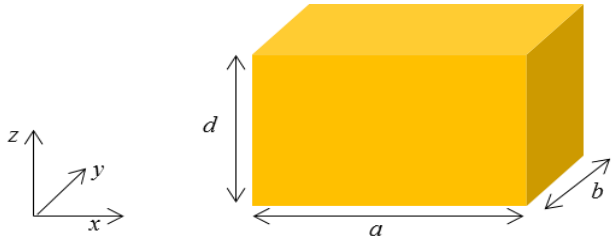

Fig. 5-1 A conventional cavity resonator.

5.1.2 Tunable Cavity Resonator

Tunable microwave filters are vital components for the next generation reconfigurable radio front-end in the wireless communication systems with multiband and multi-standard characteristics. And resonators are essential elements in the filters designs. In order to get tunable filters, first tunable resonators should be realized. The authors in [32]-[33] have proposed a capacitively- loaded cavity resonator, which has high Q, compact size, and large tunable range. Fig. 5-2 shows the cut view of a tunable cavity resonator.

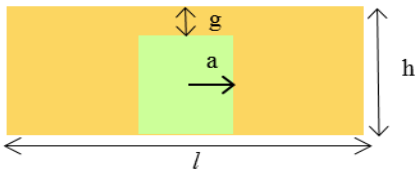

Fig. 5-2 Cut view of capacitively-loaded tunable cavity resonator.

In Fig. 5-2, it is found that a metal post is located at the center of the cavity. The metal post top and the cavity ceiling form a loaded capacitor. When the gap is small in terms of micrometers, the capacitance generated by the metal post and cavity top is very high, therefore, a small variation of the gap will make a big change of the capacitance. The resonant frequency of the cavity is then changed by the variation of the loaded capacitance. The closer the gap, the larger the loaded capacitance is. As a result, the frequency of the resonator is dramatically decreased. In this situation, the size of resonator is effectively reduced. In order to demonstrate the impacts of the loaded capacitance on the resonant frequency of the cavity resonator, a metal post of 3mm radius is placed at the center of a cylindrical cavity. The configuration of the tunable resonator is as shown in Fig. 5-2. The detailed dimensions are listed in Table 5-1. Fig. 5-3 shows the simulated resonant frequency of the tunable resonator with a varying capacitive gap. The simulation is conducted with HFSS v. 14.

Table 5-1 Detailed dimension of the tunable cavity resonator

h	a	l
5mm	3mm	236mm

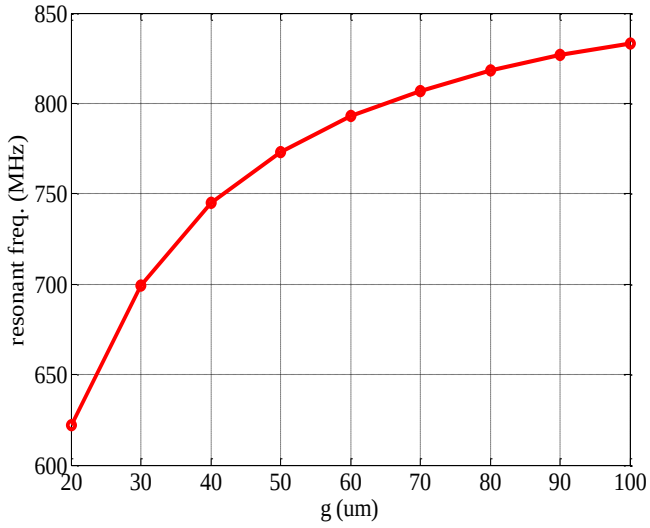

Fig. 5-3 Simulated resonant frequency of the tunable resonator with a varying gap.

According to Fig. 5-3, the gap is swept from 20μm to 100μm, and the resonant frequency is increased from around 620MHz to 830MHz. This result proves that when the gap is very small, a small variation of it will change the resonant frequency dramatically. It is observed that when the gap is 100μm, the cavity resonates at 830MHz, which is much smaller comparing with the conventional empty cavity of 900MHz resonant frequency. Thus, integrating the metal post in the cavity can reduce the size effectively. We can learn from the tunable cavity resonator that a small variation of gap between the metal post and cavity ceiling will change the frequency dramatically. This idea can be implemented in the RSA design. If the sensing material has thermal characteristics, is placed at the middle of the cavity. Then a relation between gap and temperature is established. Temperature variation will alter the gap, and then change the frequency effectively. A high sensitive temperature RSA can be realized.

5.2 Cavity Backed Slot Antenna

We learn from the tunable cavity resonator that a small variation of the gap between metal post and cavity ceiling can change the resonant frequency of the resonator effectively. If we can employ this feature in the RSA design, a high sensitive RSA can be obtained. To this end, a capacitively-loaded cavity backed slot antenna shown in Fig. 5-4 is designed. A slot antenna is cut out from a metal sheet, and an IC chip is mounted at the middle of the slot. A cavity is placed behind to the slot antenna with the sensing material located at its center. The existing of the cavity can suppress the backward radiation, thus enhance the gain of the slot antenna. In addition, it will also increase the Q factor of the slot antenna, thus narrow its bandwidth.

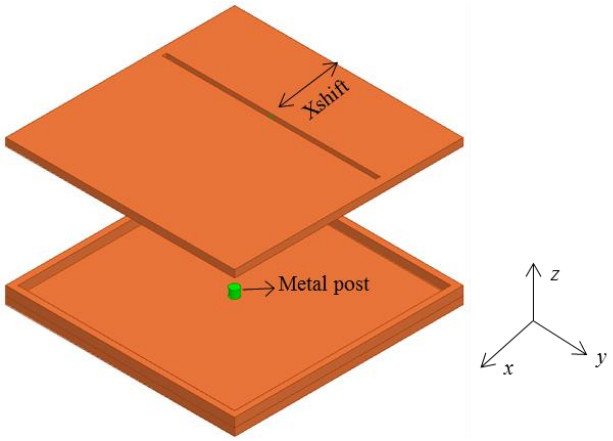

Fig. 5-4 Capacitively-loaded cavity backed slot antenna configuration.

As a RSA, there are several characteristics must be considered including antenna frequency shift with temperature ($\Delta f/\Delta T$), antenna gain, and bandwidth. Our goal is to design a high sensitive RSA. To achieve it, we first investigate how the parameters affect the RSA

performance. The parameters contains cavity, metal post cross section, gap between metal post and cavity, and slot location.

5.2.1 Cavity Effects Study

Slot antenna is a popular antenna configuration, because it can be cut out from whatever surfaces it to be mounted on. It is a λ/2 elongated slot which excited at the center. This slot behaves according to Babinet's principle [1] as a resonant radiator. This principle relates the radiated fields and impedance of a slot antenna to that of the field of a dipole antenna. The field of the slot is almost the same as the dipole antenna, but the field's components are interchanged: a vertical slot has got a horizontal electric field; and the vertical dipole has got a vertical electric field. In general, the slot antenna has unidirectional radiation pattern. In our design, a cavity is behind the slot antenna, which will suppress the backward radiation and thus enhance the directivity of the slot antenna.

As shown in Fig. 5-5, the slot is cut out from a metal layer. Behind the slot antenna, there is an empty metal cavity. To get a compact design, the cavity length is comparable to the slot length. In order to figure out the effect of the cavity to the slot performance, we start from a slot antenna cutting out from finite ground, which resonates around 900MHz. The slot length is 127mm, and the antenna is matched to the Higgs 3 chip impedance. In order to make the antenna compact, the ground size is 137mm, which is a little bit larger than the slot. The slot is 50mm away from the edge of the ground as shown in the Fig 5-5. When an empty cavity is backed to the slot antenna, it

does work like adding a parallel inductor and capacitor to the slot antenna. Thus, the characteristics of the slot antenna will be changed. Fig. 5-6 shows the S_{11} comparison between the slot antenna and cavity backed slot antenna. It is observed from the Fig. 5-6 that the cavity backed slot antenna has a higher resonant frequency than the slot antenna. This demonstrates that the cavity works more like a parallel inductor adding to the slot. Besides changing the antenna's resonant frequency, the bandwidth of the cavity backed slot antenna is narrower than the slot antenna due to more energy stored by using cavity.

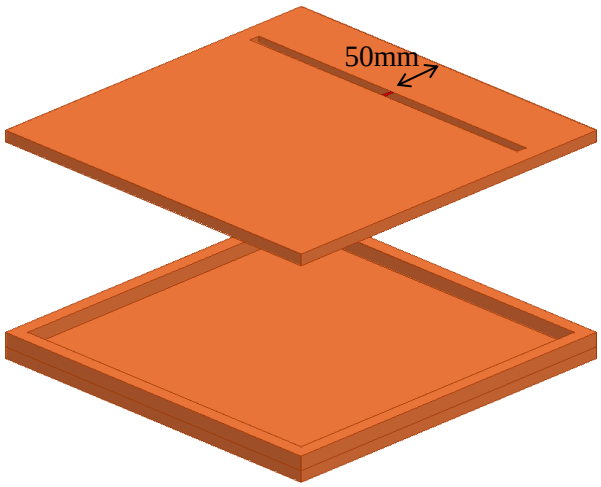

Fig. 5-5 A slot antenna is backed with empty cavity.

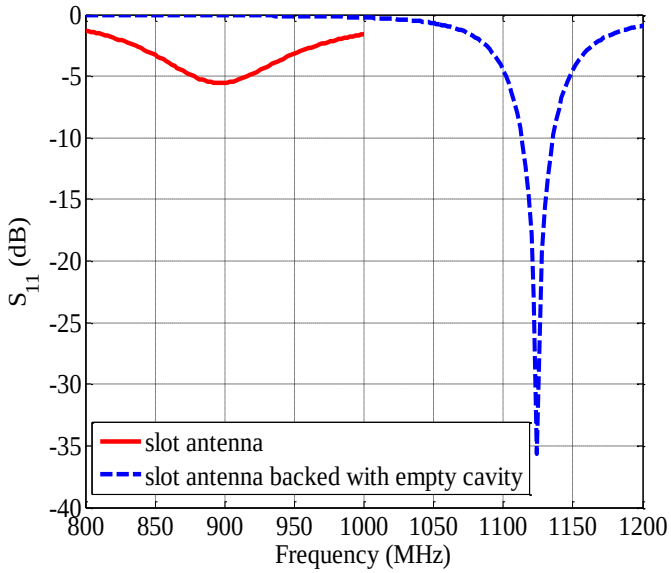

Fig. 5-6 S_{11} comparison between the slot antenna and cavity backed slot antenna.

5.2.2 Metal Post Cross Section Size Study

As mentioned before, our design goal is to get a high sensitive temperature RSA. Thus, sensing material will be placed at the center of the cavity as the metal post shown in Fig. 5-4. The material top surface and cavity ceiling form a loaded capacitor. This loaded capacitor is important to determine the RSA size. The larger the loaded capacitance, the smaller the RSA size becomes. It is known that the capacitance of a capacitor is determined by its cross section, gap, and filling material. Here, the effects of the metal post cross section size are investigated.

The capacitively-loaded cavity backed slot antenna is as shown in Fig. 5-4. It has a square cavity of 137mm side length, while the slot length is 127mm with 3mm slot width. A metal post of 5.8mm height is placed at the center of the cavity. The gap between the metal post and cavity top is

set to 0.1mm. The radius of the post is from 1mm to 4mm to explore its impact on the antenna performance.

Fig. 5-7 and Fig. 5-8 show the S_{11} and realized gain comparison between the cavity backed slot antennas with different metal post radius. It is shown from Fig. 5-7 that when the metal post radius increases, the loaded capacitance increases, and the resonant frequency of the cavity backed slot antenna decreases. When the metal post radius increases from 1mm to 4mm, the antenna resonant frequency drops dramatically from 1100MHz to around 900MHz. Meanwhile, when the metal post radius increases, the bandwidth of the antennas becomes narrower. This is because the Q factor of the antenna is increased by increasing the loaded capacitance.

It is observed from Fig. 5-8 that the realized gain value decreases with the metal radius increasing. The maximum realized gain of the RSA with 1mm post radius is 6.67dB, and the one with 4mm post radius, its realized gain drops to 5.95dB. There are two reasons for this: one is that the impedance match between the antenna and chip degrades as metal radius increases; the other is that the resonant frequency of the antenna decreases as radius increases, which make the aperture of antenna becomes smaller, thus decrease the antenna's directivity. Obviously, the realized gain bandwidth becomes narrower as the radius becomes larger. To be specifically, the 3dB realized gain bandwidth of the RSA with 1mm metal post radius is 6.17%, and the bandwidth of the RSA with 4mm radius decreases to be 2.31%, which is much narrower.

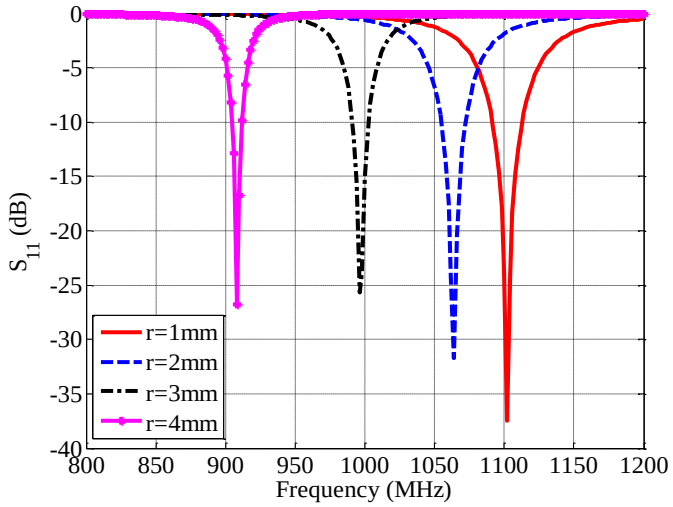

Fig. 5-7 S_{11} comparison between the cavity backed slot antennas with different metal post radius.

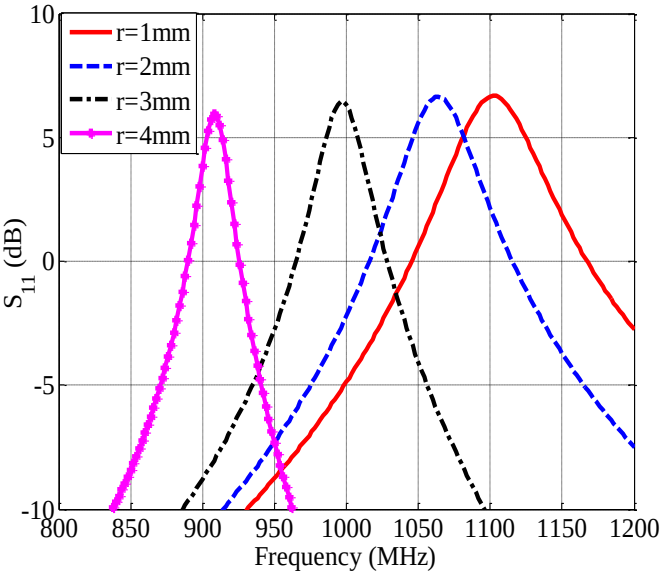

Fig. 5-8 Realized gain comparison between the cavity backed slot antennas with different metal post radius.

5.2.3 Gap Study

The mercury used cavity RSA uses the thermal expansion of mercury to tune the gap between mercury surface and cavity top. By tuning the gap, the loaded capacitance formed by the mercury and cavity are also changed. Thus the resonant frequency of the RSA is reconfigurable by temperature. The sensitivity of the RSA is closely related to the gap. In this situation, the investigation of the starting gap is important. The cavity and slot size are the same as the one used in the metal post size study, which are 137mm and 127mm, respectively. And the metal post is 5.8mm in height and its radius is 4mm.

Fig. 5-9 and Fig. 5-10 show the S_{11} and realized gain comparison between the RSAs with different gap situations. It is observed from Fig. 5-9 that when the gap is larger than 0.4mm, every 0.1mm gap variation can slightly change the resonant frequency of the RSA. To be specifically, the resonant frequency only shifts 6MHz when the gap changes from 0.6mm to 0.5mm. Obviously, during this gap range, the RSA has very limited sensitivity in terms of $\Delta f/\Delta T$. This is because large frequency variation needs large capacitance variation. For a capacitor whose cross section area and filling material are fixed, the only factor can affect the capacitor is gap. The small gap variation can change the capacitance effectively only when the two parallel metal of capacitor is in close proximity to each other. Therefore, when the gap is small than 0.4mm, a large frequency shifting is achieved.

Although the smaller gap provides better sensitivity, it would limit the temperature range the RSA can measure and also increase the difficulty in fabricate and measurement. Thus,

considering the sensitivity, temperature range, and fabrication accuracy, the original gap between metal post and cavity is set to 0.4mm.

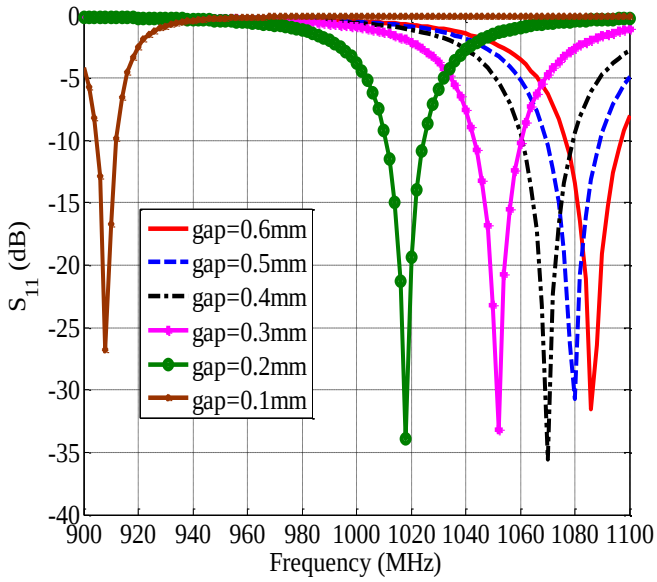

Fig. 5-9 S_{11} comparison of the RSA under different gap situations.

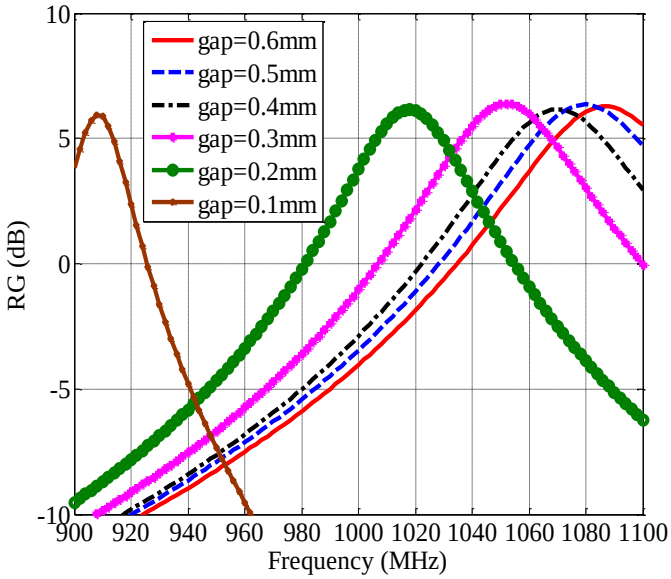

Fig. 5-10 Realized gain comparison of the RSA under different gap situations.

5.2.4 Slot Location Study

In the previous sections, the effects of cavity, metal post cross section, and gap are investigated. We learned from the cavity effects study that the usage of cavity is actually adding a parallel inductor to the slot antenna. However, how much the parallel inductor is added is related to the slot location. In this section, we focus on the slot location's effects on the antenna performance. Fig. 5-11 and Fig. 5-12 show the S_{11} and realized gain comparison of the RSAs with slot locating at different positions.

The Xshift represents the distance between the slot and the cavity edge as shown in Fig. 5-4. A large value of Xshift means the slot is near the cavity center. In this case, the two parallel inductor separated by the slot is comparable to each other, and the total added parallel inductance gets a larger value. So we can observe from the Fig. 5-11 that the resonant frequency of the antenna with slot locating near center has a lower value. On the other hand, when the slot is close to the cavity edge, the added parallel inductor is smaller, thus the resonant frequency of the RSA becomes larger, which is also illustrated in Fig. 5-11. By this study, it is clear that if one wants to get a compact design, the slot should be placed near the center of the cavity.

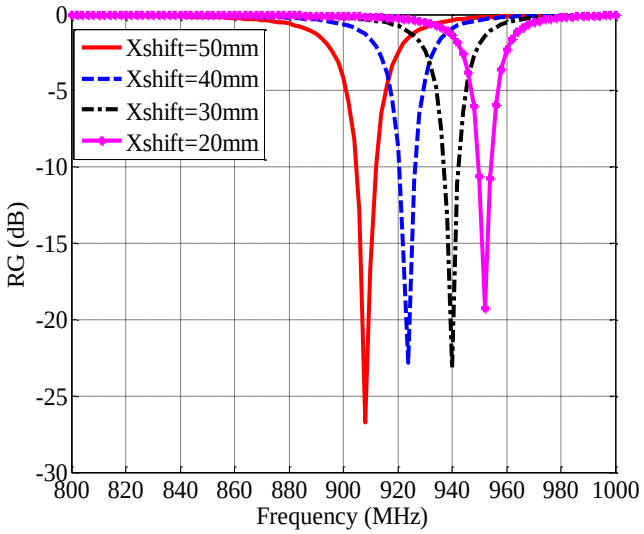

Fig. 5-11 S_{11} comparison of the RSAs with different slot locations.

One can observe from Fig. 5-12 that the realized gains of the RSAs with different slot locations are comparable with each other. The detailed information of the realized gains at resonant frequencies of the RSAs is drawn in Table 5-2. It is noticed from the Table 5-2 that, as the slot locates near the cavity edge, the realized gain bandwidth becomes narrower. The bandwidth is directly related to the Q factor of the antenna. The reason for the narrower bandwidth is that when the slot is near the cavity edge, more energy is stored around the slot, and this can be proved by the current distribution on the slot layer. Fig. 5-13 (a) and (b) show the current distributions on the RSA top layer when the slot is 20mm and 50mm away from the cavity edge. It is illustrated from the current distribution that when the slot is 20mm away from the cavity edge, more current is surrounded the slot other than radiation, thus the bandwidth of RSA in this situation is narrower. So, if a narrower bandwidth is desired, the slot should be near the cavity edge. In the RSA design,

what we want most is a high sensitivity, thus the slot is determined to place 20mm away from the cavity edge to obtain narrow bandwidth.

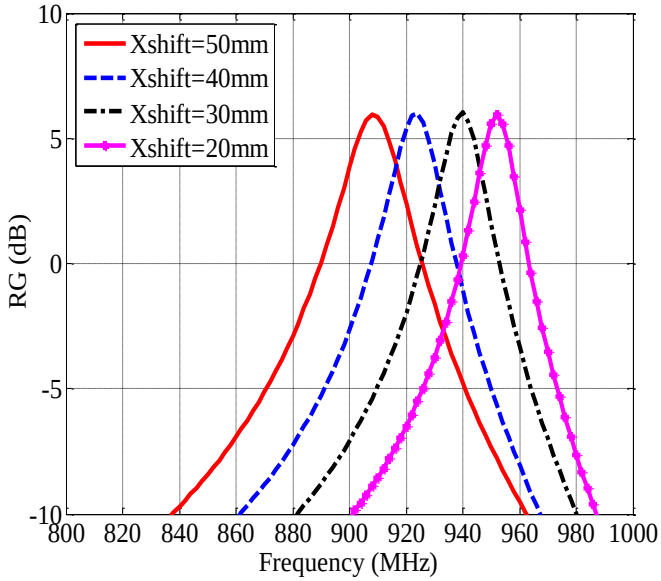

Fig. 5-12 Realized gain comparison of the RSAs with different slot locations.

Table 5-2 Detailed information of the RSAs with different slot locations

Xshift	Resonant frequency	Realized gain	Bandwidth
20mm	952MHz	5.93	1.47%
30mm	940MHz	6.02	1.7%
40mm	924MHz	5.99	1.89%
50mm	908MHz	5.95	2.31%

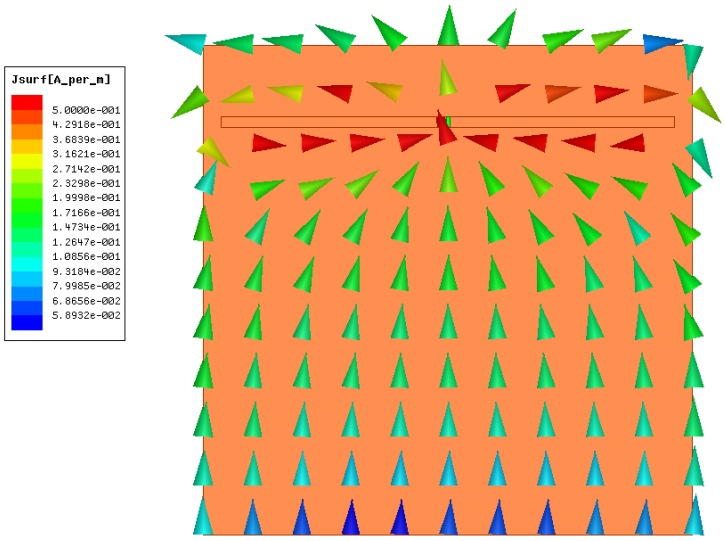

(a)

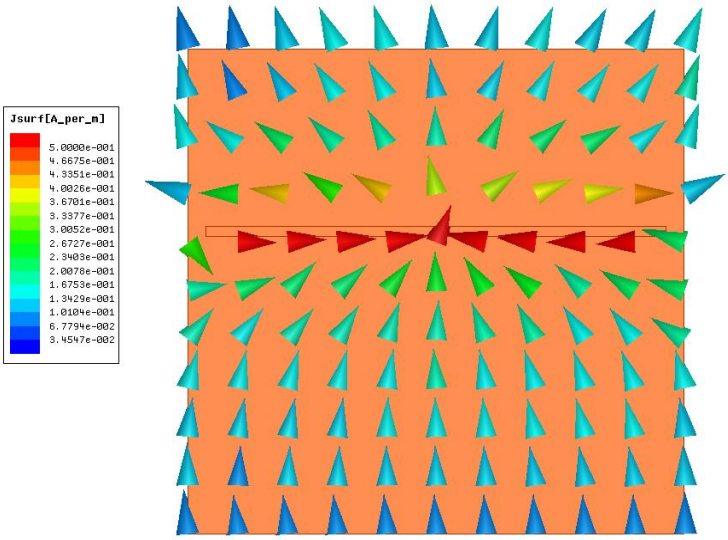

(b)

Fig. 5-13 Current distribution of the RSA with different slot locations: (a) Xshift=20mm at 952MHz, (b) Xshift=50mm at 908MHz.

5.2.5 Parameters Study Summary

In previous sections, the cavity, metal post cross section, gap, and slot location, their impacts to the slot antenna performance are studied. The existing of the cavity can enhance the antenna gain and make the bandwidth of the slot antenna narrow by increasing the Q value. The metal post introduces a loaded capacitor of the cavity backed slot antenna, which reduces the antenna size effectively. And the cross section size of the metal post is important to how much size can be reduced. The larger the cross section, the larger the loaded capacitance, the effective the antenna size is reduced. Meanwhile, the metal post with large cross section can also make the antenna have a narrower bandwidth, which is beneficial to the RSA sensitivity. The gap plays the role of tuning the loaded capacitance of the antenna. It is found that only in a small gap range, the gap variation can effectively change the resonant frequency of the antenna. This is very important for the RSA design using gap tuning to alter the antenna frequency. In addition, the location of the slot also affects the performance of the antenna. When the slot is close to the cavity edge, a narrower bandwidth is obtained. Keeping these effects in mind, and it will provide guide lines to obtain an optimum design in the following designs.

5.3 Mercury Used Capacitively-Loaded Cavity Backed Slot RSA

5.3.1 Mercury Introduction

Mercury is a chemical element which has a symbol of Hg. It is the only liquid metal at ordinary temperature and pressure. Its freezing point is -38.83℃ and boiling point is 356.73℃.

And it has a large volume thermal expansion coefficient of 180ppm/℃. Mercury has been used widely such as thermometer, mercury switches, mirror telescope, medicine. Among these applications, mercury thermometer is the one most commonly used. In the thermometer, thermal expansion of mercury is employed. Usually, in a mercury thermometer, a bulb is used to store mercury and a tiny tube with scale on it is used to read the temperature. The reason of utilizing this configuration can be easily understood from the expansion calculation method.

Fig. 5-14 shows a conventional thermometer. The relation between the mercury level and temperature can be calculated based on (5-2). The mercury stored in the bottom bulb is represented by V. As temperature increases, the mercury expands outward in the tiny tube. Assume that the tube has a cross section of A, once the change of mercury volume ΔV is obtained, the increase of mercury level Δ*l* can be calculated. To get a large Δ*l*, the cross section of tube should be as small as possible. Because of the large thermal expansion of mercury, we can use it as temperature sensing material in the capacitively-loaded cavity RSA design.

Fig. 5-14 A conventional mercury thermometer.

$$\Delta l = \frac{\Delta V}{A} = \frac{V \times 180 \times 10^{-6} \times \Delta T}{A} \tag{5-2}$$

5.3.2 Mercury Storage Methods

In the proposed capacitively-loaded cavity backed slot RSA design, mercury is selected as the temperature sensing material. The sensing principle is that the mercury is stored at the center of the cavity, and its surface forms a loaded capacitor with cavity top. The thermal expansion of mercury will change the gap between mercury and cavity top. This gap variation will alter the loaded capacitance, which consequently changes the resonant frequency of the cavity RSA. Thus, there is a relation established between the resonant frequency and temperature. And by checking the resonant frequency, the surrounding temperature can be monitored. However, Mercury is a liquid material, so how to store mercury becomes a main concern.

The mercury thermometer indicates that a two layer structure is favorable for the mercury storage, which can maximize the expansion of mercury level. Based on this, two different mercury storage methods are designed which are shown in Fig. 5-15. Both of them are two layer cylindrical structures. The bottom layers have large radius and are used to store mercury. And the top layers, their radius is much smaller comparing with the bottom ones. In this situation, when temperature changes, the mercury level could have a large increase, which means the gap will be changed effectively. The large gap variation is benefit for the RSA sensitivity.

The difference between the two methods is that in method 1, there is only one small tube on the top layer; however, in method 2, there are four small tubes on the top layer. The bottom layers of the two methods have same radius and inner height, which is 20 mm by 3.5 mm. However, their top layer radiuses are different, which is 3 mm in method 1 and 1.5 mm in method 2. It is

worthwhile to mention here that the two methods although have different top layer tube radius, but their total cross section area are the same. The reason of doing this is to verify that whether the mercury location affects the RSA sensitivity.

The cut view of the two different storage methods is shown in Fig. 5-16. The two mercury containers both have 1mm thickness, and are 0.1 mm below the cavity top. The total thickness of the mercury container is 5.8 mm.

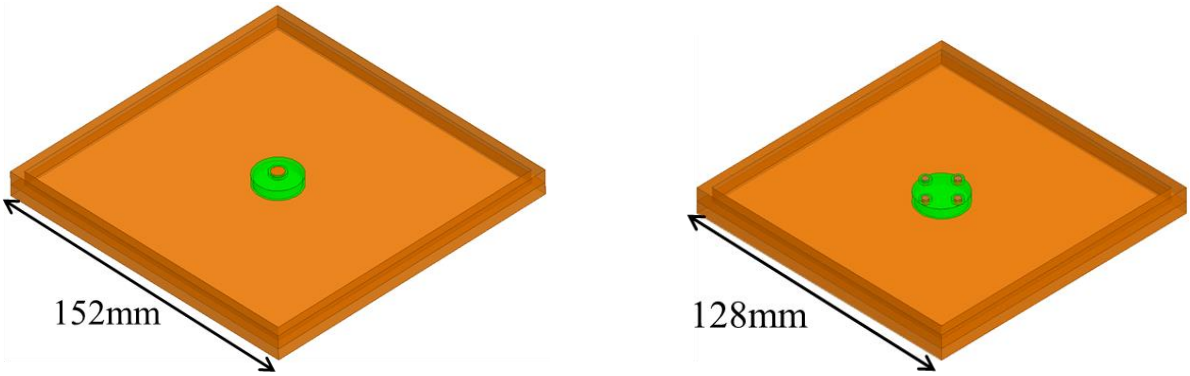

(a) (b)

Fig. 5-15 Mercury storage methods of the cavity RSA: (a) method 1, (b) method 2.

(a) (b)

Fig. 5-16 Cut views of the mercury containers: (a) method 1, (b) method 2.

5.3.3 Characteristics of the Two Mercury Used RSAs

In previous section, two mercury storage methods are presented. Both of them have the same volume and same top layer cross section. According to the mercury expansion calculation method shown in (5-2), the mercury expansions of using these two storage methods are the same. And the original gap between the mercury surface and cavity top **g**, is set to 0.4mm based on the gap study previously.

There are two cavity RSAs designed to resonate at 900MHz.One is the cavity RSA using mercury storage method 1, which has 152mm cavity length and 142mm slot length. And the other is the cavity RSA using mercury storage method 2, which has 128mm cavity length and 118mm slot length. The smaller cavity size of the RSA using method 2 is because the larger copper cross section of the top layer tubes in method 2 results in a larger loaded capacitance, which reduce the cavity size.

Fig. 5-17 (a) shows the simulated S_{11} comparison between the two RSAs using mercury storage method 1 and method 2. The detailed dimension of these two RSAs is shown in Fig. 5-15. It is observed from Fig. 5-17 (a) that the two RSAs both resonate at 900MHz and are matched well to the Higgs 3 IC chips. Fig. 5-17 (b) shows the broadside realized gain comparison of the two designs. The realized gains of method 1 and method 2 are 5.96dB and 5.47dB, respectively. It is also noticed from the Fig. 15-7 (b) that the realized gain bandwidth of method 1 design is wider than that of method 2 design. This is because in method 2 design, the larger loaded capacitance increases the antenna's Q factor, which results in a narrower bandwidth.

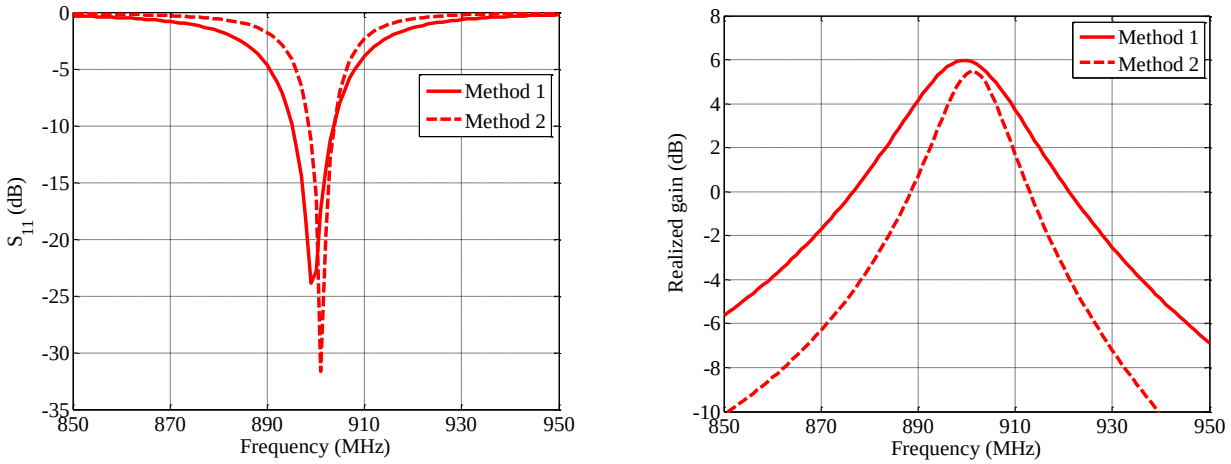

(a) (b)

Fig. 5-17 Simulated results of the mercury used RSA using mercury storage method1 and method 2: (a) S_{11} comparison, (b) realized gain comparison.

5.3.4 Sensitivity Analysis of Mercury Used Cavity RSA

In previous section, two RSAs using different mercury storage methods are illustrated. They are matched well to the chip impedance and have high realized gain. However, as a sensing antenna, besides maintaining a good antenna performance, its sensitivity is also important. In this section, the temperature sensitivities of the two RSAs are investigated. Table 5-3 shows the gap between mercury and cavity at different temperatures. As mentioned before, the original gap at 20°C is 0.4mm. Based on the (5-2), one can easily get the gap information under different temperatures. Because the mercury volume and cross section area of the two containers are the same, so the gap variations of the two RSAs are also the same.

Table 5-3 Relation between gap and temperatures

Temp. (℃)	20	30	40	50	60
Gap (mm)	0.4	0.33	0.26	0.19	0.12

Based on the information in Table 5-3, the performance of the RSAs at different temperatures is obtained. Fig. 5-18 shows the S_{11} and realized gain under various temperatures of the cavity RSA using mercury storage method 1. It is found that the RSA resonates at 900MHz at 20°C. As temperature increases, the thermal expansion of mercury will make the gap smaller. The smaller gap provides a larger loaded capacitance. As a result, the resonant frequency of the RSA decreases. The higher the temperature, the larger the frequency shifts. This is because, when the gap is small, the same gap variation affects more on the loaded capacitance. The maximum frequency variation with temperature is 13MHz/10°C, which improves a lot comparing to the water RSA of 4MHz/10°C and HDPE-BST RSA of 8MHz/10°C. Meanwhile, the realized gain of the RSA is high with a narrow bandwidth, which is 2.78%. The detailed sensitivity information in terms of $\Delta f/\Delta T$, realized gain, and realized gain bandwidth are shown in Table 5-4.

Fig. 5-19 is the S_{11} and realized gain of the cavity RSA using mercury storage method 2 under various temperatures. It is observed that this design also resonates at 900MHz at 20℃. As temperature increases, the frequency decreases as shown in Fig. 5-18. The higher the temperature, the larger the frequency shifts. The reason is mentioned before. The maximum frequency shift with temperature is around 14MHz/10°C, which is comparable to the design using mercury

storage method 1. However, the 3dB realized gain bandwidth of this design is 1.33%, which is narrower than the method 1 used design. The detailed sensitivity information is also listed in Table 5-4. Table 5-4 is a comparison table which also includes the sensitivity of the water RSA and the HDPE-BST RSA. From Table 5-4, it is notice that the sensitivity of mercury RSA designs improves effectively comparing with the designs using electrical properties of materials. Especially the realized gain and $\Delta f/\Delta T$, which are improved from -3dB to more than 5dB, and from 8MHz/10°C to 14MHz/10°C. In addition, the bandwidth of the mercury RSAs is also narrower.

In order to compare the performance of the two mercury RSAs, their resonant frequencies versus temperature and realized gain at resonance frequency under different temperatures are plotted in Fig. 5-20 (a) and (b), respectively. It is noticed from Fig. 5-20 (a), the RSAs using different mercury storage methods have similar $\Delta f/\Delta T$. This result indicates that the frequency shift of the capacitive loaded RSA is not strongly affected by the capacitor location. From Fig. 5-20 (b), one can observe that the realized gain of RSA using method 1 is 0.4dB higher than that of the RSA using method 2. This is due to larger aperture size of the method 1 used RSA. Comparing the two mercury RSAs, the one using mercury storage method 2 is favorable than the method 1 used design, because it has narrower bandwidth while maintaining comparable $\Delta f/\Delta T$ and realize gain.

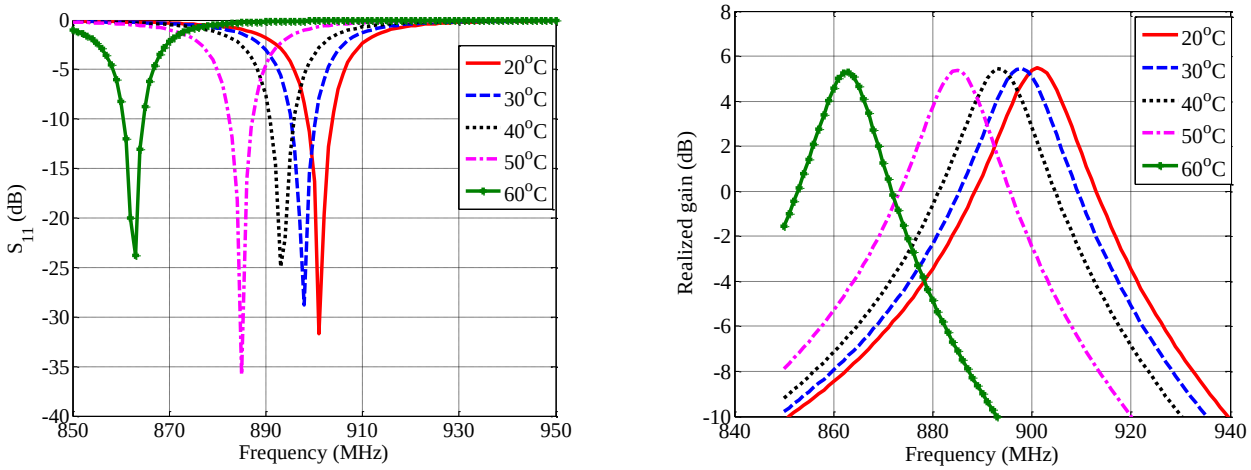

(a) (b)

Fig. 5-18 Simulated RSA performance of mercury used cavity RSA using storage method 1: (a) S_{11} at different temperature, (b) realized gain at different temperature.

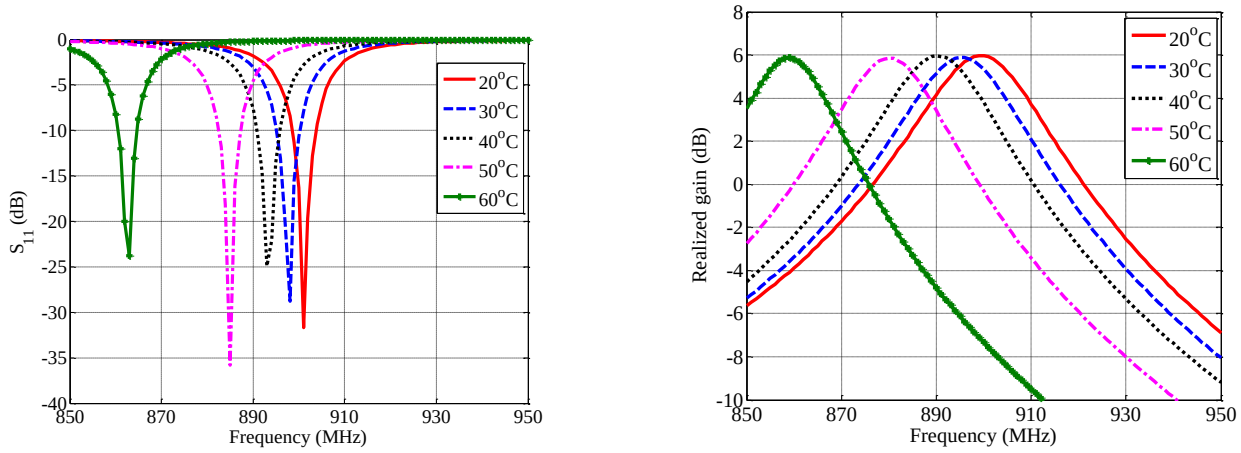

(a) (b)

Fig. 5-19 Simulated RSA performance of the mercury used cavity RSA using storage method 2: (a) S_{11} at different temperature, (b) realized gain at different temperature.

Table 5-4 Sensitivity Comparison of the water RSA, HDPE-BST RSA, and Mercury RSAs

	Water RSA	HDPE-BST RSA	Mercury RSA (Method 1)	Mercury RSA (Method 2)
Δf/ΔT	4MHz/10℃	8MHz/10℃	14MHz/10℃	13MHz/10℃
Realized gain	-3.2dB	-3.8dB	5.96dB	5.47dB
3dB bandwidth	4.33%	0.67%	2.78%	1.33%

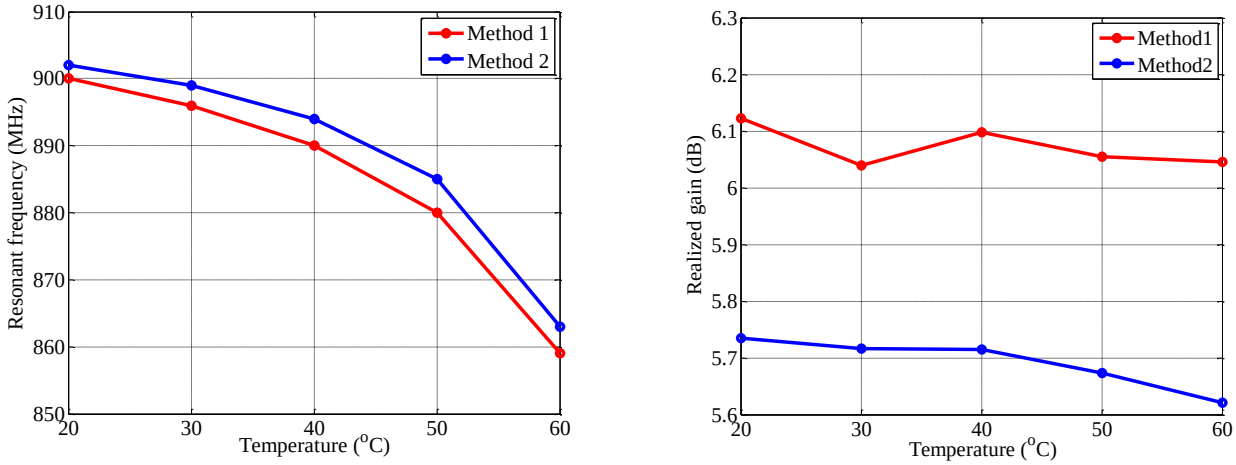

(a) (b)

Fig. 5-20 Performance comparison of the mercury used cavity RSAs: (a) frequency shift comparison, (b) maximum realized gain comparison.

5.3.5 Loss Analysis

The loss of antenna is important to determine its gain. It is known that the loss includes dielectric loss and metallic loss. The dielectric loss is attributed to bound charge and dipole relaxation phenomena in the dielectric material, which gives rise to energy loss that is indistinguishable from the loss due to the free charge conduction that is quantified by σ. The metallic loss is due to the finite conductivity of the metal material. In the mercury RSAs, the loss is mainly attributed from the metallic loss from mercury and copper.

In this section, the metallic loss of mercury and copper is investigated. The method 2 used mercury RSA proposed in previous section is used to illustrate the loss produced by mercury and copper container. It is known that mercury has a conductivity of 1.06×10^{6}, and copper has a conductivity of 5.8×10^{7} . Both of them have finite conductivity and thus produce loss. Fig. 5-21 shows the directivity and gain comparison between different loss conditions of the method 2 used mercury RSA. They are the normal design, lossless mercury, and lossless copper container. In the normal case, both mercury and copper loss exist, so it has the smallest gain, which is represented by the solid curve. When the mercury becomes lossless, which means only the copper loss exist, the gain of the RSA is comparable to the normal case. This illustrates that the mercury loss has a little contribution to the total loss. When the copper container becomes lossless, the total gain is maximum 0.2dB higher than the normal case, which demonstrates that the loss from the copper container is much higher than mercury.

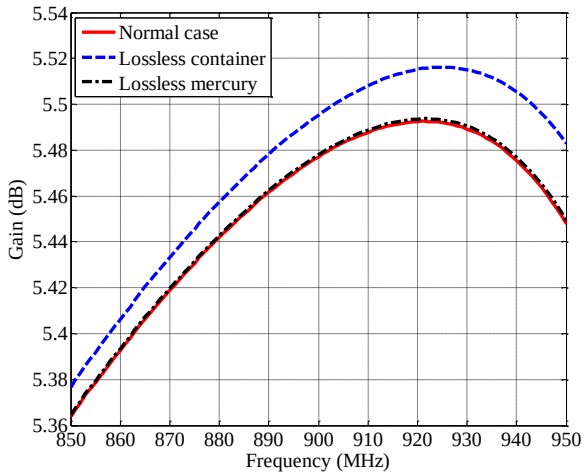

Fig. 5-21 Gain comparison of the mercury used RSA using mercury storage method 2.

5.4 Summary

Different from the RSA designs using electric properties of materials, the thermal properties of material is utilized in the RSA design in this chapter. Mercury is selected as the sensing material because it has a large thermal expansion of 180ppm/°C. In order to implement mercury in the antenna design and realize high temperature sensitivity, capacitive loaded cavity backed slot antenna is used. By placing the mercury in the container located at the cavity center, a loaded capacitor is generated between the mercury and cavity ceiling. As temperature increases, the thermal expansion of mercury changes the loaded capacitance, which results in an antenna frequency variation.

In order to properly store mercury and get good sensitivity, two different mercury storage methods are designed and analyzed. The one with four small top layer tubes are favorable, because it can make the mercury RSA has 13MHz/°C frequency shift with temperature, 5.47dB realized

gain, and 1.33% 3dB realized gain bandwidth. The mercury used cavity backed slot RSAs are proved to offer much better sensitivity than the electric properties used RSAs. However, because mercury is liquid and toxic material, it is hard to implement in the experiment. In this situation, other sensing materials should be considered to replace mercury.

CHAPTER VI

RSA USING THERMAL PROPERTIES OF MATERIAL: PTFE USED CAPACITIVELY-LOADED CAVITY BACKED SLOT RSA

The mercury used cavity RSAs have been demonstrated in last chapter. The results show that the mercury used cavity RSA possess 13MHz/10°C frequency shift with temperature and 5.47dB realized gain. Its sensitivity is much improved comparing with the designs using material's electrical properties. However, it is known that mercury is a liquid material, which makes it hard to implement in practice. Additionally, mercury is toxic which means it needs to be used carefully. All of these deficiencies restrict the employment of mercury in RSA designs.

In this chapter, a solid material, namely, Polytetrafluoroethylene (PTFE) is utilized as temperature sensing material to replace mercury due to its large thermal expansion coefficient of 140ppm/°C. Similar to the usage of mercury in RSA design, a PTFE post is also integrated in a cavity backed slot antenna to form a temperature-dependent loaded capacitor with cavity ceiling. The copper coated PTFE is placed at the center of the cavity, and in close proximity to the cavity ceiling. Because the solid status of PTFE, it can be placed very close to the cavity ceiling, which is only 0.09mm. In this small gap, the thermal expansion of PTFE has a much effective impact on the resonant frequency of the antenna. The experiment results show that the maximum $\Delta f/\Delta T$ of PTFE used RSA can achieve 40MHz/10°C, and its realized gain is 4.17dB with a 0.66% 3dB bandwidth,

which provides a 14m read range. When compared to the mercury used RSA, the RSA using PTFE has a smaller size and higher sensitivity in terms of $\Delta f/\Delta T$ and antenna bandwidth.

Although the PTFE used RSA has a high sensitivity, its size, which is 104mm by 104mm, is a little bulky. So, the method of reducing the cavity RSA size without sacrificing its sensitivity is also presented in this chapter. At last, the size of the cavity RSA is reduced 30% comparing with the conventional square one, while its sensitivity maintains 38MHz/10°C.

6.1 PTFE and Its Storage Methods

In a RSA design, sensing material is important to determine its sensitivity. In previous chapter, mercury is selected as the temperature sensing material because of its high thermal expansion coefficient. However, as mentioned before, the implementation of mercury in practice is difficult due to its liquid status. In this situation, a solid material Polytetrafluoroethylene (PTFE) is found that also has a large thermal expansion coefficient. Therefore, PTFE is chosen as the sensing material to replace mercury.

6.1.1 Characteristics of PTFE

Polytetrafluoroethylene (PTFE) has been widely used in microwave substrates and packaging applications because it exhibits excellent dielectric properties, such as low permittivity ($\varepsilon_r = 2.1$), extremely low loss tangent ($\tan\delta$=0.00001 at 800MHz). In addition, the PTFE also has the advantages of easy-machinability, good chemical resistance, high service temperature (<250°C), especially large linear coefficient of thermal expansion (>100ppm/°C). Its large thermal

expansion and easy-machinability make it a good candidate of temperature sensing material. Fig. 6-1 shows a side view of a PTFE cylinder with 6mm diameter and 5mm height. The linear thermal expansion of the proposed PTFE cylinder in height direction is measured using a thermo-mechanical analyzer in the range 25–120°C, which is also shown in Fig. 6-1. It is observed from the measurement results that the PTFE has a thermal expansion coefficient of 120ppm/°C.

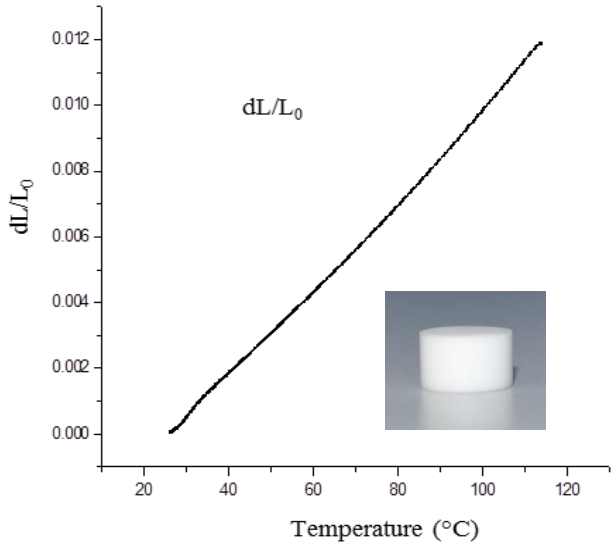

Fig. 6-1 Thermal expansion of the PTFE post in height direction.

PTFE is a dielectric material, so if used to form a loaded capacitor with the cavity ceiling, it should be coated with metal. In this chapter, the surface of PTFE is coated with copper due to its good conductivity. Fig. 6-2 shows the side view of a copper coated PTFE which has 6mm diameter and 5mm height. Its thermal expansion coefficient is measured and also shown in Fig. 6-2. It is observed from the results that from 25°C to 125°C, the linear thermal expansion coefficient of the

copper wrapped PTFE cylinder is 140ppm/°C, which is larger than 120ppm/°C of the PTFE itself due to the thermal expansion of copper. This 140ppm/°C of copper wrapped PTFE is much larger than the normal materials such as Rogers RO3003, whose thermal expansion coefficient is only 25ppm/°C. Based on the measurement results, one can easily get the relation between temperature and gap, when the PTFE is placed at the cavity.

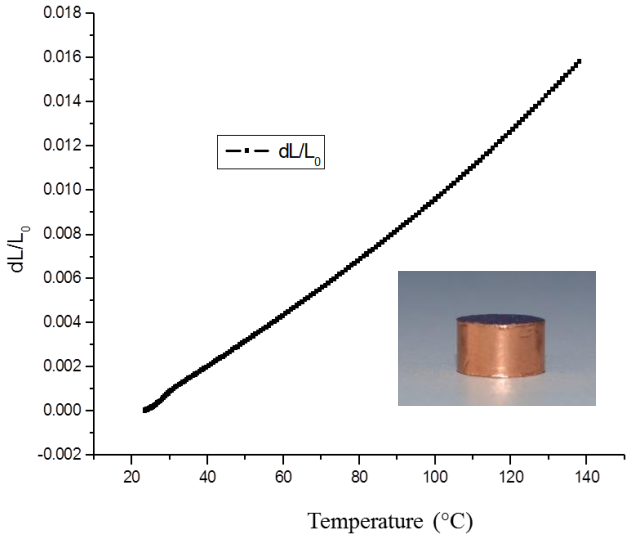

Fig. 6-2 Thermal expansion of copper wrapped PTFE post in height direction.

6.1.2 PTFE Storage Method

As mentioned before, the sensing material PTFE is placed at the center of the cavity. In order to fix it, a copper container is built there. Now, the problem is to determine the relation between the height of PTFE and the height of container to obtain a high sensitivity. The

configuration of the PTFE used RSA is shown in Fig. 6-3. The cavity is a square one with side length 80mm, and the slot on it has a length of 70mm and a width of 3mm. The slot is located 8mm away from the cavity edge. The PTFE post is placed at the center of cavity with 3mm radius. And the container used to fix it has 2.05mm thickness. The bottom cavity has a height of 11mm, where the inner side wall is 5.9mm and ground thickness is 5.1mm. The thickness of slotted cover is 5.75mm. In order to figure out the best relation between PTFE height and the container height, three PTFE storage methods are investigated as shown in Fig.6-4. In all the methods, the height of PTFE height is set to 5.81mm, which is 0.09mm behind the cavity cover.

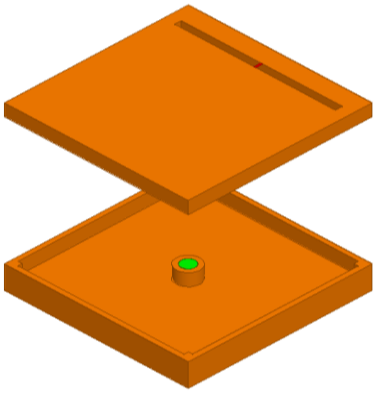

Fig. 6-3 Configuration of the PTFE used cavity.

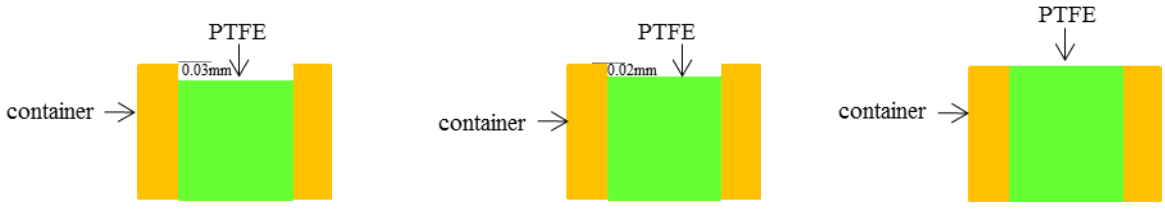

(a) (b) (c)

Fig. 6-4 PTFE storage methods: (a) method 1 where container 0.03mm higher than PTFE, (b) method 2 where container 0.02mm higher than PTFE, (c) method 3 where container and PTFE has same height.

The configuration of method 1 is shown in Fig. 6-4 (a), where the height of copper container 5.84, 0.03mm higher than the PTFE post. In this situation, the characteristics of the RSA with the gap variation are studied. Fig. 6-5 shows the S_{11} and realized gain of the RSA under different gaps, which are 0.09mm, 0.08mm, 0.07mm, and 0.06mm. It is observed from Fig. 6-5 (a) that as the gap decreases from 0.09mm to 0.06mm, the resonant frequency of the RSA drops from 890MHz to 847MHz. On the other hand, it is noticed from Fig. 6-5 (b) that maximum realized gain also decreases as gap decreases. To be specifically, the realized gain decreases from -1dB to -2dB when the gap decreases from 0.09mm to 0.06mm. This is because when the gap is small, the E filed inside it becomes much stronger which results in higher loss. In addition, in the small gap situation, the RSA resonates at a lower frequency, which results in a smaller directivity for the RSA. In one word, when the container height is 5.84mm, the RSA using this PTFE storage method 1 provides a realized gain of -1dB, which is too low. In this situation, other storage methods are investigated.

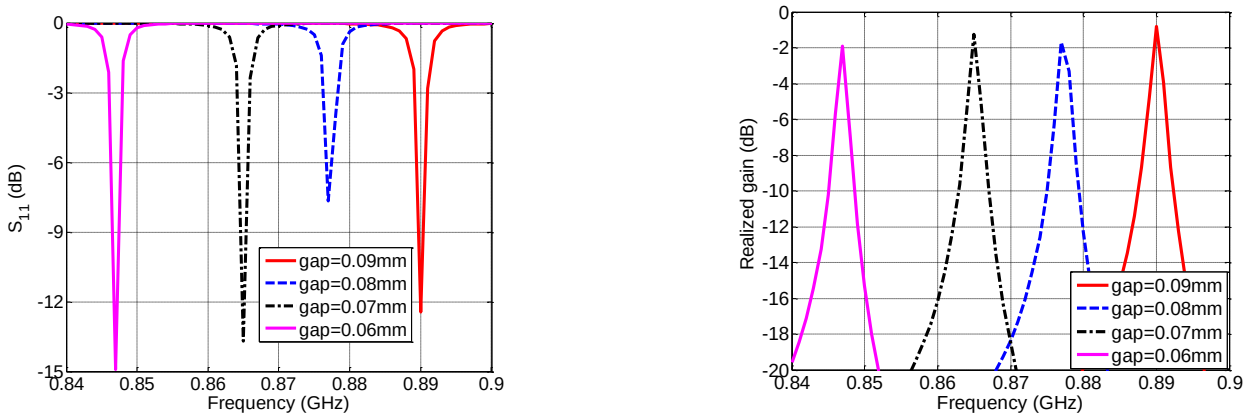

(a) (b)

Fig. 6-5 The characteristics of the RSA using storage method 1: (a) S_{11} under different gaps, (b) realized gain under different gaps.

The PTFE storage method 2 is shown in Fig. 6-4 (b), where the container has a height of 5.83mm, 0.02mm higher than the PTFE post. Other parameters of the cavity RSA are the same to that used in method 1. Similarly, the RSA characteristics under different gap situation of using storage method 2 are also studied. Fig. 6-6 shows the S_{11} and realized gain comparison of the RSA under different gaps, which are 0.09mm, 0.08mm, and 0.07mm, respectively. It is noticed from Fig. 6-6 (a) that when the gap between PTFE and cavity top is 0.09mm, the resonant frequency of the RSA is 935MHz. Comparing with the RSA using storage method 1 at same situation, which is 890MHz, the resonant frequency of the RSA increases a lot. This is because the copper container top surface and cavity ceiling also form a loaded capacitor. When the container height becomes smaller in method 2, the gap between them becomes larger which results in a smaller capacitance. That is the reason of higher resonant frequency of the RSA using method 2. As the gap between

PTFE and cavity top decreases from 0.09mm to 0.07mm, the resonant frequency also decreases from 935MHz to 907MHz. It is observed from Fig. 6-6 (b) that when the gap is 0.09mm, the realized gain of the RSA becomes 0dB, which is improved comparing with the -1dB of the method 1 used RSA. This is because gap between container and cavity top becomes bigger in method 2, which decrease the loss. In addition, the RSA resonating at higher frequency makes it possess a higher directivity. It is also noticed from the Fig. 6-6 (b) that as gap decreases, the realized gain drops a little.

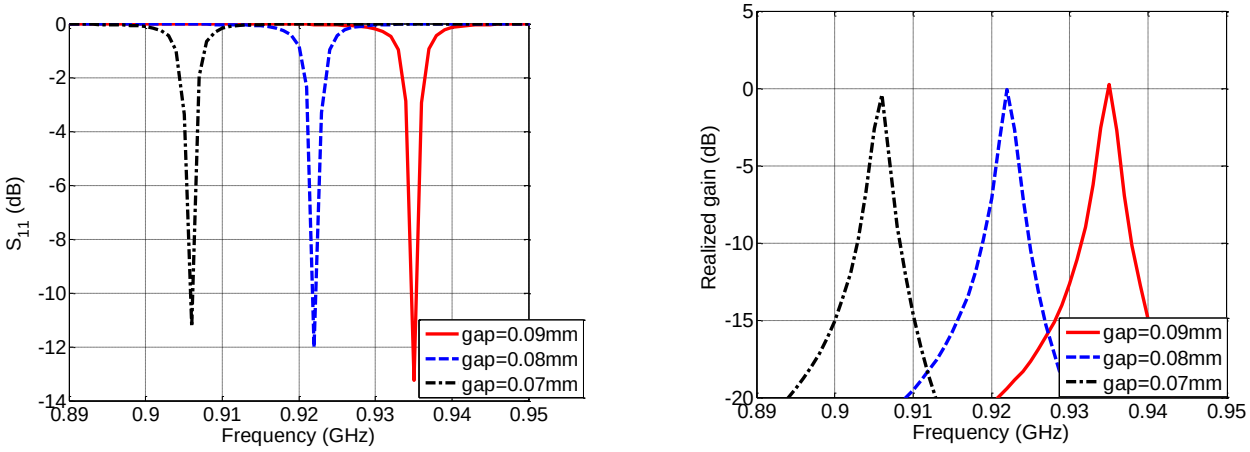

(a) (b)

Fig. 6-6 The characteristics of the RSA using storage method 2: (a) S_{11} under different gaps, (b) realized gain under different gaps.

Although the PTFE storage method 2 used RSA provides a higher realized gain, its value is still smaller than 5.47dB of the mercury used cavity RSA. Therefore, another storage method, which is method 3, is proposed here. The PTFE storage method 3 is shown in Fig. 6-4 (c), where

the container height is 5.81mm, which is the same as the PTFE. The simulated S_{11} and realized gain under different gap are shown in Fig. 6-7. It is observed from Fig. 6-7 (a) that as the gap decreases from 0.09mm to 0.07mm, the resonant frequency of the RSA decreases from 1009MHz to 972MHz. And its realized gain drops from 1.7dB to 0.93dB. The RSA using method 3 has the best realized gain. This is because the gap between container and cavity top becomes large which reduce the loss. In addition, the frequency shift with temperature of this one is higher than the one using method 2 in the same gap variation. To be specifically, when the gap changes 0.02mm, the RSA using method 2 has a frequency shift of 28MHz. However, the RSA using method 3 can provide 37MHz. Thus, the PTFE storage method 3 is used in the following designs.

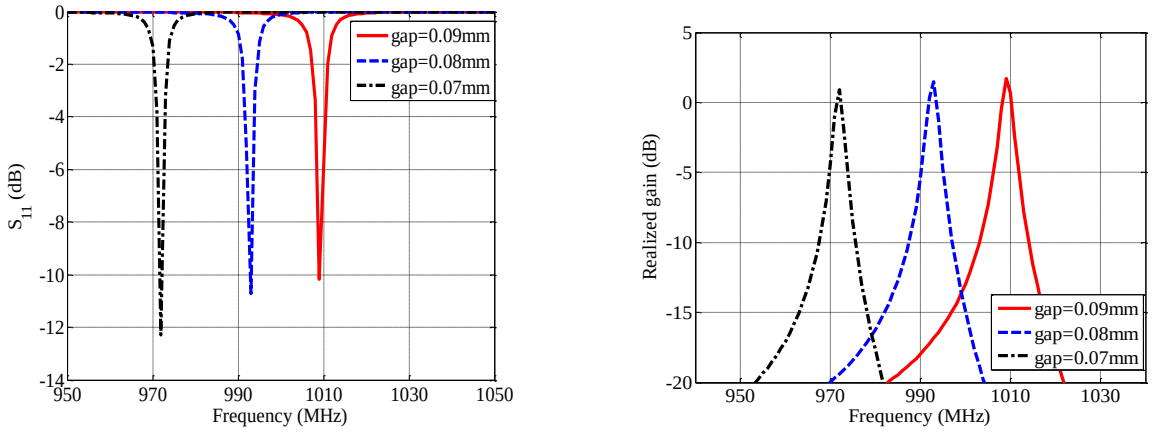

(a) (b)

Fig. 6-7 The characteristics of the RSA using storage method 3: (a) S_{11} under different gaps, (b) realized gain under different gaps.

6.2 PTFE Used Capacitively-Loaded Cavity Backed Slot RSA

6.2.1 An Optimum Design of the PTFE Used Cavity Backed Slot RSA

As mentioned before, the cavity backed slot antennas (CBSAs) [34]-[35] are usually high gain and narrow bandwidth, which are beneficial for the RSA designs. Different from the conventional CBSA, in order to design a high sensitivity RSA, PTFE is integrated at the center of the CBSA to form a temperature dependent loaded capacitor. In order to fix it and constrain its radial expansion, the PTFE is placed in a copper container. In previous section, the relation between container and PTFE are investigated. And the results show that when the PTFE height is the same as the container, the RSA has a better sensitivity. Thus, in the followings, the container height is set to the same as the PTFE's. Theoretically, the smaller the gap between PTFE and cavity top, the more effective its variation on altering the loaded capacitance, the higher the sensitivity is obtained. However, one must consider the fabrication accuracy, thus the gap between the center container and cavity top is decided to be 0.09mm.

It is obviously that to obtain a high sensitivity, the thermal expansion of the PTFE, which relates to the original height of objects, should be as large as possible. However, when considering the cavity thickness in design, a compromise should be made between the size and sensitivity of the RSA. Therefore, a PTFE with thickness 5.81mm at 20°C is selected. By calculation, its thermal expansion is 8 μ m/10°C.

From the previous gap study, it is indicated that the frequency shift of the PTFE used cavity RSA with gap variation is large. In the experiment, the Tagformace device is used to measure the

performance of the RSA. The Tagformance has a frequency sweep from 800MHz to 1000MHz. To guarantee the resonant frequencies of the RSA are always in this range, the RSA is designed to resonate at 920MHz at the room temperature of 20°C, when gap is 0.09mm. By considering the fabrication issues, an optimum PTFE used cavity RSA is designed as shown in Fig. 6-8 (a). The detailed dimension of the RSA design is shown in Table 6-1. The cavity is made of copper due to its good conductivity. The whole cavity has a volume of 104 by 104 by 16mm, where 16mm is the total height of the cavity including 11mm of the cavity bottom and 5mm of the cover. And the 11mm cavity bottom is composed of 5.1mm ground and 5.9mm side walls. The reason of choosing such a thick cavity ground and cover is to reduce the deformation of the copper in fabrication and measurement. Fig 6-8 (b) shows the slotted cover, where the slot is located 20mm away from the edge. And a Higgs 3 chip is mounted on the middle of the slot. Fig. 6-9 (c) and (d) shows the top view of the cavity bottom and the top view of the center container with PTFE inside.

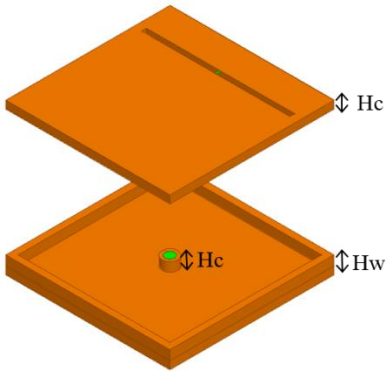

(a)

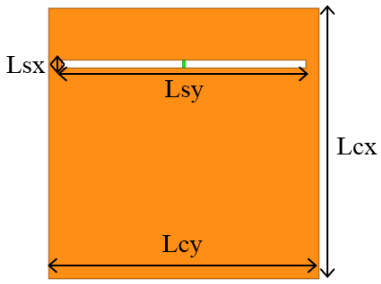

(b)

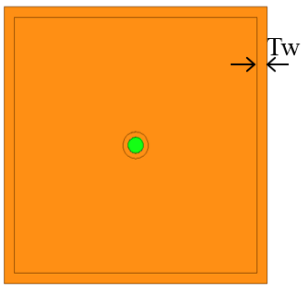

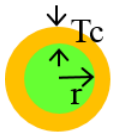

(c) (d)

Fig. 6-8 Configuration of the optimum PTFE used cavity RSA: (a) prospective view, (b) top view of cover, (c) top view of cavity, (d) top view of center container.

Table 6-1 Dimensions of the optimum PTFE used cavity RSA design

Lcx/Lcy	Lsx	Lsy	Hc	Tc	r	Hw	Tw	Hc
104	94	3	5.81	2	3	5.9	4	5

Fig. 6-9 shows the simulated S_{11} of the proposed cavity RSA. It is noticed that the RSA resonates at 920MHz with a narrow bandwidth as expected. The gap between PTFE and cavity ceiling is 0.09mm. And in Fig. 6-10 the radiation pattern of directivity and gain of the RSA at 920MHz are plotted. It is observed that the directivity of the RSA is 5.2dB directivity and its gain is 4.4dB. In addition, the front to back ratio (FTBR) of the RSA is high, which is 7dB. The high gain and FTBR is because the cavity of the RSA plays a role of metal shield to reduce the backward radiation, thus enhance its gain. Its broadside realized gain is plotted in Fig. 6-11 which is 4.17dB and has a 3dB bandwidth of only 0.66%. This high gain and narrow bandwidth is favorable for the RSA design. Fig. 6-12 shows the theoretical read range of the cavity RSA calculated based on Friis formula, which is around 15mm at 920MHz.

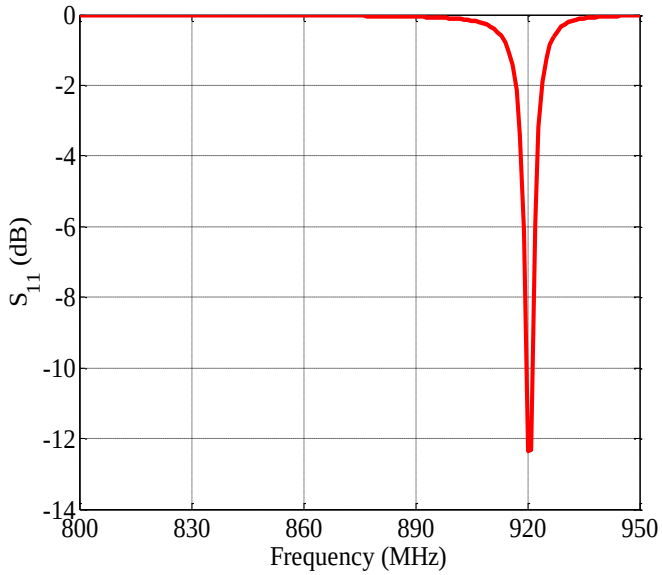

Fig. 6-9 Simulated S_{11} of the optimum RSA design when the gap is 0.09mm at 20°C.

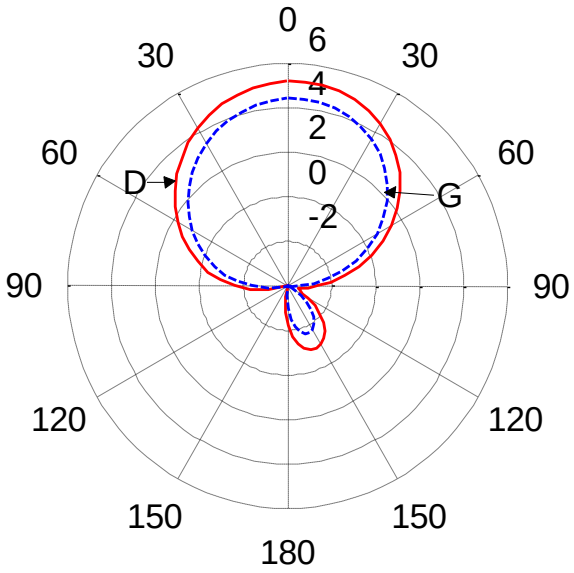

Fig. 6-10 Simulated radiation pattern of directivity and gain of the RSA at 920MHz.

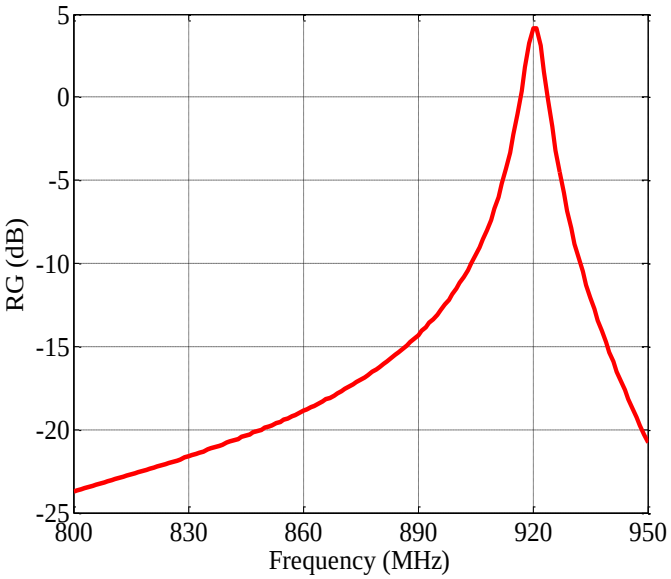

Fig. 6-11 Simulated broadside realized gain of the RSA when gap is 0.09mm at 20°C.

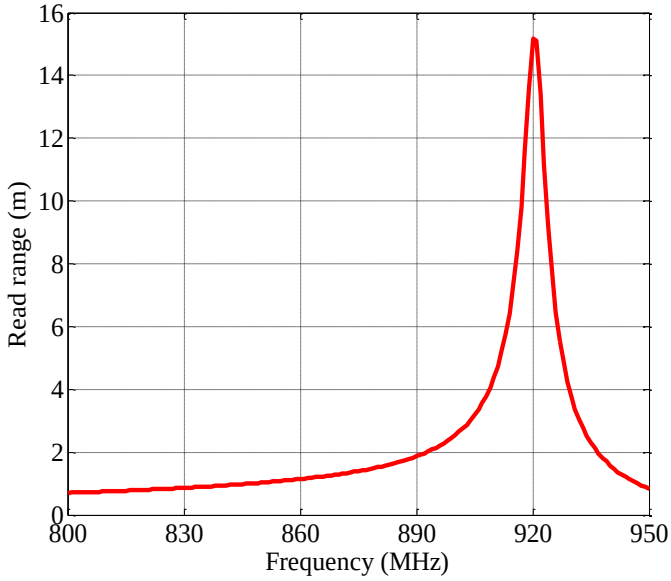

Fig. 6-12 Theoretical read range of the cavity RSA when gap is 0.09mm at 20°C.

6.2.2 Temperature Sensitivity Analysis

The proposed cavity RSA uses the thermal expansion of the PTFE to change the gap between PTFE and cavity top, therefore reconfigure the RSA's resonant frequency. In this situation, the relation between temperature and gap is important to determine the RSA's sensitivity. Table 6-2 shows the gap information under different temperatures. As mentioned before, the height of the copper coated PTFE is 5.81mm, where the copper layer is 0.05mm.Thus the copper coated PTFE has a 0.09 mm gap to the cavity top at 20°C. As temperature increases, the gap becomes smaller. The variation is about 8 μ m/10°C. Based on the information shown in Table 6-2, the RSA's characteristics at different temperatures can be obtained using HFSS.

Figure 6-13 shows the simulated S_{11} under various temperatures. It shows that RSA's resonant frequency is strongly affected by the temperature. To be specifically, as the temperature increases from 20°C to 40°C, the resonant frequency of the RSA drops from 920MHz to 843MHz. Finally, a 40MHz/10℃ frequency shift with temperature is obtained. And Fig. 6-14 shows the simulated realized gain at broadside direction of the RSA under different temperatures. The realized gain at 20°C is around 4.17dB and decreases as temperature increases. This is because as temperature increases, the gap becomes smaller which results in a stronger E filed. Thus, the loss is increased. Meanwhile, as the gap decreases, the realized gain bandwidth becomes narrower. This is because the loaded capacitance is increased which results in a higher Q factor of the RSA. The detailed information of the RSA's sensitivity is drawn in Table 6-3. One can calculate the theoretic read range of the RSA based on the realized gain by Friis formula. The read range of the RSA

under different temperatures is illustrated in Fig. 6-15. It is observed that this cavity RSA has a read range as far as 15m.

Table 6-2 Relation between temperatures and gap

Temperature (°C)	20	30	40
Gap (mm)	0.09	0.082	0.074

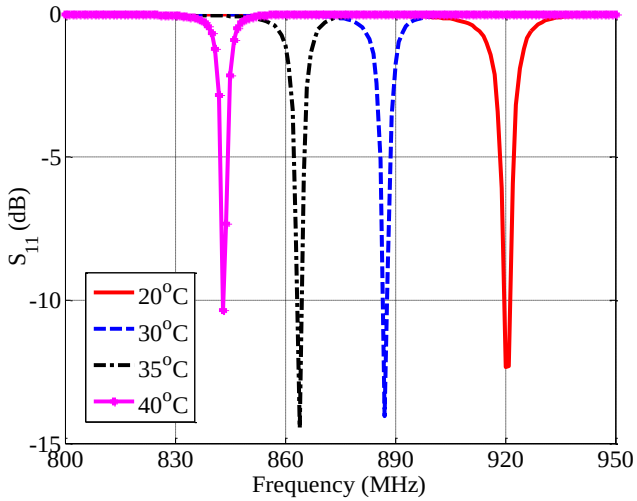

Fig. 6-13 Simulated S_{11} of the optimum RSA under various temperatures.

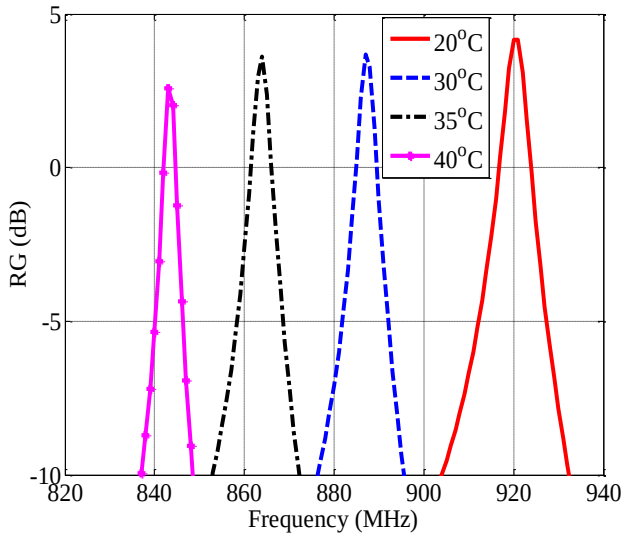

Fig. 6-14 Simulated realized gain of the optimum RSA under various temperatures.

Table 6-3 Sensitivity of the optimum RSA

Temperature (°C)	20	30	35	40
Resonant freq. (MHz)	920	887	864	843
Realized gain (dB)	4.17	3.7	3.6	2.6
Realized gain bandwidth	0.66%	0.56%	0.43%	0.24%

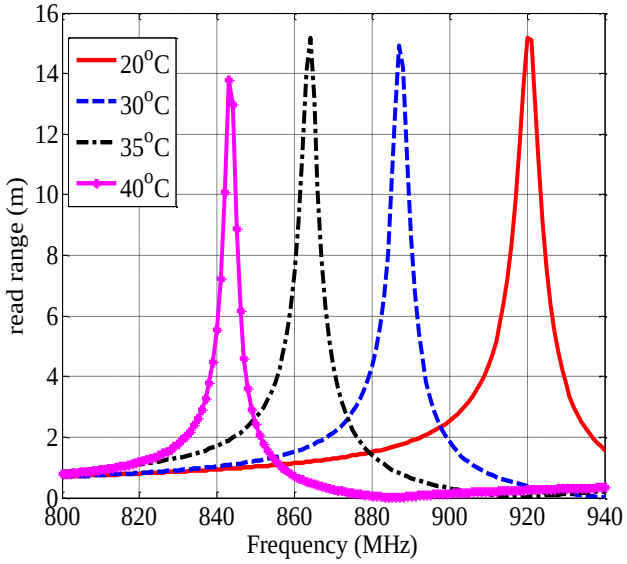

Fig. 6-15 Simulated broadside read range of the optimum RSA under different temperatures.

6.2.3 Experiments Setup and Results

In order to validate the simulation results, the cavity RSA is fabricated with copper. The fabrication prototype is shown in Fig. 6-16. There are totally 16 holes in the side wall and cavity top, where the screws are used to make the two parts of the cavity hermetically touched. Copper coated PTFE is placed in the center container. Theoretically, the gap between the PTFE and cavity ceiling is 0.09mm at 20°C.

The RSA is placed face to face to a reader in an anechoic chamber as shown in Fig. 6-17. The distance between the reader and the RSA is 0.5m. The reader sends out the electromagnetic waves, and the RSA backscatters the incoming wave under the control of IC and sensor. By measuring the backscattered power, the read range of the RSA can be calculated. The equation used to obtain the read range is the same one used in previous chapters.

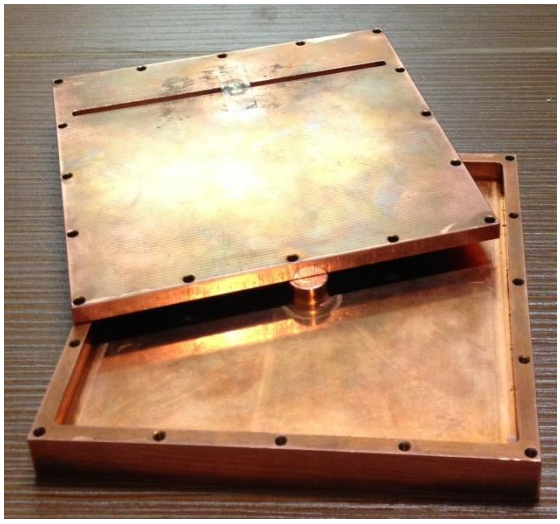

Fig. 6-16 Fabrication prototype of the PTFE used cavity RSA.

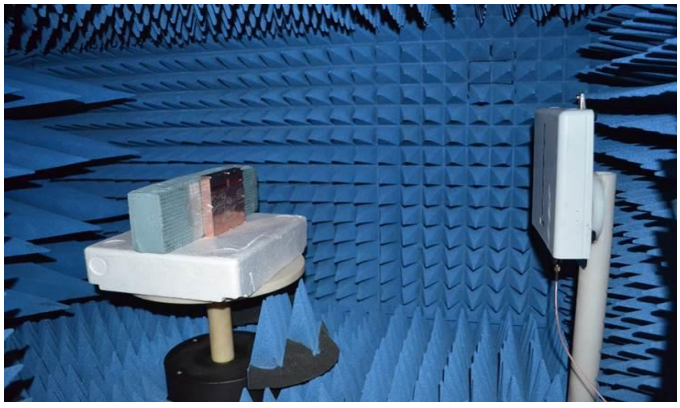

Fig. 6-17 Measurement setup of the PTFE used cavity RSA.

In order to validate its temperature sensitivity, the RSA is heated by an electronic heating platform outside the chamber. Figure 6-18 (a) shows the measured read range under different temperatures. It is observed that the RSA resonates at 917MHz with a 14m read range at 22°C, which are similar to the theoretical results. When the temperature increases, the resonant frequency decreases dramatically as expected. Finally, a maximum 40MHz/10°C frequency shift

is obtained. Although the measured temperature is 40°C due to the scope of the measurement facility, the RSA is able to monitor higher temperature. The measurement is repeated three times to validate the performance of the RSA. Fig. 6-18 (b) and (c) shows the measured read ranges of the RSA under different temperature in the second and third measurement, respectively. Both of them have read range more than 12m, and comparable frequency shift with temperature to the results obtained in first measurement. In order to get a clear comparison, Fig. 6-19 shows the resonant frequency of the RSA at different temperature among the simulation and three times measurements. They are in good agreement.

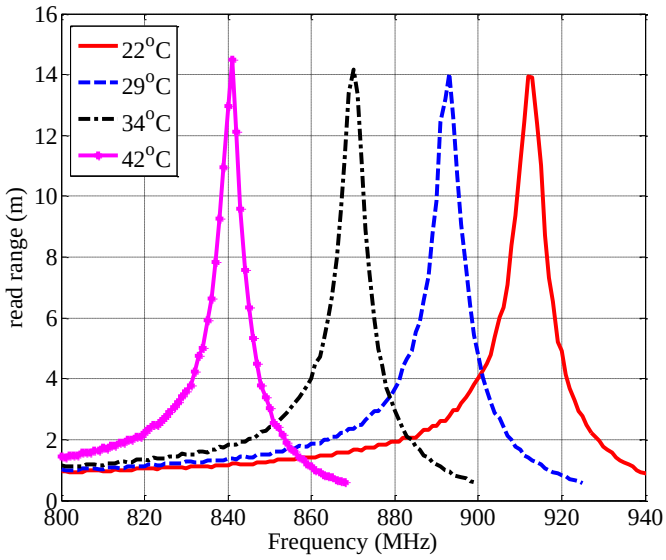

(a)

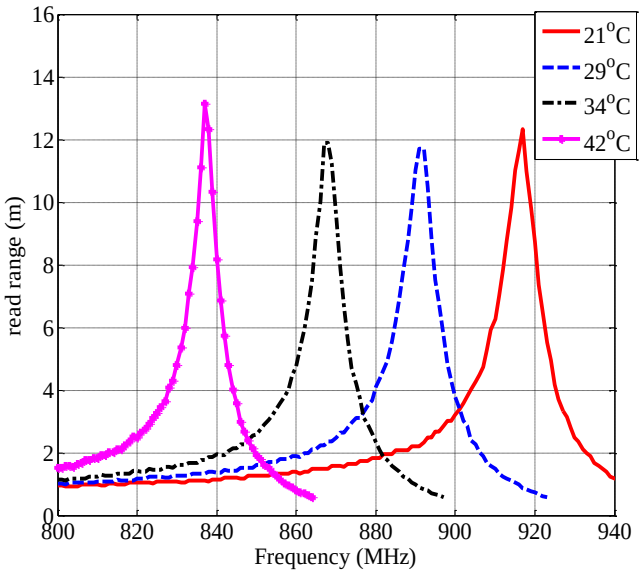

(b)

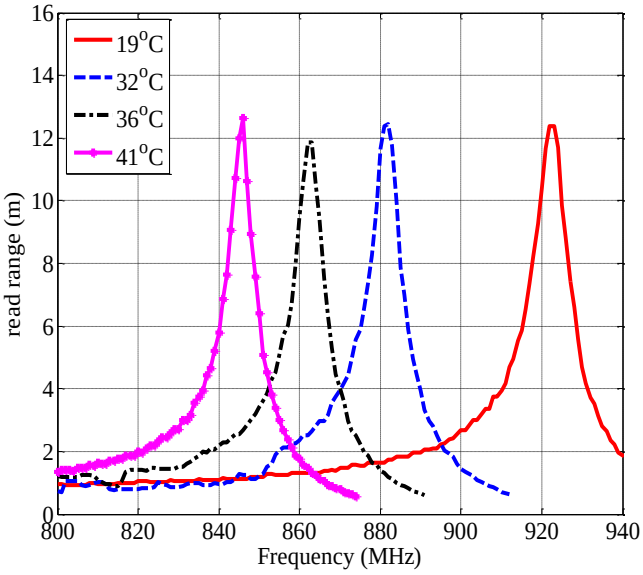

(c)

Fig. 6-18 Measured read range of the PTFE used cavity RSA: (a) first time measurement, (b) second time measurement, (c) third time measurement.

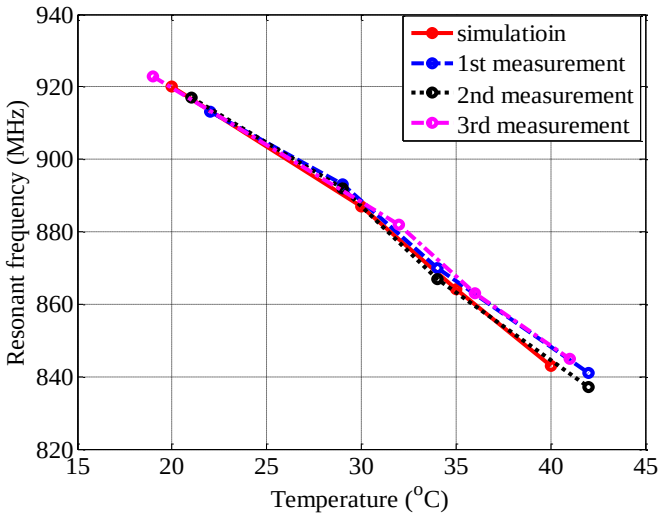

Fig. 6-19 Resonant frequency of the RSA under different temperatures comparison between simulation and measurements.

Besides measuring the RSA from low temperature to high temperature three times to verify its validation, it is also measured from high temperature to low temperature to confirm the results. Fig. 6-20 shows the measured read range of the RSA in different heating procedures. Fig. 6-20 (a) shows the read range measured from low to high temperatures. And Fig. 6-20 (b) shows the read range measured from high to low temperatures. It is seen that no matter the temperature is from high to low or low to high, the RSA performance is stable. A more clear comparison is shown in Fig. 6-21, where the resonant frequency of the RSA at different temperatures using two different measurement procedures is plotted. It is observed that the two results agree with each other.

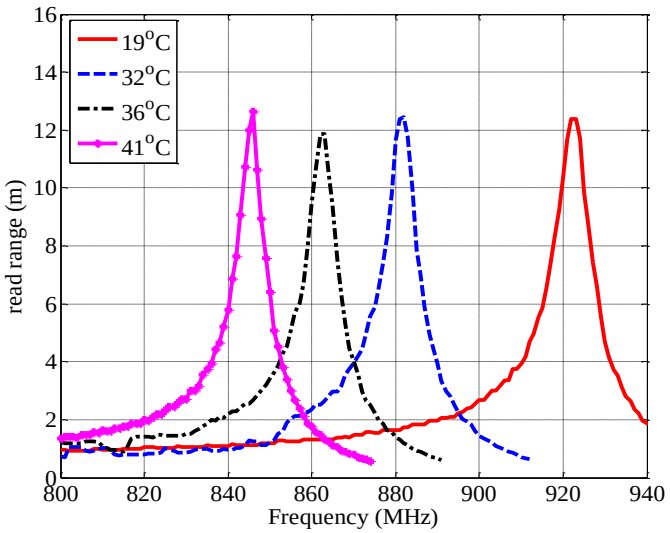

(a)

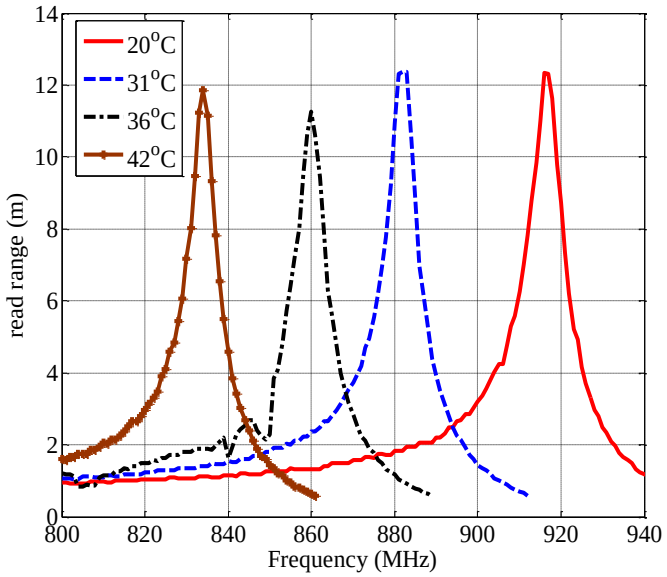

(b)

Fig. 6-20 Measured read range of the RSA in different heating procedures: (a) measurement is conducted from low temperature to high temperature, (b) measurement is conducted from high temperature to low temperature.

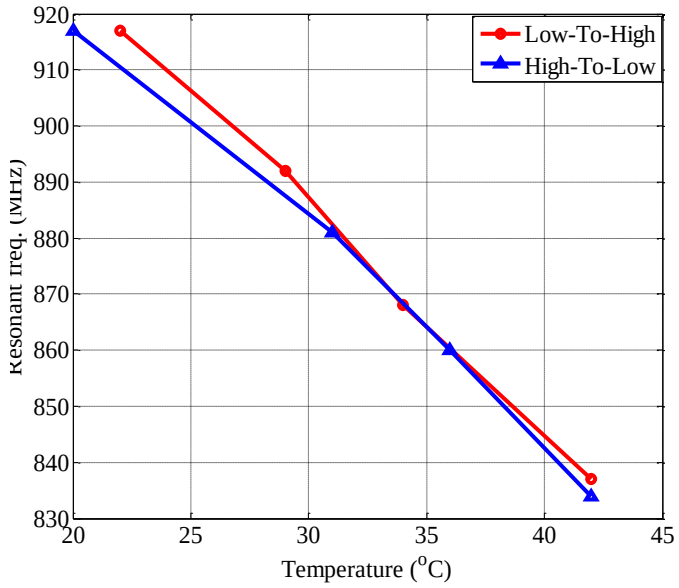

Fig. 6-21 Resonant frequency of the RSA at different temperatures using different measurement procedures.

6.3 Size Reduction of the PTFE Used Cavity RSA

The PTFE loaded cavity RSA introduced previously offers a temperature sensitivity of 40MHz/10°C, which is the best result for the known frequency reconfigurable sensing antennas. However, its size of 104mm is a little bulky which restricts its deployment. Therefore, in the following section, the size reduction methods of the PTFE used cavity RSA are investigated.

There are several methods can be used to reduce the cavity size. One is to increase the loaded capacitance of the RSA by decreasing the gap. This method can significantly reduce the cavity size. However, the fabrication accuracy is difficulty to satisfy. The other is to use a high dielectric material in the cavity to reduce its size. This method also can reduce the cavity size. However the integration of high dielectric material will introduce more loss to the RSA. In this

situation, the method used to reduce the cavity size herein is to change the configuration of the RSA itself. To be specifically, the cavity is designed in rectangular shape instead of square one as shown before. The cavity length is reduced in the direction which is perpendicular to the slot, while maintaining the length of the other side. Besides the size reduction, another PTFE storage method is also introduced in the following sections.

6.3.1 New PTFE Storage Method

In the previous RSA designs, the PTFE post is placed inside a copper container which located at the center of the cavity. Both the container and PTFE have same height to realize a good sensitivity. This condition is easy to satisfy in simulation. However, when it comes to the measurement, there are two things must be guaranteed: one is the gap between the container and cover, the other is the height alignment of the PTFE and container. Although the container can fix the PTFE post, the usage of it introduces difficulty to fabrication and measurement. In this situation, a new PTFE storage method by using copper pin to fix the PTFE post is introduced. The copper pin is also located at the center of the cavity as shown in Fig. 6-22. And the PTFE drilled with a hole will be fixed by the copper pin. This method is simple and easy to implement in fabrication. Meanwhile, there is no need to do the alignment with container which makes the measurement also easy to conduct.

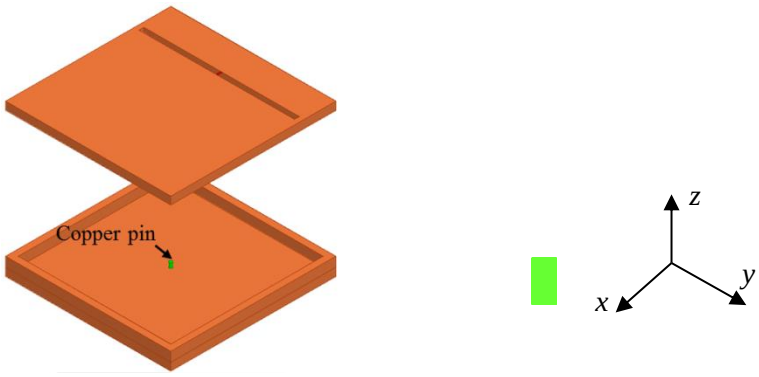

(a) (b)

Fig. 6-22 The new PTFE storage method by using copper pin: (a) RSA configuration, (b) the copper pin.

Before investigating the size reduction method of the cavity RSA, the impact of the new PTFE storage method is studied. Starting from the square cavity RSA with the new PTFE storage method, the side length of the cavity is 104mm, the slot size and position are the same as the PTFE cavity using copper container as shown in Fig. 6-8. The RSA is also designed to resonate at 920MHz. In order to achieve this goal, the gap between the copper wrapped PTFE and cavity ceiling is set to be 0.09mm, and the PTFE radius is 5mm. The PTFE is wrapped with copper, which has a thickness of 0.05mm. The simulated S_{11} is shown in Fig. 6-23. It is observed that the RSA resonates at 921MHz. And the realized gain at broadside at 921MHz is 4.15dB with 3dB bandwidth 0.65%, which is shown in Fig. 6-24. This result is comparable to the 4.17dB of the container used RSA. Based on the results shown in Fig. 6-23 and Fig. 6-24, it is learned that the RSA using copper pin to fix the PTFE post has the similar characteristics of the one using container.

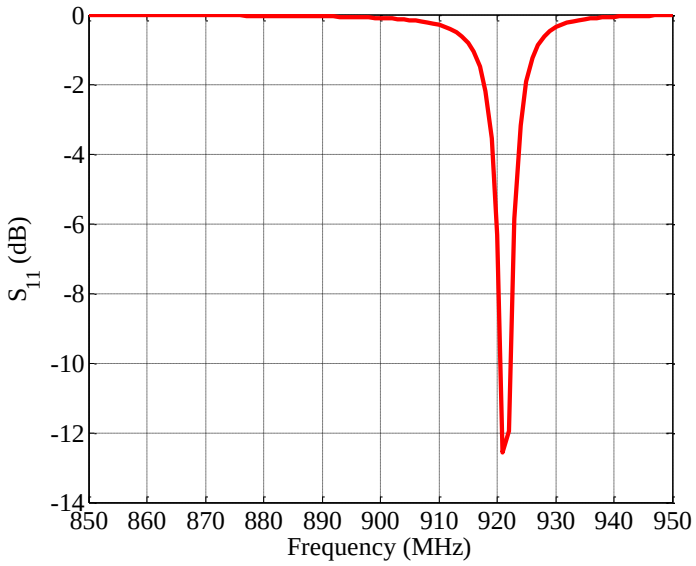

Fig. 6-23 S_{11} of the square cavity RSA using new PTFE storage method.

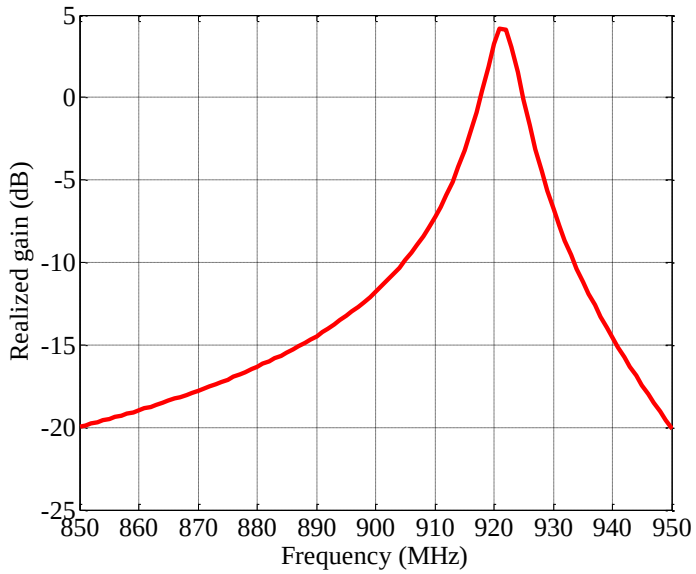

Fig. 6-24 Broadside realized gain of the square cavity RSA using new PTFE storage method.

6.3.2 Size Reduction of the Cavity RSA

As shown in Fig. 6-22, slot aligns with the *y* direction, and the current flow is along the *x* direction. It is known that the resonant frequency of RSA is mainly determined by the slot length. In order to obtain a compact design, the cavity length along *x* direction is reduced, while maintaining the other parameters. In this situation, the resonant frequency of the RSA has no big change. However, because the radiation of the RSA is mainly attributed by the current of the surface, thus as we decrease the cavity size in *x* direction, the directivity of the RSA will be decreased. The simulation results of the cavity with different *x* direction side length are shown in Fig. 6-25. The cavity length in *x* direction is reduced from 104mm to 64mm with 10mm step, while the cavity length in *y* direction keeps 104mm. It is observed that when the side length reduced from 104mm to 84mm, the resonant frequency of the RSA is almost the same. As the cavity size keeps reduced, the resonant frequency of the RSA increases a little. This is because the cavity works like a parallel inductor to the slot antenna, when its size reduced, the parallel inductance decreased, thus the resonant frequency of the RSA is increased.

Fig. 6-26 shows the broadside realized gain comparison between the RSA with different cavity side lengths. It is seen that the as the cavity size reduces, the realized gain of the RSAs decreases. The reduced realized gain is due to two reasons: one is the degraded match between the chip and RSA, the other is the compact size caused smaller directivity. The detailed information about the S_{11} and realized gain at different cavity side length are listed in Table 6-4. The realized gain drops from 4.15dB to 2.6dB when the cavity size decreased from 104mm to 64mm. The design goal is to obtain a compact size RSA with moderate realized gain resonating at 920MHz.

Based on this, the cavity size is selected to be 74mm, because at this side length, the realized gain and resonant frequency of the RSA both meets the requirements.

Table 6-4 Detailed information of the RSA with different side lengths

Lcx	Lcy	Resonant frequency	Realized gain
104	104	921	4.15
94	104	921	4.11
84	104	922	3.76
74	104	926	3.19
64	104	935	2.6

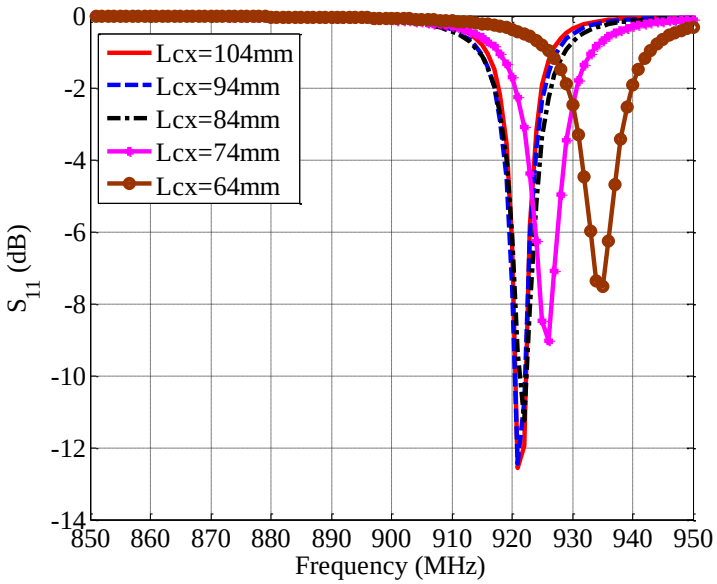

Fig. 6-25 S_{11} comparison between the RSAs with different side lengths.

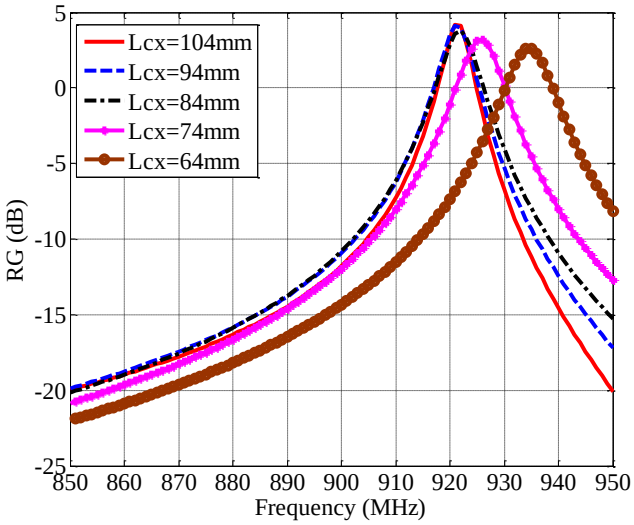

Fig. 6-26 Realized gain comparison between the RSAs with different side lengths.

6.3.3 New Capacitively-loaded Rectangular Cavity RSA

Based on the analysis of the previous section, a new rectangular cavity RSA using PTFE material is shown in Fig. 6-27. The cavity size is 98mm by 74mm, which is 30% size reduced comparing with the square one. A slot with 3mm width is cut out from a copper layer of 5mm thickness. An IC chip is mounted at the center of the slot to realize the wireless identification. A small copper pin is located at the center of cavity with 0.8mm radius and 3mm height to fix the copper coated PTFE. The copper coated PTFE with a radius of 5.18mm and height of 5.81mm is 0.09mm from the cavity ceiling. When the gap is 0.09mm at 20°C, the simulated S_{11} and realized gain are shown in Fig. 6-28 and Fig. 6-29, respectively. From Fig. 6-28, it can be seen that the impedance match between chip and antenna is not as good as the square cavity design. This is because when the cavity becomes more compact, the imaginary part of the RSA impedance is too

inductive to get a good match with chip due to the smaller parallel inductance added by the cavity. This is the drawbacks of using compact cavity size. And from Fig. 6-29, it is observed that the maximum realized gain of the rectangular RSA is 3.1dB with a 1% 3dB bandwidth, which is smaller than the square one of 4.17dB.

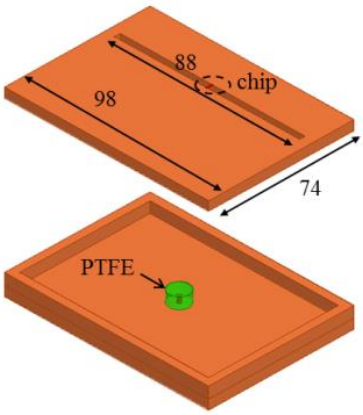

Fig. 6-27 Configuration of the PTFE used rectangular cavity RSA.

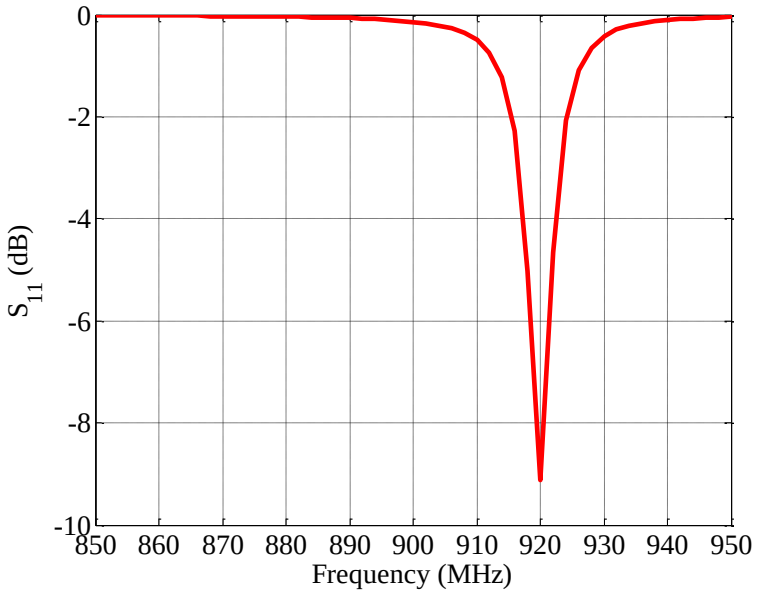

Fig. 6-28 S_{11} of the PTFE used rectangular cavity RSA.

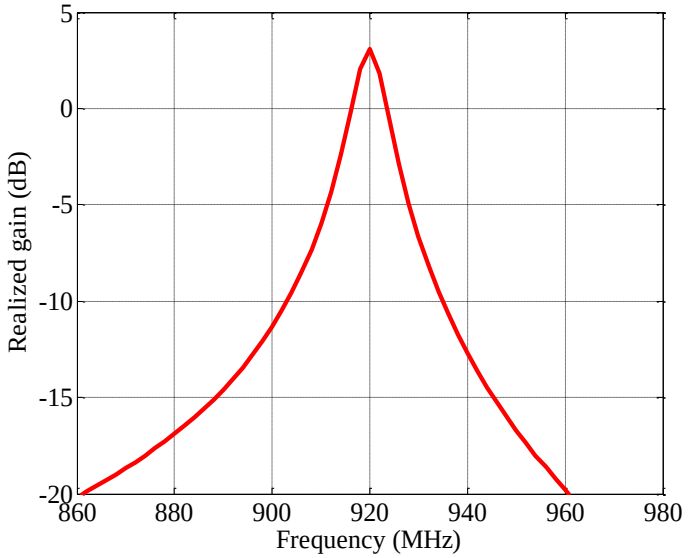

Fig. 6-29 Broadside realized gain of the PTFE used rectangular cavity RSA.

6.3.4 Temperature Sensitivity of the PTFE Used Rectangular Cavity RSA

The thermal expansion of the PTFE can be calculated based on its thermal expansion coefficient and the temperature variation, which is around 8μm/10°C. According to this information, the RSA performance at different temperatures can be simulated by the HFSS. Fig. 6-30 shows the realized gain of the RSA under different temperature. It is seen from the Fig. 6-30 that as temperature increases, the realized gain of the rectangular RSA decreases. To be specifically, the realized gain decreased from 3.1dB to 0.81dB, when the temperature increases from 20°C to 50°C. There are three contributing factors to the decreased realized gain. The first one is that the impedance match between RSA and IC chip degrades. The second one is that as the PTFE approaching the cavity top with temperature increasing, the metallic loss increases. The last

one for the smaller realized gain is that in high temperature, the RSA resonates at lower frequency, which results in a smaller directivity.

Table 6-5 shows the sensitivity comparison between the square cavity RSA and the new rectangular RSA. One can observe from the table that the size of the rectangular RSA is 30% less than the square one. However, these two designs possess similar Δf/ΔT and bandwidth. The only difference is the realized gain. The realized gain of the rectangular one is 1dB less than the square one.

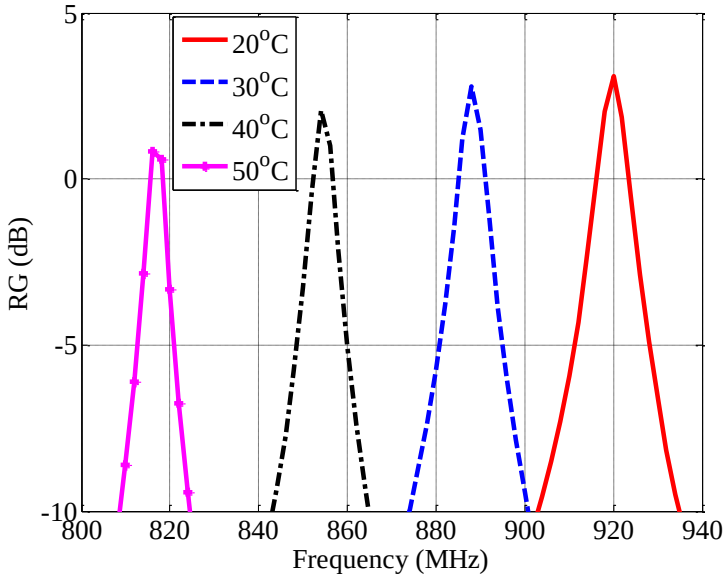

Fig. 6-30 Realized gain of the RSA under different temperatures.

Table 6-5 Sensitivity comparison between the rectangular cavity and square cavity RSAs

	Size	Δf/ΔT	RG	BW
Square cavity	104x104 mm^2	40MHz/10°C	4.17dB	0.66%
Rectangular cavity	98x74 mm^2	38MHz/10°C	3.1dB	1%

6.4 Summary

In this chapter, a solid material PTFE is selected as the temperature sensing material due to its 140ppm /°C thermal expansion coefficient. Similar to mercury, the PTFE is also placed at the center of a cavity backed slot antenna to form a temperature dependent loaded capacitance with cavity top. Because of its solid status, the PTFE post can be in close proximity to the cavity top, which is only 0.09mm.As a result, the PTFE used RSA has a higher sensitivity comparing to the mercury used RSA. The experimental results show that the PTFE used cavity RSA can realize 40MHz/10°C frequency shift with temperature and 14m read range, which is the best sensitivity in the known frequency reconfigurable RSA designs.

Although the PTFE used RSA possess good sensitivity, it is a little bulky, which constrains its application areas. Therefore, in this chapter, the size reduction method of the RSA is also investigated. The new compact cavity RSA is obtained by making the square cavity to a rectangular one. By understanding the resonating principle of the cavity RSA, one can reduce the cavity size in the direction perpendicular to the slot without changing its resonant frequency much. However, in this case, the antenna directivity will be sacrificed a little.

Besides reducing the cavity size, a new PTFE storage method is also introduce. In this method, a copper pin is used to fix the PTFE post instead of copper container. By doing this, the fabrication and measurement difficulty are decreased. Combing the new PTFE storage method and rectangular cavity, we get a compact RSA design. This new design provides a temperature sensitivity of 38MHz/10°C, 3.1dB realized gain, and 1% 3dB realized gain bandwidth. This sensitivity is comparable with the conventional square cavity. The only difference is the realized

gain of the new one is 1dB less. Although the compact design has a smaller realized gain, its size is 30% reduced comparing with the conventional one. One may realize that the tradeoff between the RSA size and gain always exists. Thus, in the design procedure, a compromise is always needed to get an optimum design which best meets the design goal.

CHAPTER VII

CONCLUSIONS

7.1 Summary

Reconfigurable sensing antennas are the antennas, which realize the environmental sensing functionality by reconfiguring their characteristics, such as resonant frequency, RCS. They have simple structure, which mainly consists of antenna and sensor unit. The sensor unit is directly integrated as part of the antenna. When compared with the conventional sensor node used in WSN, the RSA has the advantages of simple structure, passive, and cost efficient. These features make the RSA become valuable candidate in large scale WSN deployment. If integrated with the RFID IC chip, the RSA can realize wireless identification besides wireless sensing, which make them also suitable for the emerging RFID sensing applications.

Because the importance of RSA in both the WSN and RFID sensing areas, in this dissertation, the systematic investigation about RSAs, especially temperature sensing RSAs are done, including its concept introduction, state of the art designs, and the design and analysis of new high sensitivity RSAs. In order to obtain high temperature sensitivity, two different sensing mechanisms are investigated. They are the electrical properties of materials and thermal properties of materials. For each sensing mechanism, two different RSAs are designed, fabricated, and measured. They are the water used RSA and HDPE-BST based RSA of using materials' electrical

properties; the mercury used cavity RSA and PTFE loaded cavity RSA of using materials' thermal properties. Their sensitivity is evaluated with $\Delta f/\Delta T$, realized gain, and realized gain bandwidth. Table 7-1 shows the details comparison of the four RSAs. It is observed that the PTFE loaded cavity RSA possesses the best sensitivity of 40MHz/10°C frequency shift with temperature, 4.17dB broadside realized gain, and 0.66% 3dB realized gain bandwidth This PTFE loaded RSA is the one which provides the best sensitivity in the frequency reconfigurable RSAs.

Table 7-1 Sensitivity comparison of different RSAs

	Water RSA	HDPE-BST RSA	Mercury RSA	PTFE RSA
$\Delta f/\Delta T$ (MHz/10°C)	4MHz/10°C	8MHz/10°C	13MHz/10°C	40MHz/10°C
Realized gain (dB)	-3.2dB	-3.9dB	5.47dB	4.17dB
Realized gain bandwidth	4.33%	0.6%	1.33%	0.66%

The most important contributions of this dissertation are as follows:

- Firstly, the concept of the reconfigurable sensing antennas is introduced;
- Secondly, different sensing mechanisms are investigated and summarized;
- Thirdly, thermal expansion properties of materials are firstly used in the continuous temperature monitoring.
- Furthermore, the best temperature sensitivity of the frequency reconfigurable RSAs are obtained by the PTFE loaded cavity design.

7.2 Future Work

Although the RSAs in this dissertation are passive and can realize high sensitivity, there are still future works need to be done. First thing is to further reduce the cavity RSA size. Although the rectangular cavity RSA has a side length of 74mm by 98mm with a whole thickness of 11mm, which is 30% size reduced comparing with the square one; its size is still big. One can use the substrate integrated cavity to further reduce the size, or instead of using straight slot, use meander slot to make the design compact.

In addition, one can also investigate new sensation mechanism and implement it is RSA design. For example, the element whose capacitance or inductance is environmental dependent can be integrated in the RSA design.

Nowadays, most of the research work is focus on RSA designs only to use new material or high sensitivity. One can build a measurement system to fulfill a real time temperature monitoring in practice.

BIBLIOGRAPH

[1]. C. A. Balanis, Antenna Theory Analysis and Design, 3rd edition, John Wiley & Sons. Inc., 2005.

[2]. J. Huang and A. C. Densmore, "Microstrip patch array for antenna for mobile satellite vehicle application," *IEEE Trans. Antenna and Prog*., vol 39, pp. 1024-1030, Jul. 1991.

[3]. J. Liang, C. Chiau, X. Chen, and C. G. Parini, "Study of a printed circular disc monopole antenna for UWB systems," *IEEE Trans. Antenna and Prog*., vol. 53, pp. 3500-3504, Nov. 2005.

[4]. J. D. Boerman and J. T. Bernhard, "Performance Study of Pattern Reconfigurable Antennas in MIMO Communication Systems**,**" *IEEE Trans. Antennas Propag.*, vol. 56, no. 1, pp. 231 – 236, Jan. 2008.

[5]. P. J. B. Clarricoats, A. D. Monk, and H. Zhou, "Array-fed reconfigurable reflector for spacecraft applications**,**" *IEE Proceedings Microwaves, Antennas and Propagation*, vol. 141, no. 6, pp. 531-535, Dec. 1994.

[6]. B. A. Cetiner, H. Jafarkhani, Qian Jiang-Yuan, Yoo Hui Jae, A. Grau, and F. De Flaviis, "Multifunctional reconfigurable MEMS integrated antennas for adaptive MIMO systems," *IEEE Communications Magazine*, vol. 42, no. 12, pp. 62-70, Dec. 2004.

[7]. S. Nikolaou, R. Bairavasubramanian, C. Lugo, Jr., I. Carrasquillo, D. C. Thompson, G. E. Ponchak, J. Papapolymerou, and M. M. Tentzeris, "Pattern and frequency reconfigurable annular slot antenna using PIN diodes," *IEEE Trans. Antennas Propag.*, vol. 54, no. 2, pp. 439-448, Feb. 2006.

[8]. E. W. Jacobs, D. W. ogliatti, H. Nguyen, D. J. Albares, C. T. Chang, and C. K. Sun, "Photo-injection p-i-n diode switch for high-power RF switching," *IEEE Microwave Theory and Techniques*, vol. 50, no. 2, pp. 413-419, Feb. 2002.

[9]. N. Behdad and K. Sarabandi, "A varactor-tuned dual-band slot antenna," *IEEE Trans. Antennas Propag.*, vol. 54, no. 2, pp. 401-408, Feb. 2006.

[10]. https://people.hofstra.edu/geotrans/eng/ch5en/appl5en/meatcoldchain.html

[11]. http://www.bulgarianbuildingservices.com/eco-green-building/energy-efficient-house-design/

[12]. F. Yang, Q. Qiao, J. Virtanen, A. Z. Elsherbeni, L. Ukkonen and L. Sydänheimo "Reconfigurable sensing antenna: a slotted patch design with temperature sensation," *IEEE Antenna Wireless Propag. Lett*., vol. 1, pp. 632–635, June 2012.

[13]. Q. Qiao, L. Zhang, F. Yang, Z. Yue and A. Z. Elsherbeni, "Reconfigurable sensing antenna with novel HDPE-BST material for temperature monitoring," *IEEE Antenna Wireless Propag. Lett.*, vol. 12, pp. 1420-1423, 2013.

[14]. Z. Jiang, F. Yang, "Reconfigurable RFID tag antenna for wireless temperature monitoring," in *Proc. IEEE Antennas Propag. Society Int. Symp*. Chicago, IL, Jul. 8-14, 2012, pp. 1-2.

[15]. R. Bhattacharyya, C. Floerkemeier, and S. Sarma, "RFID tag antenna based temperature sensing," *IEEE International Conf.* on RFID, pp. 8-15, Apr. 2010.

[16]. K. Chang, Y. H. Kim, Y. J. Kim and Y. J. Yoon, "Functional antenna integrated with relative humidity sensor using synthesised polyimide for passive RFID sensing," *Electronics Lett.*, vol. 43, no.5, pp. 7-8, Mar. 2007.

[17]. J. Virtanen, L. Ukkonen, T. Björninen and L. Sydänheimo, "Printed humidity sensor for UHF RFID system," *IEEE Sensor Application Symp.*, pp. 269-272, Feb. 2010.

[18]. C. Occhiuzzi, A. Rida, G. Marrocco, and M. M. Tentzeris, "CNT-based RFID passive gas sensor," *IEEE MTT-S Int. Symp*., pp. 1-4, Aug. 2011.

[19]. C. Occhiuzzi, S. Cippitelli, and G. Marrocco, "Modeling, design and experimentation of wearable RFID sensor tag," *IEEE Trans. Antennas Propag*., vol. 58, no. 8, Aug. 2010.

[20].Higgs™-3 EPC Class 1 Gen 2 RFID Tag IC, http://www.alientechnology.com/docs/products/Alien-Technology-Higgs-3-ALC-360.pdf, Product Overview.

[21]. D. M. Dobkin, The RF in RFID: Passive UHF RFID in Practice, Newnes Press. 2007.

[22]. http://rfid-handbook.de/about-rfid.html

[23]. A. Vaz, A. Ubarretxena, I. Zalbide, D. Pardo, H. Solar, and A. García-Alonso, "Full passive UHF tag with a temperature sensor suitable for human body temperature monitoring," *IEEE Trans. Circuits Syst*., vol. 57, pp. 95-99, Feb. 2010.

[24]. U. Kaatze, "Complex permittivity of water as a function of frequency and temperature," Journal of Chemical & Engineering Data, vol. 34 (4), pp.371-374, 1989.

[25]. Ansoft HFSS, ver. 14, Ansoft Corporation, Canonsburge, PA, 2012.

[26]. A. Z. Elsherbeni and V. Demir, The Finite-Difference Time-Domain Method for Electromagnetics with MATLAB Simulations, SciTech Publishing, Inc, Raleigh, NC.

[27]. Voyantic Ltd., Alien Tagformance overview, available at: http://www.voyantic.com.

[28]. Regulatory status for using RFID in the EPC Gen 2 band (860 to 960 MHz) of the UHF spectrum, http://www.gs1.org/docs/epcglobal/UHF_Regulations.pdf.

[29]. Alien Technology, Higgs 2 Datasheet, online: www.alientechnology.com/docs/products/DS H2. pdf, last accessed, February 4, 2010.

[30].http://www.rogerscorp.com/acm/products/10/RT-duroid-5870-5880-5880LZ-High-Frequency-Laminates.aspx

[31] D. M. Pozar, Microwave Engineering, Third Edition, John Wiley & Sons Inc., Mar. 2005.

[32]. X. Liu, L. P. B. Katehi, W. J. Chapell and D. Peroulis, “High-Q Tunable Microwave Cavity Resonators and Filters using SOI-based RF MEMS Tuners,” Journal of Microelectromechanical Syst., vol. 19, no. 4, pp. 774-784, Aug. 2010.

[33]. X. Liu , L. P. B. Katehi , W. J. Chappell and D. Peroulis "A 3.4–6.2 GHz continuously tunable electrostatic MEMS resonator with quality factor of 460–530", IEEE MTT-S Int. Microw. Symp. Tech. Dig., pp.1149 -1152 2009.

[34]. S. A. Long, “Experimental study of the impedance of cavity backed slot antennas,” IEEE Trans. Antennas Propag., vol. 23, no. 1, Jan. 1975.

[35]. C. A. Lindberg, “A shallow-cavity UHF crossed slot antenna,” IEEE Trans. Antennas Propag., vol. 17, no. 5, Sep. 1969.

LIST OF PUBLICATIONS

[1] Q. Qiao, F. Yang and A. Z. Elsherbeni "A high sensitivity RFID temperature sensor tag design using PTFE material," *IEEE AP-S International Symposium*, Memphis, TN, July 2014, *under review*.

[2] F. Yang, Q. Qiao, L. Zhang, Z. Yue and A. Z. Elsherbeni, "High-Sensitivity RFID Sensing Antennas: From Sensing Mechanism Selections to Antennas Structure Designs," *IEEE URSI-GA*, Beijing, Aug. 2014, under review.

[3] Q. Qiao, Z. Fu, F. Yang, L. Zhang, A. Z. Elsherbeni, and Z. Yue, "High sensitivity capacitively-loaded reconfigurable cavity backed slot antennas for temperature applications," *IEEE Trans. Antennas and Propagations, in press.*

[4] Q. Qiao, L. Zhang, F. Yang, Z. Yue and A. Z. Elsherbeni, "Reconfigurable sensing antenna with novel HDPE-BST mateiral for temperature monitoring," *IEEE Antenna Wireless Propagation Letters*, vol. 12, pp.1420-1423, 2013.

[5]. F. Yang, Q. Qiao and Atef. Z. Elsherbeni, "Reconfigurable sensing antennas: concept, design, and applications," *IEEE Antenna Propagation Wireless Communication Conference*, pp. 748-752, Torino, Italy, Sep. 2013.

[6]. Q. Qiao, L. Zhang, F. Yang, Z. Yue and A. Z. Elsherbeni, "UHF RFID temperature sensor tag using novel HDPE-BST composite material," *IEEE APS International Symposium*, Florida, USA, July, 2013.

[7] F. Yang, Q. Qiao, J. Virtanen, A. Z. Elsherbeni, L. Ukkonen and L. Sydänheimo "Reconfigurable sensing antenna: a slotted patch design with temperature sensation," *IEEE Antenna Wireless Propagation Letters*, vol. 1, pp. 632–635, June 2012.

[8]. Q. Qiao, F. Yang and A. Z. Elsherbeni, "Read range and sensitivity study of RFID temperature sensors," *IEEE AP-S International Symposium*, Chicago, USA July, 2012.

[9]. F. Yang, Q. Qiao, Z. Jiang, "Reconfigurable sensing antennas: a low-cost passive wireless sensing method," *IEEE AP-S International Symposium*, Chicago, USA July, 2012.

[10]. Q. Qiao, J. Virtanen, F. Yang, L. Ukkonen, A. Z. Elsherbeni and L. Sydänheimo, "UHF RFID sensor tags for temperature sensation," *IEEE AP-S International Symposium*, Spokane, Washington, July, 2011

[11]. Q. Qiao, F. Yang, A. Z. Elsherbeni, "Bandwidth enhancement of circularly polarized patch antenna using lumped LC matching circuit", The 27th International Review of Progress in Applied Computational Electromagnetics (ACES), Williamsburg, Virginia, 27-31 Mar., 2011.

VITA

Qian Qiao was born in 1984 in Baoji, China. She received her Bachelor of Science degree in electronic engineering from Northwestern Polytechnical University, Xi'an, China, in 2006. She also received her Master of Science in 2009 from the same department. She joined The University of Mississippi in 2009 as a research assistant and graduate student in the center of applied electromagnetic systems research (CEASR), where he earned his Ph.D in 2014. From Feb. 2012 to Apr. 2013, she worked as a cooperation researcher in Microwave and Antenna Research Institute of Tsinghua University, China. During the Ph.D study in University of Mississippi, her research interests include patch antenna, RFID tag, reconfigurable sensing antennas for temperature monitoring. She focuses on investigating different sensing materials and sensing mechanism in the RSA designs. She has published 10 papers in IEEE journal and proceedings. She is currently a student member of IEEE.